Acta Numerica (2009), pp. 111–241
doi: 10.1017/S0962492906400015
© Cambridge University Press, 2009
Printed in the United Kingdom

Adaptivity with moving grids

Chris J. Budd
Centre for Nonlinear Mechanics,
University of Bath, Bath BA2 7AY, UK
E-mail: mascjb@bath.ac.uk

Weizhang Huang
Department of Mathematics,
University of Kansas,
Lawrence, Kansas 66045, USA
E-mail: huang@math.ku.edu

Robert D. Russell
Department of Mathematics,
Simon Fraser University,
Burnaby V5A 1S6, Canada
E-mail: rdr@cs.sfu.ca

In this article we survey r-adaptive (or moving grid) methods for solving time-dependent partial differential equations (PDEs). Although these methods have received much less attention than their h- and p-adaptive counterparts, particularly within the finite element community, we review the substantial progress that has been made in developing more robust and reliable algorithms and in understanding the basic principles behind these methods, and we give some numerical examples illustrative of the wide classes of problems for which these methods are suitable alternatives to the traditional ones.

More specifically, we first examine the basic geometric properties of moving meshes in both one and higher spatial dimensions, and discuss the discretization process for PDEs on such moving meshes (both structured and unstructured). In particular, we consider the issues of mesh regularity, equidistribution, alignment, and associated variational methods. An overview is given of the general interpolation error analysis for a function or a truncation error on such an adaptive mesh. Guided by these principles, we show how to design effective moving mesh strategies. We then examine in more detail how these strategies can be implemented in practice. The first class of methods which we consider are based upon controlling mesh density and hence are called position-based methods. These make use of a so-called moving mesh PDE (MMPDE) approach and variational methods, as well as optimal transport methods. This is followed by an analysis of methods which have a more Lagrange-like interpretation, and due to this focus are called velocity-based

https://doi.org/10.1017/S0962492906400015 Published online by Cambridge University Press

methods. These include the moving finite element method (MFE), the geometric conservation law (GCL) methods, and the deformation map method. Finally, we present a number of specific types of examples for which the use of a moving mesh method is particularly effective in applications. These include scale-invariant problems, blow-up problems, problems with moving fronts and problems in meteorology. We conclude that, whilst r-adaptive methods are still in their relatively early stages of development, with many outstanding questions remaining, they have enormous potential and indeed can produce an optimal form of adaptivity for many problems.

CONTENTS

1 Introduction 112
2 Moving mesh basics 121
3 Location-based moving mesh methods 154
4 Velocity-based moving mesh methods 193
5 Applications of moving mesh methods 201
References 231

1. Introduction

1.1. Motivation

Time-dependent systems of partial differential equations (PDEs) often have structures that evolve significantly as the integration of the PDEs proceeds. These can be interfaces, shocks, singularities, changes of phase, high vorticity or regions of complexity. Associated with such structures are the evolution of small length (and time) scales, rapid movement of the solution features and the possibility of finite time blow-up of a component of the solution. Frequently associated are also conservation laws, usually linked to underlying symmetries. Examples of these phenomena occur in many applications, such as gas and fluid dynamics, conservation laws, nonlinear optics, free boundary problems, combustion, detonation, meteorology, mathematical biology and nonlinear optics. To solve such PDEs numerically it is typical to impose some form of spatial mesh and then to discretize the solution on this mesh by using a finite element, finite volume, finite difference, or collocation method. However, this strategy may not be effective in the case of structures that involve small length scales, leading to large localized errors. In such cases it is often beneficial to use some form of non-uniform mesh, adapted to the solution, on which to perform all of the computations. The advantages of doing this can be a reduced overall error, better conditioning of the system, and better computational efficiency. Unfortunately, introducing the extra level of complexity to the system through adaptivity

https://doi.org/10.1017/S0962492906400015 Published online by Cambridge University Press

can also lead to additional computational cost and possible numerical instability. Mesh adaptation should thus be used with care and appropriate analysis where possible.

1.2. Adaptivity on a moving mesh

Adaptive methods for solving partial differential equations broadly fit into three categories. The most extensively developed are *static regridding methods*, in which a mesh is updated at each time level. The most widely used of these are *h-refinement methods*, which form the basis of many commercial codes. Usually such codes start with an initially uniform mesh, and then locally coarsen or refine this by the inclusion or deletion of mesh points. The strategy for doing this is normally guided by some *a posteriori* estimate of the solution error, and may consider problems in which the error is due to the solution geometry (such as re-entrant corners) or high derivatives. In *p-refinement methods* some finite element discretization of the PDE is used with local polynomials of some particular order. This order is then increased or decreased in accordance with the solution error. These methods may be combined with *h*-refinement methods and with careful *a posteriori* estimates to give *hp* methods (Ainsworth and Oden 2000). The principal objective of the *hp* methods is to obtain solutions within prescribed error bounds by such refinement procedures. There is not usually an upper bound on the number of points used in the calculation. Such methods have now been developed to a high degree of sophistication. However, they are necessarily rather complex, need not take advantage of any dynamic properties of the underlying solution, and the *a posteriori* error estimates rely heavily on certain assumptions on the solution which may be hard to verify for strongly nonlinear problems.

The *r-refinement* (relocation refinement) moving mesh methods which will form the substance of this article are a more recent development than *hp* methods. Whilst not as widely used as *h*- or *p*-adaptive methods, *r*-adaptivity has been used with success in many applications including computational fluid mechanics (Tang 2005), phase field models and crystal growth (Mackenzie and Mekwi 2007*a*), and convective heat transfer (Ceniceros and Hou 2001). It also has a natural application to problems with a close coupling between spatial and temporal length scales, such as in problems with symmetry, scaling invariance and self-similarity (Barenblatt 1996, Budd and Williams 2006), where the mesh points become the *natural coordinates* for an appropriately rescaled problem. Less is known about the behaviour of *r*-adaptive methods than of the much more extensively developed *hp* methods, and (at least in higher dimensions) they have yet to become part of established large numerical codes. In particular, as we shall see in this article, many outstanding open questions remain on

https://doi.org/10.1017/S0962492906400015 Published online by Cambridge University Press

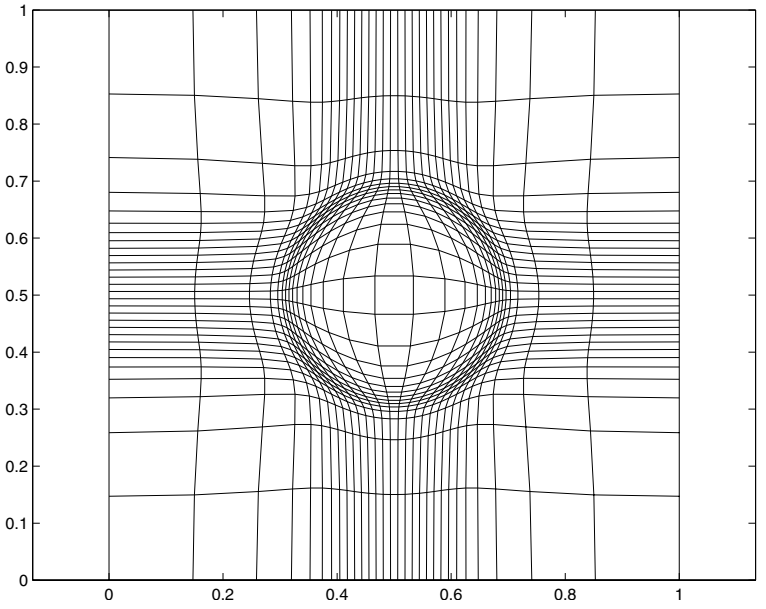


Figure 1.1. A logically rectangular mesh, moved to concentrate points around a ring in an evolving singular solution of the nonlinear Schrödinger equation. Note the good radial symmetry of the adapted mesh around the ring.

their convergence, the nature of the meshes that they generate and the error estimates that can be obtained when using them to solve PDEs with rapidly evolving structures. As a consequence, much of the analysis of such methods has been for one-dimensional problems, and the one-dimensional PDE solver MOVCOL (Huang and Russell 1996, Russell, Williams and Xu 2007) and the celebrated continuation code AUTO (for solving two-point boundary value problems amongst others) both make use of r-adaptive methods. However, r-refinement methods show great potential for solving a much greater range of problems, as we hope to demonstrate in this article.

The r-refinement methods start with a uniform mesh and then *move* the mesh points, keeping the mesh topology and number of mesh points fixed as the solution evolves. Hence the use of the alternative name of *moving mesh methods* for such procedures. The mesh points are then concentrated into regions where the solution has 'interesting behaviour', usually typified by a rapid variation of either the solution or one of its (higher) derivatives. The objective of this approach is to get the smallest error possible for the number N of mesh points used, and to try to obtain error estimates which depend upon the value of N but *not* on the solution itself. For example, if the solution evolves a boundary layer of width ϵ (with ϵ decreasing as

https://doi.org/10.1017/S0962492906400015 Published online by Cambridge University Press

time advances), then ideally the mesh points should concentrate into this boundary layer so that the solution error is *independent of* ϵ. The moving mesh methods typically work by generating a mapping from a regular (logical or computational) domain into a physical domain in which the underlying equation is posed. The location, or the velocity, of the mesh points is then determined by solving a system of *auxiliary partial differential equations*, often called the *moving mesh equations*. In all cases a vector or a scalar *monitor function* (or functions) is used to guide the position of the mesh. The monitor function is usually designed to give an estimate of some measure of the solution error which is then *equidistributed* over each mesh cell. The monitor function is usually constructed in one of three ways. It may depend upon *a priori solution estimates* (such as arclength or curvature), on *a posteriori error estimates* (such as the solution residual, as used in moving finite element methods (Baines 1994), or estimates of the derivative jump across element boundaries (Tang 2005)), or on some underlying *physics* related to the solution, such as the potential temperature or the vorticity in a meteorological problem (Budd and Piggott 2005). In the case of *scale-invariant* problems, such physical estimates are often optimal. When using such methods, much care has to be taken in preventing mesh tangling and ensuring mesh regularity and isotropy (where relevant). A discussion of this will form a significant part of Section 2. We also require that discretizations of the underlying PDE on such meshes (in either the computational or the physical domain) should retain important properties of the underlying physical solution, such as conservation laws and scaling structures (Tang 2005). Provided that these conditions are carefully considered, r-adaptive methods can be used with considerable success for many time-evolving systems. Examples of these include computational fluid dynamics (Yanenko, Kroshko, Liseikin, Fomin, Shapeev and Shitov 1976), groundwater flow (Huang and Zhan 2004, Huang, Zheng and Zhan 2002), blow-up problems (Budd, Huang and Russell 1996, Budd and Williams 2006, Ceniceros and Hou 2001, Ren and Wang 2000), chemotaxis systems (Budd, Carretero-Gonzalez and Russell 2005), reaction–diffusion systems (Zegeling and Kok 2004), the nonlinear Schrödinger equation (Sulem and Sulem 1999, Ceniceros 2002, Budd, Chen and Russell 1999*a*), phase change problems (Mackenzie and Robertson 2002, Mackenzie and Mekwi 2007*a*, Tan, Lim and Khoo 2007), shear layer calculations (Tang 2005), gas dynamics (Li and Petzold 1997, Li, Petzold and Ren 1998), hyperbolic conservation laws with high Mach number (Li and Petzold 1997, Tang 2005, Stockie, Mackenzie and Russell 2000, Tang and Tang 2003), problems with high vorticity (Ceniceros and Hou 2001), magneto-hydrodynamics (Tan 2007) and meteorological problems (Budd and Piggott 2005). More details of such applications are given in Section 5. In Figure 1.1 we give an example of an r-adaptive mesh which has evolved to capture the structure of a singular

https://doi.org/10.1017/S0962492906400015 Published online by Cambridge University Press

solution of the nonlinear Schrödinger equation which has its support concentrated around a ring.

All r-adaptive methods have intimate connections with the geometry of mapping one domain to another. They thus have intimate links with problems in differential geometry such as optimal transport (Brenier 1991, Gangbo and McCann 1996), mean curvature flows (Huang 2007) and harmonic mappings (Dvinsky 1991). A natural application of such ideas arises in image processing, and r-adaptivity has close connections with such image processing procedures as image segmentation and image de-noising (Sapiro 2003).

There are advantages and disadvantages to each of the strategies outlined above. As discussed earlier, the *hp* methods have been in use for a long time and are now well established in many commercial codes. There is a significant body of analysis supporting their use. In contrast, r-adaptive methods are more recent and are less well understood. A significant criticism which has often been made of them is that their implementation usually requires the solution of *auxiliary* partial differential equations for the mesh, which must be solved in parallel to the underlying partial differential equation. This requires significant additional computational cost. Furthermore, the equations to be solved to determine a suitable mesh can often be very stiff, and thus expensive to solve. Furthermore, the methods get the best estimates for a given N rather than errors necessarily lower than a specified tolerance. However, r-adaptive methods do have significant advantages in certain applications. Firstly, from a computational point of view, it is convenient to work with the same number of mesh points and the same mesh topology. This makes the linear algebra rather easier, as the matrices considered have a constant sparsity structure, and there is no need for any form of nested data structure to keep track of the node points (an issue which always complicates the use of h-refinement methods). The discretization strategy on the mesh is also easier, especially with a finite element method, as the constancy in the mesh topology and connectivity implies that there is no possibility of hanging nodes. There are further, structural advantages to r-refinement methods. One of these is that the movement of the mesh points may well correspond to natural structures of the PDE itself. An obvious example is Lagrangian-based methods for fluid flow problems, in which mesh points move with the fluid flow. A further such example is given by the use of r-refinement methods for PDEs with natural scaling symmetries, in which the mesh points automatically follow the motion of natural similarity variables (and indeed the use of the r-refinement method becomes equivalent to the use of an appropriate coordinate transformation). A third advantage of r-refinement is that, under certain circumstances, the adaptive strategy when coupled with the PDE can be regarded as one (large) dynamical system, which may then be amenable to a combined analysis. One limitation

https://doi.org/10.1017/S0962492906400015 Published online by Cambridge University Press

of having a *fixed* number of points means that it may never be possible to resolve all of the fine structures of a PDE as it evolves (although it is surprising what can be done with often a relatively small number of mesh points). Also, all r-adaptive methods are, in principle, prone to *mesh tangling*, in which lines connecting the mesh points can cross over during the evolution. This generally leads to severe instabilities in the system and a failure of the solution routine. Mesh tangling is often associated with *mesh racing*, where some mesh points move very fast during the evolution, frequently leading to a stiff set of equations to solve. The disadvantages of having to solve an auxiliary set of partial differential equations are less severe than they might originally appear to be. Firstly, the combined system of mesh and underlying equations may be much smaller than the original system defined on a uniform mesh for the *same level of accuracy*. Indeed, in Section 5 we will give an example of the solution of focusing behaviour in the one-dimensional nonlinear Schrödinger (Sulem and Sulem 1999) equation (which can be written as four real first-order PDEs), where a discretization of the PDE on a set of $N = 81$ moving mesh points is able to resolve singular structures with a length scale of 10^{-5}, and outperforms discretizations on uniform meshes with 10^5 mesh points. Hence the additional 81 auxiliary equations for the mesh gives a method which outperforms one with 10^5 equations, giving a very significant cost reduction. Secondly, although the equations describing the mesh are indeed stiff in general, we do not need (in general) to solve them exactly. After all, it is the underlying solution of the PDE that we are interested in, and not the mesh on which it is solved. Thus a quite rough approximation to the solution of the moving mesh equations will often deliver a mesh more than adequate for the task of resolving the structures of the underlying PDE. Indeed, we will argue in Section 3 (and demonstrate by example in Section 5) that a relaxed version of the moving mesh equations can be solved using a simple explicit method, will deliver similar performance for much stiffer equations than the meshes obtained by more computationally expensive methods. Indeed, they may well be stable, more regular, and deliver a better mesh quality than solving the exact equations for the mesh. Finally, one of the main applications of hp methods is to solve otherwise regular PDEs on irregular domains, typically with re-entrant corners, that introduce significant errors due to a lack of solution regularity at the corner. The r-adaptive methods as described in this paper are not really the right tool for this job (though see the results in Touringy (1998)). However, a combination of h and r methods may well prove optimal in this case, where the h method is used to mesh around the corner and the r method to follow any evolving solution structure. Future attempts to combine these two types of adaptive refinement in a general context should prove to be most interesting.

https://doi.org/10.1017/S0962492906400015 Published online by Cambridge University Press

1.3. Computation on moving meshes

The problem of computing solutions of PDEs using a moving mesh method separates into three related problems.

(1) As described, we need some monitor function to guide the mesh evolution, which is typically constrained either to equidistribute this function, or to relax towards an equidistributed state. In practice, whatever the choice of monitor function, some spatial (and temporal) smoothing is usually employed.

(2) Having determined the monitor function, we must determine a mesh that equidistributes it in some way. The equidistribution problem itself is a nonlinear algebraic problem, and several techniques have been developed to solve this problem, *e.g.*, a variational method, the geometric conservation law, moving mesh PDEs and optimal transport methods.

(3) The underlying PDE is then discretized, either on the mesh in the computational domain or in the original physical domain (in the latter case a finite element or finite volume method is usually employed (Tang 2005)). The underlying partial differential equation and the mesh equations can then be solved either simultaneously, typically by using the method of lines (Huang, Ren and Russell 1994), or alternatively (often by using a predictor–corrector method). The first method avoids the need for any interpolation from one mesh to another, but is usually associated with having to solve stiff differential equations. Alternating solutions can be implemented using either the quasi-Lagrange approach (Huang and Russell 1997*b*) or the rezoning approach (Tang 2005). The former transforms time derivatives to those along mesh trajectories and avoids interpolation of the physical solution from the old mesh to the new one. However, it has the disadvantages that it has to deal with extra convection terms caused by mesh movement and may cause a time lag in mesh movement. On the other hand, the rezoning approach solves the physical PDE on a fixed mesh over a time step but requires interpolation from one mesh to another (which often has to be done very carefully to preserve conservation laws). We will consider both methods in detail in this article.

We are currently in a situation where the mesh formulation problem, mesh generation and the solution of PDEs on a moving mesh are generally well understood in one spatial dimension. Reliable and efficient moving mesh methods exist (and are implemented in a number of packages) which are based on such formulations and can be used to solve time-evolving PDEs in one spatial dimension, with associated error estimates in certain cases. Indeed, for such problems the use of moving mesh PDEs to evolve the mesh coupled with a method of lines approach has proved to be very effective, and

https://doi.org/10.1017/S0962492906400015 Published online by Cambridge University Press

also amenable to analysis. In this article we will be able to give a detailed description of the theory, implementation and application of such methods. However, the problem of mesh movement, and the discretization of PDEs on such meshes, is much less understood in higher dimensions, and this will form the bulk of the discussion in this paper.

1.4. A historical survey

Moving meshes and the use of adaptive strategies to minimize estimates of the solution error have a rich and diverse literature. Moving mesh methods can be classified according to the mesh movement strategy into two groups (Cao, Huang and Russell 2003): *velocity-based* methods and *location-based* methods. The first group is referred to as velocity-based since the methods directly target the mesh velocity and obtain mesh point locations by integrating the velocity field. Methods in this group are more or less motivated by the Lagrange method in fluid dynamics, where the mesh coordinates, defined to follow fluid particles, are obtained by integrating flow velocity. A major effort in the development of these methods has been to avoid mesh tangling, an undesired property of the Lagrange method. This type of method includes those developed in Anderson and Rai (1983), Cao, Huang and Russell (2002), Liao and Anderson (1992), Miller and Miller (1981), Miller (1981), Petzold (1987) and Yanenko *et al.* (1976). The method of Yanenko *et al.* is of Lagrange type. In the work of Anderson and Rai, mesh movement is based on attraction and repulsion pseudo-forces between nodes motivated by a spring model in mechanics. The moving finite element method (MFE) of Miller and Miller has aroused considerable interest. It computes the solution and the mesh simultaneously by minimizing the residual of the PDEs written in a finite element form. Penalty terms are added to avoid possible singularities in the mesh movement equations; see Carlson and Miller (1998*a*, 1998*b*). A way of treating the singularities but without using penalty functions has been proposed by Wathen and Baines (1985). Liao and Anderson (1992) and Cai, Fleitas, Jiang and Liao (2004) use a deformation map approach. Cao *et al.* (2002) develop the GCL method based on the geometric conservation law (see Section 4). Similar ideas have been used by Baines, Hubbard and Jimack (2005) and Baines, Hubbard, Jimack and Jones (2006) for fluid flow problems.

The second group is referred to as *location-based* because the methods directly control the location of mesh points. Methods in this group typically employ an adaptation functional and determine the mesh or the coordinate transformation as a minimizer of the functional. For example, the method of Dorfi and Drury (1987) can be linked to a functional associated with equidistribution principle (Huang *et al.* 1994). The moving mesh PDE (MMPDE) method developed in Cao, Huang and Russell (1999*b*), Huang *et al.* (1994)

https://doi.org/10.1017/S0962492906400015 Published online by Cambridge University Press

and Huang and Russell (1997*a*, 1999) moves the mesh through the gradient flow equation of an adaptation functional, which includes the energy of a harmonic mapping (Dvinsky 1991) as a special example. A combination of the MMPDE method with local refinement is studied in Lang, Cao, Huang and Russell (2003). Li, Tang and Zhang (2002) and Tang and Tang (2003) also use the energy of a harmonic mapping as their adaptation functional, but discretize the physical PDE in the rezoning approach.

So far a number of moving mesh methods and a variety of variants have been developed and successfully applied to practical problems; see the review articles of Cao *et al.* (2003), Eisman (1985, 1987), Hawken, Gottlieb and Hansen (1991), Thompson (1985), Thompson, Warsi and Mastin (1982) and Thompson and Weatherill (1992), and the books of Baines (1994), Carey (1997), Knupp and Steinberg (1994), Liseikin (1999), Thompson, Warsi and Mastin (1985) and Zegeling (1993). In particular, Hawken *et al.* (1991) give an extensive overview and references on moving mesh methods before 1990. In addition to the references cited above, we would also like to bring the reader's attention to the recent interesting work of Bank and Smith (1997), Beckett, Mackenzie and Robertson (2001*a*), Budd *et al.* (1996), Calhoun, Helzel and LeVeque (2008), Ceniceros and Hou (2001), Chacón and Lapenta (2006), Lapenta and Chacón (2006), Di, Li, Tang and Zhang (2005), Huang and Zhan (2004), Mackenzie and Robertson (2002), Ren and Wang (2000), Stockie *et al.* (2000), Tang and Tang (2003) and Zegeling and Kok (2004) on moving mesh methods and their applications.

1.5. Outline of this article

The purpose of this Introduction has been to give an underlying motivation for the theory and application of (adaptive) moving meshes. In Section 2 we will consider in detail the geometry of possible meshes (with special regard to equidistribution and isotropy), and the nature of discretizations of differential equations on them. In Section 3 we then look in detail, and with reference to many examples, at 'location-based' meshes in which the *local density* of the mesh points is controlled by a monitor function. These include *moving mesh PDE* (MMPDE) methods, variational methods and optimal-transport-based methods. This discussion will look at moving meshes in both one and higher dimensions and compare the strategies used for these two cases. In Section 4 we will then look at *velocity-based* methods, such as the geometric conservation law (GCL) methods and the moving mesh finite element methods, in which the *velocity* of the mesh points, rather than their position, is controlled. The concluding section, Section 5, will then look at some examples in much more detail, considering scale invariance, blow-up problems, problems with convection and moving fronts, phase change and combustion problems, and problems arising in meteorology.

https://doi.org/10.1017/S0962492906400015 Published online by Cambridge University Press

2. Moving mesh basics

In this section we will give an overview of the main aspects of adaptive moving mesh generation, and will concentrate on the nature of the *geometry* of an adapted mesh, the equidistribution and variational approaches to defining a mesh, and the relation of the mesh to solution (truncation and interpolation) errors. The *movement* of the mesh and the way that it can be *coupled to a partial differential equation* will be discussed briefly, but will mainly be the subject of Sections 3 and 4.

As described in the Introduction, in an r-adaptive procedure a fixed number of mesh points are *moved* in response to some user-designed condition. Any r-adaptive method has two main features, a description of the *optimal geometry* of the mesh (which is related both to intrinsic properties of the mesh regularity and to the structure of the underlying solution of the PDE) and a *strategy for evolving the mesh towards this optimal geometry*. Optimal mesh geometries are typically expressed in terms of equidistribution measures (related to the solution of the underlying PDE by monitor functions) or using variational principles, and we review these here. *Movement strategies* are generally methods for determining either the *location* of the mesh points or the *velocity* of the mesh points. We discuss both briefly in this section, and then in more detail in Sections 3 and 4.

Essential to mesh adaptation is the ability to control the shape, size and orientation of mesh elements, and hence to control the error of the solution of the underlying PDE. This is done in three steps. Firstly an estimate of the solution error and/or mesh quality is made. Secondly the mesh is aligned and moved according to this estimate. Thirdly the solution of the underlying PDE is advanced on the new mesh. Typically this can be in response to some structure of the solution of a PDE which is evolving in the space supporting the mesh; however, there are more general circumstances (such as in image processing) where we might wish to evolve a mesh in a manner independent of any PDE.

In this section we will study the geometry of the meshes that arise from various adaptive strategies, considering such aspects as local element size, skewness and orientation as well as considering both isotropic and anisotropic meshes, and looking at solution error estimation and control.

2.1. Mesh-mapping functions

To describe an r-adaptive mesh we consider a *fixed computational domain* $\Omega_C \subset \mathbb{R}^n$, in which most of the computations associated with the PDE will be made. The domain Ω_C will have the usual Lebesgue measure and may have a non-trivial topology. We now consider there to be a *fixed* mesh τ_C on the computational domain. This can either be uniform or non-uniform, depending on the nature of the underlying problem, and in the simplest

https://doi.org/10.1017/S0962492906400015 Published online by Cambridge University Press

case will be a uniform set of logical rectangles. It can also be triangular, and usually takes this form when a finite element or finite volume method is used to discretize the PDE in the *physical* domain. Alternatively, if a finite difference or a spectral method is used to discretize the PDE in the *computational domain* then a regular rectangular mesh may be more appropriate. Note that we have a lot of *a priori* freedom in the choice of the computational domain Ω_C, and hence when Ω_C is *simply connected* it is often convenient to consider it to be a logically rectangular domain, so that

$$\Omega_C = [0,1]^n.$$

To describe a computational mesh in the case of such simply connected domains we typically divide $\Omega_C \subset \mathbb{R}^n$ into N^n *uniform, regular tetrahedra or cuboids* of side proportional to $1/N$ and volume proportional to $1/N^n$, and we will initially assume that this is the case. In the r-adaptive procedure considered in this section we consider the mesh points to be joined in a simple (logically rectangular or triangular) network, the topology of which (and consequently the ordering of the nodes in the network) is fixed for most (if not all) of the time during the computation. Indeed, it is this constancy of ordering which makes the r-adaptive procedure very attractive for finite element and related computations.

To derive a moving mesh, the computational domain with its associated mesh is then mapped to a *physical domain* $\Omega_P \in \mathbb{R}^n$, in which the underlying PDE is posed. We assume that there is an invertible, *adaptive mesh generating* function

$$\mathbf{F} : \Omega_C \to \Omega_P$$

describing this map, so that $\mathbf{F}$ is *smooth* on the interior of Ω_C and continuous on Ω_C. Throughout this article we will denote variables in Ω_C by Greek letters, *e.g.*, $\boldsymbol{\xi}$, and in Ω_P by Roman letters, $\mathbf{x}$, and consider the function $\mathbf{F}(\boldsymbol{\xi}, t)$ to be *time-dependent*. The action of the function $\mathbf{F}$ on the fixed mesh τ_C generates a *moving mesh* τ_P in the physical domain. An example of such a mesh is given in Figure 2.1, in which a uniform rectangular mesh in Ω_C is mapped to a mesh τ_P. (This map was constructed by using the optimal transport method described in Section 3.)

In the case where τ_C is a uniform rectangular mesh, the resulting mesh τ_P in the *physical space* is then (in the representative example of a two-dimensional system) given by the points $(X_{i,j}, Y_{i,j})$, where $\mathbf{F} = (x, y)$ and

$$X_{i,j} = x\left(\frac{i}{N}, \frac{j}{N}\right), \quad Y_{i,j} = y\left(\frac{i}{N}, \frac{j}{N}\right). \tag{2.1}$$

We assume further that the boundary of $\partial\Omega_C$ of Ω_C is mapped by $\mathbf{F}$ to the boundary of $\partial\Omega_P$ of Ω_P. In some r-adaptive strategies (such as the multi-equidistribution and/or variational strategies described in Huang and

https://doi.org/10.1017/S0962492906400015 Published online by Cambridge University Press

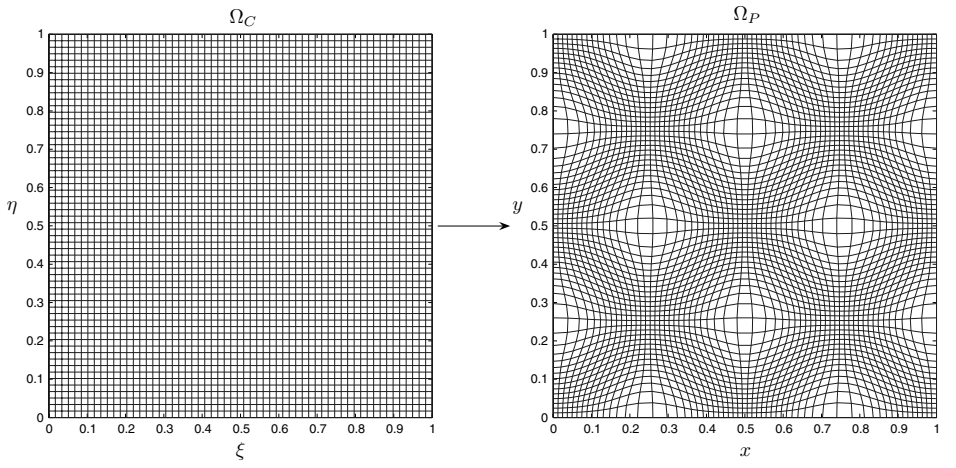


Figure 2.1. A typical map $(x(\xi,\eta), y(\xi,\eta))$ from a computational domain Ω_C to a physical domain Ω_P.

Russell (1999), the map $\mathbf{F}$ is augmented with a second map,

$$\partial F : \partial\Omega_C \to \Omega_P,$$

which explicitly describes the map from one boundary to another. This has the advantage of close control of the meshing strategy right up to the boundary, but has the disadvantage of introducing extra complexity into the system. In other algorithms, such as the optimal mapping strategy (Delzanno, Chacón, Finn, Chung and Lapenta 2008, Budd and Williams 2006), the boundary map is obtained automatically as part of the algorithm. This is an attractive feature from the perspective of algorithmic complexity, although it does lead to a reduction of control of the boundary points.

The great merit of this approach is that it transforms the problem of finding (and describing) a mesh in Ω_P (which in the case of h-adaptive methods can require subtle data structures, including hierarchical trees) into the much simpler problem of describing the function $\mathbf{F}$. Much of this article is devoted to deriving suitable equations for $\mathbf{F}$ and seeking effective solution strategies for them. It goes without saying that it should not be more difficult to find $\mathbf{F}$ than to solve the underlying PDE, and indeed that many such functions $\mathbf{F}$ may give appropriate meshes on which to solve the PDE. The properties of the mesh τ_P then follow immediately from the structure of the map $\mathbf{F}$. This simple observation is a key to the success of r-adaptive methods, as it allows the use of powerful mathematical tools to describe, construct and control the mesh behaviour. These include the application of methods from differential geometry (especially the theory of optimal transport) to describe the static structure of τ_P, and methods

https://doi.org/10.1017/S0962492906400015 Published online by Cambridge University Press

from the theory of dynamical systems to describe its evolution. The latter is especially appropriate when coupled to the partial differential equations which are often solved to find $\mathbf{F}$. The unity that r-adaptive meshes give for both solving the underlying PDE, and finding the mesh, is a significant advantage of r-adaptivity over other adaptive approaches.

2.2. Static mesh properties: skewness, regularity and smoothness

We consider first some immediate properties of the mesh τ_P which are related to the function $\mathbf{F}$. Broadly speaking these divide into *local* and *global* properties. The *global* properties relate to the isotropy of the mesh, orthogonality issues and the behaviour close to boundaries. We discuss these presently.

The *local* properties relate to the size and shape of the elements of τ_P. If τ_C is divided into logical regular rectangular or triangular elements τ_C^e, then these are mapped to elements τ_P^e in τ_P. These elements will then be distorted rectangles/triangles, possibly with small angles at the vertices. Locally we can characterize each such element by the size h_e of the largest side and (in two dimensions) the radius ρ_e of the largest inscribed circle. If a partial differential equation is discretized over τ_P using (say) a finite element method in two dimensions, then the error in the solution has contributions from the size and the shape of the elements, as well as from the derivatives of the solution itself. For example, if the solution u is interpolated over τ_p^e by a piecewise linear interpolant $\Pi(u)$, then the following *a priori* error estimates are standard (Johnson 1987):

$$\begin{aligned} \max_{\tau_p^e} |\Pi(u) - u| &\leq 2h_e^2 \max \left| \frac{\partial^2 u}{\partial x_i \partial x_j} \right|, \\ \max_{\tau_p^e} \left| \frac{\partial}{\partial x_i} \big(\Pi(u) - u\big) \right| &\leq 6 \frac{h_e^2}{\rho_e} \max \left| \frac{\partial^2 u}{\partial x_i \partial x_j} \right|. \end{aligned} \tag{2.2}$$

An adapted mesh will usually aim to control the size and the shape of each element so that, for any particular solution u, the overall error is controlled. Thus, for example, if the second derivatives of u are large over τ_p^e, then the error (2.2) can be controlled locally by taking h_e to be small, and ensuring that h_e/ρ_e remains bounded. We discuss these issues in detail later in this section. (See Cao (2005, 2007*a*) and Chen, Sun and Xu (2007) for a very complete analysis of this problem.)

Both the size and the shape of the mesh elements can be described in terms of the local properties of F, and in particular its Jacobian J, given by

$$J = \frac{\partial F}{\partial \xi}. \tag{2.3}$$

The following is immediate.

https://doi.org/10.1017/S0962492906400015 Published online by Cambridge University Press

Condition 2.1. For the map to be locally well-posed we require that J should be both bounded and invertible at all points in Ω_C.

2.2.1. Mesh scaling

The local scaling factor $1/\rho$ of the transformation (also called the *adaptation factor*) is given by

$$\Lambda \equiv 1/\rho = \det(J) \equiv |J|.$$

Assuming that J has a full set of singular values $\lambda_1, \ldots, \lambda_n$, the local stretching is given by the determinant

$$\Lambda = |\lambda_1||\lambda_2| \cdots |\lambda_n|. \tag{2.4}$$

The adaptation factor controls the (possibly higher-dimensional) *area* $|\tau_P^e|$ of the element τ_P^e so that

$$\rho|\tau_C^e| = |\tau_P^e|. \tag{2.5}$$

The area $|\tau_p^e|$ implicitly enters into the expression (2.2). Indeed, in so-called *shape-regular* two-dimensional meshes there exist constants α and β such that, for all elements $\tau_p^e \in \tau_p$, we have

$$\alpha|\tau_p^e| \leq h_e^2 \leq \beta|\tau_p^e|.$$

Accordingly, many moving mesh methods (such as those based on equidistribution or variational methods) aim to control the adaptation factor. Scale-invariant methods relate the adaptation factor to local length scales of the underlying PDE. It is easily possible for the adaptation factor to vary over *many orders of magnitude*, particularly when the adaptive method is being used to compute singular structures in the underlying PDE in which the solution u and/or its derivatives vary over similar orders of magnitude.

2.2.2. Mesh skewness

In the case of one-dimensional meshes, control of the adaptation factor for each element completely describes the mesh. In higher dimensions many more mesh properties are important, such as the local rotation or the skewness of the mesh. A special class of *irrotational* meshes control the local element rotation by requiring that J is symmetric, so that

$$J^T = J,$$

or equivalently that

$$\boldsymbol{\nabla}_{\boldsymbol{\xi}} \times \mathbf{F} = \mathbf{0}.$$

This is by no means true of all such mappings, but it can be shown (Delzanno *et al.* 2008, Brenier 1991) that meshes in an averaged sense closest to uniform meshes have this property.

The shape of the element τ_P^e, in particular the existence of any small

https://doi.org/10.1017/S0962492906400015 Published online by Cambridge University Press

angles, is also important in the error estimate (2.2). A measure of this is the local *mesh skewness*. A measure for the *local skewness* s of the mesh is then given by

$$s = \frac{\max|\lambda_i|}{\min|\lambda_j|}. \tag{2.6}$$

Other measures of mesh skewness are also referred to as shape or quality measures. Liu and Joe (1994) investigate several shape measures for tetrahedra and show that they are equivalent to each other. Denote the four vertices of a tetrahedron τ_P^e by $a_0, \ldots, a_3$, and define the so-called edge matrix as $E = [a_1 - a_0, a_2 - a_0, a_3 - a_0]$. Let $\hat{e}$ be a regular tetrahedron having the same volume as τ_P^e. Denote the corresponding vertices and the edge matrix of $\hat{e}$ by $\hat{a}_0, \ldots, \hat{a}_3$ and $\hat{E}$, respectively. Then one of the shape measures for τ_P^e is defined by

$$\eta(\tau_P^e) = \frac{3\big[\det((E\hat{E}^{-1})^T(E\hat{E}^{-1}))\big]^{\frac{1}{3}}}{\operatorname{trace}((E\hat{E}^{-1})^T(E\hat{E}^{-1}))}.$$

Notice that the $\eta(\tau_P^e)$ ranges from 0 to 1, with $\eta(\tau_P^e) = 1$ for a regular tetrahedron and $\eta(\tau_P^e) = 0$ for a flat tetrahedron. A geometric quality measure is introduced by Huang (2005*a*) for measuring the shape of a simplicial element in any dimension. Let τ_P^e be a simplicial element in n dimensions and let $\hat{K}$ be an n-simplex with unit edge length. There exists a unique invertible affine mapping

$$F_e : \hat{K} \to \tau_P^e, \quad \tau_P^e = F_e(\hat{K}).$$

Denote the Jacobian matrix of F_e by F_e'. Then the geometric measure is defined by

$$Q_{\text{geo}}(\tau_P^e) = \frac{\operatorname{trace}((F_e')^T F_e')}{d[\det((F_e')^T F_e')]^{\frac{1}{d}}}.$$

Notice that $Q_{\text{geo}}(\tau_P^e)$ ranges from 1 to ∞, with $Q_{\text{geo}}(\tau_P^e) = 1$ for a regular n-simplex and $Q_{\text{geo}}(\tau_P^e) = \infty$ for a flat d-simplex. Interestingly, for tetrahedra these two shape measures have the relation $Q_{\text{geo}}(\tau_P^e) = 1/\eta(\tau_P^e)$. To see this, we first notice that $\hat{K}$ and $\hat{e}$ are similar. Thus, the mapping $G_e : \hat{e} \to \tau_P^e$ is related to F_e by

$$G_e = cF_e, \quad G_e' = cF_e'$$

for some positive constant c. Then the edge matrices E and $\hat{E}$ are related by

$$E = G_e'\hat{E} = cF_e'\hat{E}.$$

Using this relation we can rewrite $\eta(\tau_P^e)$ as

$$\eta(\tau_P^e) = \frac{3\big[\det((F_e')^T F_e')\big]^{\frac{1}{3}}}{\operatorname{trace}((F_e')^T F_e')} = \frac{1}{Q_{\text{geo}}(\tau_P^e)}.$$

https://doi.org/10.1017/S0962492906400015 Published online by Cambridge University Press

It is shown by Huang (2005*a*) that measures s defined in (2.6) and Q_{geo} are mathematically equivalent.

Some other quality measures can be found in Liseikin (1999, Chapter 3), Knupp (2001) and Shewchuk (2002). Again, a good adaptive method aims to control some or all of these measures of skewness, either explicitly or implicitly throughout the calculation, and we discuss this later in this section. In the case of scale-invariant meshes we shall show that, whilst the adaptation factor changes a great deal, *the skewness hardly varies.* More generally, it should be noted that whereas the adaptation factor often changes a great deal in a mesh, the skewness generally does not. To control terms in the error expression (2.2) arising from large solution gradients, it is generally more important to vary the adaptation factor. If this results in a locally larger value of the skewness then this can usually be tolerated.

2.2.3. Mesh smoothness and regularity

The smoothness or regularity of a mesh is a measure of how much the mesh elements vary over the mesh. This can be important since the accuracy and error in the numerical solution of partial differential equations generally depend upon the type of discretization, the quality of the mesh, the treatment of boundary conditions, and so on. A uniform mesh has the highest degree of regularity, which can lead to particularly low error estimates on such meshes. It is sometimes claimed that only uniform meshes have such low estimates, but in fact, as we shall see, they share this with sufficiently regular meshes. Although there is generally no simple relationship between the smoothness of the mesh and the error (see Veldman and Rinzema (1992)), for most problems and most discretization methods, abrupt variations in the mesh will cause a deterioration in the convergence rate and an increase in the error (Thompson *et al.* 1985), or indeed in the accuracy of the approximation of a function over the mesh. Moreover, most discrete approximations of spatial differential operators have much larger condition numbers on an abruptly varying mesh than they do on a gradually varying one, and these ill-conditioned approximations may result in stiffness in the time integration for time-dependent problems.

The smoothness of a mesh can be expressed in terms of the regularity of the underlying mesh function $\mathbf{F}$.

Definition. A mesh τ_P has degree of regularity r if $\mathbf{F} \in C^r(\Omega_C)$.

The regularity of $\mathbf{F}$ can often be achieved by determining $\mathbf{F}$ as a solution of a PDE system or a minimizer of a functional as in variational mesh generation methods. In many cases it is possible to have strong control over the derivatives of $\mathbf{F}$ allowing guaranteed regularity of the mesh τ_P. It should be noted that an obvious way to determine a mesh is to prescribe the Jacobian function J exactly (Brackbill and Saltzman 1982). However,

https://doi.org/10.1017/S0962492906400015 Published online by Cambridge University Press

it is in general very hard to do this, and instead some property of J (such as its determinant) is prescribed, and this is then used to determine the mesh.

A mesh can also be made smoother by some direct methods. For example, (weighted) Laplace smoothing is often used in *hp* adaptation (see Carey (1997)). In this strategy, the coordinates of an interior mesh point are adjusted so that they become the (weighted) average of the coordinates of its neighbouring points. Typically this is carried out in a Jacobian or Gauss–Seidel fashion. When this is the case, Laplace smoothing can be viewed as the application of the Jacobian or Gauss–Seidel iteration to the solution of a discretization of the partial differential equation

$$-\Delta_{\boldsymbol{\xi}}(\hat{x},\hat{y}) = (x,y), \tag{2.7}$$

where $\Delta_{\boldsymbol{\xi}}$ is the Laplacian operator applied in the computational domain. In r-adaptive methods based on equidistribution, on the other hand, a smoother mesh is often obtained indirectly by smoothing the monitor function M used for controlling mesh adaptation and movement. We will describe this strategy presently.

When calculating solutions to a (partial) differential equation on a non-uniform mesh it is essential that there is a strong control on the mesh variation. For one-dimensional meshes for which we have a mesh function $x(\xi)$, mesh points $X_i = x(i\Delta\xi)$ and local mesh spacing given by $\Delta_i = X_{i+1} - X_i$ then the *grid size ratio* or *local stretching factor* r is given by

$$r = \frac{\Delta_i}{\Delta_{i-1}}. \tag{2.8}$$

In a uniform mesh we have that $r = 1$. For many calculations on a non-uniform mesh, we require instead that

$$r = 1 + \mathcal{O}(\Delta_i). \tag{2.9}$$

Such grids are termed *quasi-uniform* (Li *et al.* 1998, Zegeling 2007, Kautsky and Nichols 1980, Kautsky and Nichols 1982), and normally lead to truncation (and approximation) errors of the same order as uniform meshes (Veldman and Rinzema 1992). We note that

$$r = 1 + \frac{\Delta_i - \Delta_{i-1}}{\Delta_i} = 1 + \frac{X_{i+1} - 2X_i + X_{i-1}}{X_i - X_{i-1}}.$$

Consequently, as $\Delta_i \approx \Delta\xi x_\xi$, *etc.*, we have

$$r = 1 + \Delta_i \frac{x_{\xi\xi}}{x_\xi^2} + \mathcal{O}(\Delta_i^2).$$

Thus the mesh is quasi-uniform provided that

$$\Lambda \equiv \frac{x_{\xi\xi}}{x_\xi^2} = \mathcal{O}(1). \tag{2.10}$$

https://doi.org/10.1017/S0962492906400015 Published online by Cambridge University Press

The condition (2.10) plays an important role in our subsequent analysis of the errors of computations on both static and moving non-uniform meshes. The ratio between lengths of adjacent elements is also used in Dorfi and Drury (1987) and studied by Verwer, Blom, Furzeland and Zegeling (1989).

The concept of quasi-uniformity has natural extensions to higher dimensions augmented with small angle conditions. For example, in two dimensions, if we have a triangulation τ_P then this is *shape-regular*, ensuring control over small angles, if, for each element $\tau_e \in \tau_p$ with area $|\tau_e|$, longest side of length h_e and interior circle of diameter ρ_e, we have a constant σ_1 such that

$$\max_{\tau_e} \frac{h_e}{\rho_e} \leq \sigma_1. \tag{2.11}$$

Such a shape-regular mesh is then *quasi-uniform* if there is a second constant σ_2 for which

$$\frac{\max_{\tau_e \in \tau_p} |\tau_e|}{\min_{\tau_e \in \tau_P} |\tau_e|} \leq \sigma_2. \tag{2.12}$$

As in the one-dimensional case, quasi-uniform meshes have similar error estimates to uniform ones (Johnson 1987). However, it is often much harder to achieve this for time-dependent problems.

2.3. Mesh calculation, mesh tangling and mesh racing

The function $\mathbf{F}$ must be determined as part of the process of calculating τ_P. This map can be calculated either explicitly or implicitly. In the explicit method, an equation is derived for $\mathbf{F}$ which is expressed in terms of the *position* of the mesh points. This (usually large and nonlinear) system is then solved to find $\mathbf{F}$ and hence to determine the location of the mesh. This procedure lies at the heart of a number of equidistribution *position-based* methods for calculating the mesh, such as the moving mesh partial differential equation, optimal transport and variational methods.Typically such methods *cluster* the mesh points where high precision is required, and the location of points of *density* of the mesh points moves as the solution evolves (in a similar manner to a longitudinal wave passing down the length of a spring, whilst the coils of the spring do not move very far from their equilibrium positions).

In an alternative procedure, the *velocity* $\mathbf{v}$ of the mesh points in τ_P is determined. This is given by

$$\mathbf{v} = \mathbf{F}_t. \tag{2.13}$$

The mesh point positions are updated using this velocity. This approach is very closely linked with particle and Lagrangian methods and includes methods such as GCL, MFE and the deformation map method. (Using the analogy above, such methods are like moving the whole spring.)

https://doi.org/10.1017/S0962492906400015 Published online by Cambridge University Press

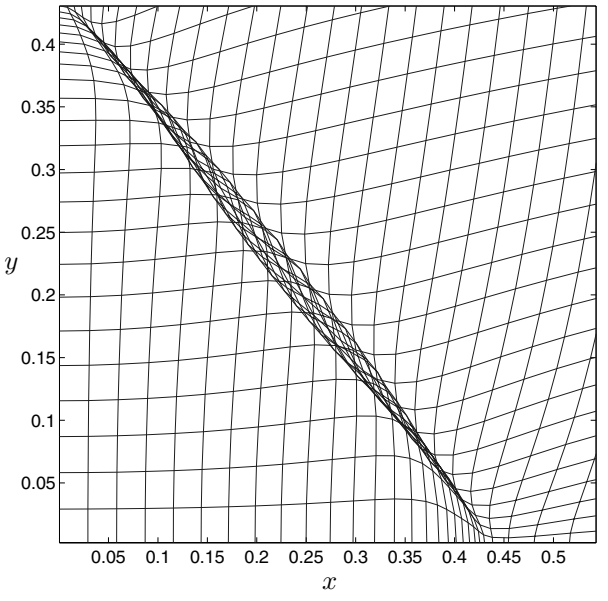


Figure 2.2. An example of a mesh which has tangled whilst attempting to resolve a front.

In general, position-based methods tend to produce smoother meshes, and are much less prone to the problem of *mesh tangling* than velocity-based methods. Mesh tangling occurs when the lines connecting adjacent mesh points intersect. An example of this is given in Figure 2.2, in which we see an attempted calculation of a solution front for Burgers' equation which has led to a tangled mesh through the use of an inappropriately large time step in evolving the mesh.

Mesh tangling can occur either locally or globally and can often arise in Lagrangian-type methods computing solutions with high vorticity. It is associated with a local loss of inevitability of the map $\mathbf{F}$ or, equivalently, at a point for which $\Lambda = \det(J) = 0$. If Λ is controlled throughout the evolution of the mesh, then mesh tangling can be avoided. Position-based methods usually try to do this (see the calculations using the optimal transport and MMPDE methods), hence their robustness to mesh tangling. Of course, control of Λ for all time is impossible, as any equations describing the time evolution of $\mathbf{F}$ will inevitably be discretized in time. If this discretization is too coarse then mesh tangling may result.

Mesh racing is related to mesh tangling and occurs if $\mathbf{v}$ is too large relative to the evolutionary behaviour of the underlying system being solved (so that the mesh evolves more rapidly than the solution of the underlying PDE). Mesh racing can occur for a variety of reasons, such as an inappropriate

https://doi.org/10.1017/S0962492906400015 Published online by Cambridge University Press

choice of adaptivity strategy, gross mesh distortion or problems when the moving mesh interacts with a fixed boundary. In a purely *Lagrangian* setting a moving mesh used to calculate (for example) a fluid flow might seek to have $\mathbf{v}$ equal to the local velocity of the fluid particles. In practice, as we will demonstrate, such a procedure can lead to mesh tangling in the presence of flows with high vorticity, and mesh racing when the fluid particles leave the boundary and the mesh labelling has to be reassigned. In practice (and in a manner to be made precise presently) it is often optimal for the mesh points to move in a similar manner to the particles, but not to follow their motions too precisely.

The connectivity of a mesh reflects how adjacent nodes are connected together. In an h-adaptive mesh connectivity can be a significant issue, and changes every time a local mesh refinement step is implemented. This causes additional overheads in setting up the equations of any discretization on this mesh, as the connectivity matrix needs to be constantly updated. In contrast, in an r-adaptive method, the connectivity of the moving mesh is usually determined by the connectivity of the underlying computational mesh, which usually does not change during the calculation, and we can presume to be relatively simple. A significant benefit of this approach is that various mesh-smoothing methods can use this constant connectivity and can (for example) exploit fast spectral methods which take advantage of the constant mesh connectivity in the computational domain. As an example, if the functions $(x(\xi,\eta), y(\xi,\eta))$ determine a particular mesh, then it is possible to construct a smoother mesh from this. One example is given by

$$(\hat{x},\hat{y}) = \left(I - \gamma\Delta_\xi\right)^{-1}(x,y), \tag{2.14}$$

where Δ_ξ is the Laplacian operator applied in the *computational domain* and γ is chosen appropriately. An important reason for constructing a smoother mesh is to avoid significant variation in mesh size between adjacent elements. We presently consider the effect of this on the solution error. This procedure was introduced by Huang and Russell (1997*a*). The Laplacian operator can be inverted very rapidly on a simply connected uniform rectangular mesh by using a fast spectral method, for example the fast cosine transform. This smoothing procedure also damps out the creation of certain chess board modes that can lead to a deterioration of the mesh quality.

2.4. Mesh topology

The discussion so far has been restricted to the use of moving meshes mapping one convex region, indeed logically rectangular regions, to logically rectangular regions. There is no real problem mapping a logically rectangular region Ω_C to another convex region. For example, the article by Calhoun *et al.* (2008) describes in detail how a logically rectangular mesh

https://doi.org/10.1017/S0962492906400015 Published online by Cambridge University Press

can be mapped to both circular and spherical domains. This is especially useful for calculations in meteorology involving whole Earth models. However, moving mesh methods are not ideal for mappings to and from non-convex regions, due to the inherent singularities associated with re-entrant corners. See Dvinsky (1991) for a brief discussion of this point. The issue of refining a mesh close to such a corner where the geometry of the solution and the associated singularity is (of course) known *a priori* has been extensively covered in the literature of h-adaptive methods: see, for example, Ainsworth and Oden (2000), Johnson (1987) and many other texts. This approach can be very naturally coupled with a moving mesh approach by using an h-adaptive method to construct a mesh in the *computational domain*, which is refined close to the re-entrant corner. This mesh can then be mapped, in a similar manner to that described earlier, to a moving mesh in the *physical domain*. We will not pursue this further here as this article is largely concerned with the construction of meshes adapted to the evolving structures of time-dependent PDEs.

2.5. Equidistribution and monitor functions

Having considered the general aspects of the mesh geometry and the mesh function $\mathbf{F}$, we now consider the issues associated with calculating appropriate functions $\mathbf{F}$ to give meshes with certain properties. There are several general approaches to this, and we consider two closely related methods: equidistribution-based and variational-based. Both methods generate meshes determined by suitable *monitor functions*, which are typically determined both by properties of the solution of the underlying partial differential equation and by other considerations of the mesh regularity.

2.5.1. Equidistribution

At the heart of many r-adaptive methods is the concept of *equidistribution*, introduced as a computational device by de Boor (1973). Equidistribution is a widely used means of prescribing the *optimum geometry* of the mesh, but many different strategies have been devised to move the mesh towards this optimum state, leading to a variety of moving mesh methods. In a certain sense, all meshes equidistribute some function, and to motivate equidistribution we consider the fundamental Radon–Nikodym theorem from measure theory. To do this we consider an invertible mesh mapping function F which maps an arbitrary set A in Ω_C to an image set $B = F(A)$ in Ω_P. We can induce a measure $\nu(B)$ on Ω_P by $\nu(B) = |A|$, where $|A|$ is the usual Lebesgue measure on Ω_C. We then have the following.

Theorem 2.2. (Radon–Nikodym) If ν is a well-defined Borel measure on Ω_P, then there is a non-negative measurable function $M : \Omega_P \to \mathbb{R}$ such

https://doi.org/10.1017/S0962492906400015 Published online by Cambridge University Press

that

$$\nu(B) = \int_B M(\mathbf{x})\ \mathrm{d}\mathbf{x},$$

for any Borel subset B of Ω_P, where $\mathrm{d}\mathbf{x}$ is the usual Lebesgue measure on Ω_P. Furthermore M is unique up to sets of Lebesgue measure zero.

Proof. See Capiński and Kopp (2004). □

The Radon–Nikodym theorem shows that for any invertible map $\mathbf{F}$ we can find a unique function $M(\mathbf{x})$ such that, for any set $A \subset \Omega_C$, we have

$$\int_A \mathrm{d}\mathbf{x} = \int_{\mathbf{F}(A)} M(\mathbf{x})\,\mathrm{d}\mathbf{x}. \tag{2.15}$$

Note, however, that (other than the special case of one dimension) the same function M may be associated with many different maps.

The function $M(\mathbf{x}) > 0$ is a function of $\mathbf{x}$ and t, but is more usually defined in terms of the solution $u(\mathbf{x}, t)$ of the underlying PDE, so that we might have

$$M(\mathbf{x}, t) \equiv M(\mathbf{x}, u(\mathbf{x}, t), \boldsymbol{\nabla} u(\mathbf{x}, t), \ldots, t).$$

In this context M is usually called a *scalar monitor function*, and is chosen to be large when the mesh points need to be clustered, for example if the solution of the underlying problem has a high gradient. In this case the Lebesgue measure of the set B may be small even if the measure $\nu(B)$ is not. This may occur, for example, in the neighbourhood of a solution singularity or a sharp front. An obvious example of a monitor function is some estimate of the truncation error in the calculation of the solution of the underlying PDE, and this was the original motivation of the equidistribution approach of de Boor (1973). Loosely speaking, equidistributing the error in calculating the solution of a PDE over all mesh elements is a necessary condition for finding a global minimum of that error (Johnson 1987)

Assume now that we know the scalar function M and consider how we might determine an appropriate map $\mathbf{F}$. To do this we introduce an arbitrary non-empty set $A \subset \Omega_C$ in the computational domain, with a corresponding image set $\mathbf{F}(A, t) \subset \Omega_P$. The map $\mathbf{F}$ *equidistributes the respective scalar monitor function* M if the Stieltjes measures of A and $\mathbf{F}(A, t)$, normalized over the measure of their respective domains, are the same. This implies that

$$\frac{\int_A \mathrm{d}\boldsymbol{\xi}}{\int_{\Omega_C} \mathrm{d}\boldsymbol{\xi}} = \frac{\int_{\mathbf{F}(A,t)} M(\mathbf{x}, t)\,\mathrm{d}\mathbf{x}}{\int_{\Omega_P} M(\mathbf{x}, t)\,\mathrm{d}\mathbf{x}}. \tag{2.16}$$

https://doi.org/10.1017/S0962492906400015 Published online by Cambridge University Press

It follows from a change of variable that

$$\frac{\int_A \mathrm{d}\boldsymbol{\xi}}{\int_{\Omega_C} \mathrm{d}\boldsymbol{\xi}} = \frac{\int_A M(\mathbf{x}(\boldsymbol{\xi},t),t)|J(\boldsymbol{\xi},t)|\,\mathrm{d}\boldsymbol{\xi}}{\int_{\Omega_P} M(\mathbf{x}(\boldsymbol{\xi},t),t)\,\mathrm{d}\mathbf{x}}. \tag{2.17}$$

As the set A is arbitrary, the map $\mathbf{F}(\boldsymbol{\xi},t)$ must (for all $(\boldsymbol{\xi},t)$) obey the identity

$$M(\mathbf{x}(\boldsymbol{\xi},t),t)|J(\boldsymbol{\xi},t)| = \theta(t), \quad \text{where } \theta(t) = \frac{\int_{\Omega_P} M(\mathbf{X}(\boldsymbol{\xi},t),t)\,\mathrm{d}\mathbf{x}}{\int_{\Omega_C} \mathrm{d}\boldsymbol{\xi}}. \tag{2.18}$$

We shall refer to (2.18) as the *equidistribution equation*. This equation must always be satisfied by the map $\mathbf{F}(\boldsymbol{\xi},t)$. It is the central equation of much of mesh generation, and we shall show presently that it is strongly connected to a variational representation of the mesh transformation.

2.5.2. Choice of a scalar monitor function

The choice of a scalar monitor function M appropriate to the accurate solution of a PDE is difficult, problem-dependent, and the subject of much research. We do not consider this in detail here but give a brief review of various choices used for certain problem classes. The function M can be determined by *a priori* considerations of the geometry or of the physics of the solution. An example is the generalized solution arclength given by

$$M = \sqrt{1 + c^2|\boldsymbol{\nabla}_{\mathbf{x}} u(x)|^2}, \quad \text{or alternatively } \ M = \sqrt{1 + c^2|\boldsymbol{\nabla}_{\boldsymbol{\xi}} u(x(\xi))|^2}. \tag{2.19}$$

The first of these is often used to construct meshes which can follow moving fronts with locally high gradients (Winslow 1967, Huang 2007). A careful analysis of the application of arclength-based monitor functions to the resolution of the solution of singularly perturbed PDEs is given in Kopteva and Stynes (2001). Ceniceros and Hou (2001) successfully used the second monitor function (with u being the temperature) to resolve small scale singular structures in Boussinesq convection. It is also common to use monitor functions based on the (potential) vorticity, or curvature, of the solution (Beckett and Mackenzie 2000), and these have been used in computations of weather front formation (Budd and Piggott 2005, Budd, Piggott and Williams 2009, Walsh, Budd and Williams 2009). In certain problems, moving fronts are associated with changes in the physics of the solution. An example is problems with phase changes, where the phase front occurs at those points $(x_m)_i$ at a temperature $T = T_m$. In such cases it is possible to construct meshes which resolve behaviour close to the phase boundary by using the monitor function $M = a/\sqrt{b|x - x_m| + c}$, where $|x - x_m| = \min|x - (x_m)_i|$ (Mackenzie and Mekwi 2007*a*). Alternatively, M can be linked to estimates of the solution error. A significant calculation in

https://doi.org/10.1017/S0962492906400015 Published online by Cambridge University Press

which M was determined in terms of *a priori* error estimates (typically proportional to the higher derivatives of the solution or estimates of these) was given in Dorfi and Drury (1987), and is discussed in more detail presently. More recently, monitor functions determined by *a posteriori* error estimates have been constructed. An example of these, in the context of a piecewise linear finite element approximation u_h to a function u, is $M = \sqrt{1+\alpha\zeta^2}$, where

$$|u-u_h|^2_{1,\Omega_P} \sim \zeta^2(u_h) \equiv \sum_{\text{l: interior edge}} \int_l [\boldsymbol{\nabla} u_h.n_l]^2_l \,\mathrm{d}l \tag{2.20}$$

and $[.]_l$ is the jump in the computed solution along the element edges. This monitor function is used by Tang (2005) to compute solutions adaptively to the Navier–Stokes equations with thin shear layers and/or high Mach numbers. Similarly, in a series of papers studying both isotropic and anisotropic meshes (Huang 2001*a*, 2001*b*, 2005*a*, 2005*b*, 2007), Huang explicitly considers monitor functions which are designed to control the regularity, alignment and quality of the mesh. These include monitor functions which are based as estimates of the interpolation error of the computed solution, and we consider them presently. Other measures of mesh quality can be incorporated into the monitor function including maximum and minimum angle conditions (Zlamal 1968, Babuška and Rheinboldt 1979), conditions on aspect ratio and quantities that combine both shape and solution behaviour (Berzins 1998). Finally, it is sometimes possible in the case of PDEs with *strong scaling structures* (such as problems related to combustion and gas dynamics) to find suitable monitor functions which give meshes reflecting the natural scales of the problem (Budd and Williams 2006). We give an example of these in Section 5, looking at a PDE which has solutions which blow up in a finite time. In this case we need a fine mesh when the solution is large, and take $M(u) = \sqrt{a^2+b^2u^{2p}},\ p>0$.

We note at this stage that most choices of monitor function need a degree of smoothing and regularization to perform effectively, and we will consider this presently.

2.5.3. Matrix-valued monitor functions

The monitor function defined above is a scalar measure and is effective in the specification and generation of certain isotropic meshes. However, much greater freedom in mesh calculation may be required when calculating anisotropic meshes, and in this case a *matrix-valued monitor function* $\mathbf{M}$ can be used. In this case the meshes are defined via the metric determined by an $n \times n$ matrix-valued monitor function that specifies the shape, size and orientation of the elements throughout the physical domain Ω_P. Huang (2007) defines a matrix-valued monitor function $\mathbf{M}(\mathbf{x})$ using the

https://doi.org/10.1017/S0962492906400015 Published online by Cambridge University Press

identity

$$J^{-T}J^{-1} = \left(\frac{\int_{\Omega_P}\sqrt{\det(\mathbf{M})}\,\mathrm{d}\mathbf{y}}{|\Omega_C|}\right)^{-\frac{2}{n}}\mathbf{M}(\mathbf{x}), \tag{2.21}$$

which is closely linked to the equidistribution principle for the scalar function. Indeed, the mesh satisfies an *equidistribution equation*

$$|J|\sqrt{\det(\mathbf{M})} = \frac{\int_{\Omega_p}\sqrt{\det(\mathbf{M})}\,\mathrm{d}\mathbf{y}}{|\Omega_C|}. \tag{2.22}$$

It also follows an *alignment condition*

$$\frac{1}{n}\mathrm{trace}(J^{-1}\mathbf{M}^{-1}J^{-T}) = \det(J^{-1}\mathbf{M}^{-1}J^{-T})^{\frac{1}{n}}. \tag{2.23}$$

A matrix monitor function $\mathbf{M}$, together with a proper boundary correspondence, then specifies a mesh via the conditions (2.22) and (2.23). Presently we relate these conditions of alignment and equidistribution to mesh quality and interpolation error, and show how to construct monitor functions that give explicit control over mesh quality.

2.6. Moving mesh PDEs, variational principles and harmonic maps

2.6.1. Moving the mesh to an equidistributed state

The equidistribution equation must be solved to find a mesh which equidistributes the monitor function M, and this equation must be augmented with additional conditions to obtain a unique map $\mathbf{F}$. Indeed, the equidistribution principle has different consequences in one dimension from higher dimensions. In one dimension it (together with boundary conditions) uniquely defines the map $\mathbf{F}(\boldsymbol{\xi}, t)$. In this case the strategies for moving the mesh are all similar (or indeed trivially equivalent), and rely on either exactly solving the equidistribution equation (2.18), or relaxing towards a solution of some differentiated form of (2.18).

An important set of examples of the relaxation methods, which we will consider in detail (both in one and higher dimensions) in Section 3, are the variety of *moving mesh PDE* (MMPDE) methods. An example is MMPDE6, given by

$$-\epsilon x_{\xi\xi} = (Mx_\xi)_\xi. \tag{2.24}$$

Here $0 < \epsilon \ll 1$ is a *relaxation time* over which the mesh evolves to the equidistributed state.

However, uniqueness of the solution of the equidistribution equation is lost in higher dimensions. Informally, this is because there is a unique interval (up to translation) of prescribed length in one dimension, but there is an uncountable number of sets of prescribed area in higher dimensions. Thus the equidistribution principle needs to be augmented with some additional

https://doi.org/10.1017/S0962492906400015 Published online by Cambridge University Press

conditions if it is to be applied in dimension $n > 1$. The determination of these additional conditions is neither straightforward nor unique, and leads to a variety of different methods for mesh generation, for which control of mesh skewness and other geometric properties must also be considered. Two examples of the additional conditions might be to impose an irrationality condition in the computational domain so that $\nabla_{\boldsymbol{\xi}} \times \mathbf{F} = 0$ (Budd and Williams 2006) – which is the basis of the optimal transport methods – or to require that the mesh velocity is irrotational in the physical domain so that $\nabla_{\mathbf{x}} \times \mathbf{v} = 0$ (Cao *et al.* 2002) – which is the basis of the GCL methods. The augmented equations can then be solved in a number of ways to find the mesh: by directly solving the nonlinear system, which can be expensive; by differentiating the condition and solving the resulting differential equations which leads to the GCL methods we will consider in Section 4; by relaxing towards a solution of the system, which leads to the MMPDE methods in one and higher dimensions; or to have a global variational principle associated with the error and to find the gradient flow equations associated with it. We consider the latter now, with more details in Section 3.

2.6.2. Variational methods in one dimension and links to equidistribution
An alternative strategy for determining a mesh, also based on an appropriate monitor function, is the variational method. In such a method the stationary points determine the optimal mesh, and the associated gradient flow equations towards the stationary points determine a suitable mesh motion strategy.

Suppose that $I(\boldsymbol{\xi})$ is a certain functional and that the mesh generation strategy is equivalent to minimizing I over a certain function space. Finding the Euler–Lagrange equations then leads to a gradient flow equation to evolve the mesh towards the equilibrium state (a stationary point of I), which is given by

$$\frac{\partial \xi}{\partial t} = -\frac{\delta I}{\delta \xi}. \tag{2.25}$$

This can then lead directly to an MMPDE to move the mesh by introducing some additional local control on the mesh movement in the form

$$\frac{\partial \xi}{\partial t} = -\frac{P}{\tau}\frac{\delta I}{\delta \xi}, \tag{2.26}$$

where P is a positive differential operator and $\tau > 0$ is a parameter for adjusting the time scale of the mesh movement. In one dimension, equidistributing the scalar monitor function M is exactly equivalent to minimizing the functional

$$I(\xi) = \frac{1}{2}\int_0^1 \frac{1}{M}\left(\frac{\partial \xi}{\partial x}\right)^2 \mathrm{d}x. \tag{2.27}$$

https://doi.org/10.1017/S0962492906400015 Published online by Cambridge University Press

If the function P in (2.26) is taken to be

$$P = \left(\frac{M}{\xi_x}\right)^2,$$

then we obtain MMPDE5 (see Section 3 for an alternative derivation),

$$\frac{\partial x}{\partial t} = \frac{1}{\tau}\frac{\partial}{\partial \xi}\left(M\frac{\partial x}{\partial \xi}\right). \tag{2.28}$$

This equation can be used to evolve the one-dimensional mesh towards an equidistributed state. It also has a natural generalization to the PMA equation derived from the *optimally transported meshes* we will consider in Section 3.

2.6.3. Variational methods in higher dimensions

Motivated by (2.27) we can consider a generalization to two dimensions, which is essentially a form of *equidistribution in each coordinate direction* (Huang and Russell 1997*b*, 1999). This is given by

$$I(\xi,\eta) = \frac{1}{2}\int_{\Omega_P}\left[\boldsymbol{\nabla}\xi^T\mathbf{M}^{-1}\boldsymbol{\nabla}\xi + \boldsymbol{\nabla}\eta^T\mathbf{M}^{-1}\boldsymbol{\nabla}\eta\right]\mathrm{d}x\,\mathrm{d}y, \tag{2.29}$$

where $\mathbf{M}$ is now a symmetric positive definite matrix-valued monitor function, which is a generalization of the original scalar monitor function. The Euler–Lagrange equations which define the coordinate transformation at the steady state are then given by

$$\boldsymbol{\nabla}\cdot(\mathbf{M}^{-1}\boldsymbol{\nabla}\xi) = 0, \quad \boldsymbol{\nabla}\cdot(\mathbf{M}^{-1}\boldsymbol{\nabla}\eta) = 0, \tag{2.30}$$

where *all derivatives are expressed in terms of the physical variables* so that $\boldsymbol{\nabla} = (\partial_x, \partial_y)^T$. A moving mesh PDE can then be obtained via the gradient flow equations, given by

$$\frac{\partial \xi}{\partial t} = -\frac{P}{\tau}\frac{\delta I}{\delta \xi}, \quad \frac{\partial \eta}{\partial t} = -\frac{P}{\tau}\frac{\delta I}{\delta \eta}, \tag{2.31}$$

and we will give more details of this procedure in Section 3. A special case of this system is given by

$$\mathbf{M} = wI, \tag{2.32}$$

where w is known as the (scalar) weight function. This corresponds to one-dimensional equidistribution and in the steady state gives the equations

$$\boldsymbol{\nabla}\cdot\left(\frac{1}{w}\boldsymbol{\nabla}\xi\right) = 0, \quad \boldsymbol{\nabla}\cdot\left(\frac{1}{w}\boldsymbol{\nabla}\eta\right) = 0. \tag{2.33}$$

Finding a mesh which satisfies this is called *Winslow's variable diffusion method* (Winslow 1967, 1981).

https://doi.org/10.1017/S0962492906400015 Published online by Cambridge University Press

2.6.4. Harmonic maps

Another method closely related to (2.29) is the method based on *harmonic maps* (Dvinsky 1991). It defines the coordinate transformation used for mesh adaptation as a harmonic map minimizing the functional

$$I(\xi,\eta)=\frac{1}{2}\int_{\Omega_P}\sqrt{\det(\mathbf{M})}\left[\boldsymbol{\nabla}\xi^T\mathbf{M}^{-1}\boldsymbol{\nabla}\xi+\boldsymbol{\nabla}\eta^T\mathbf{M}^{-1}\boldsymbol{\nabla}\eta\right]\mathrm{d}x\,\mathrm{d}y, \tag{2.34}$$

where, once again, $\mathbf{M}$ is a matrix-valued monitor function. We note that in this case the matrix-valued function $\mathbf{M}$ cannot be chosen to be a scalar monitor function (see Winslow (1967)) as this would lead to no mesh adaptivity in two dimensions. Brackbill and Saltzman (1982) generalize Winslow's idea and define the needed coordinate transformation by minimizing a combination of three functionals characterizing adaptivity, smoothness, and orthogonality, respectively. Its final functional takes the form

$$\begin{aligned}I(\xi,\eta)=\theta_a\int_{\Omega_P}w|J|\,\mathrm{d}x\,\mathrm{d}y+\theta_s\int_{\Omega_P}(\boldsymbol{\nabla}\xi^T\boldsymbol{\nabla}\xi+\boldsymbol{\nabla}\eta^T\boldsymbol{\nabla}\eta)\,\mathrm{d}x\,\mathrm{d}y\\+\theta_o\int_{\Omega_P}(\boldsymbol{\nabla}\xi^T\boldsymbol{\nabla}\eta)^2\,\mathrm{d}x\,\mathrm{d}y,\end{aligned} \tag{2.35}$$

where w is the (scalar) weight function and θ_a, θ_s, and θ_o are positive parameters. Notice that the three integrals on the right-hand side have different dimensions. As a consequence, the choice of the parameters may depend on specific applications. Directional control is further considered by Brackbill (1993). Variational methods have also been developed based on mechanical models; see Jacquotte (1988), Jacquotte and Coussement (1992) and de Almeida (1999). Dvinsky (1991) also discusses the advantages and disadvantages of formulating the harmonic map method in the physical domain and in the computational domain. However, numerical results show that the method formulated in the computational domain produces crossover meshes for a non-convex physical domain, whereas the method formulated in the physical domain leads to non-singular meshes.

2.7. Mesh quality, isotropy and alignment

The methods discussed in Section 2.6 are primarily based on physical and/or geometric considerations. Although they have been applied with a degree of success to numerical solution of a variety of PDEs, it is unclear how mesh concentration is controlled precisely through the monitor function for these methods. This is important because a clear understanding of the effect of the monitor function on mesh concentration will lead to a better choice of the monitor function as well as a better design of the mesh adaptation method itself. Moreover, neither of the methods, or their choice of the monitor function, is directly connected to any sort of error analysis. (A qualitative

https://doi.org/10.1017/S0962492906400015 Published online by Cambridge University Press

analysis of the effect of the monitor function on mesh concentration is given by Cao, Huang and Russell (1999*b*) for the functional (2.29).)

A variational method based on appropriate functionals which addresses these issues has been developed based on the equidistribution and alignment conditions (2.22) and (2.23) in Huang (2001*b*), Huang and Sun (2003) and Huang (2007). Recall that, for a given matrix-valued monitor function $\mathbf{M}(\mathbf{x})$, the condition (2.22) specifies the size of elements while (2.23) determines the shape and orientation of elements. The main idea of the variational method in this context is to then generate a coordinate transformation that closely satisfies these two conditions.

2.7.1. A functional for mesh alignment

First consider the alignment condition (2.23). Let the eigenvalues of the matrix $J^{-1}\mathbf{M}^{-1}J^{-T}$ be $\lambda_1, \ldots, \lambda_n$. By the arithmetic-mean/geometric-mean inequality, the desired coordinate transformation can be obtained by minimizing the difference between the two sides of the inequality

$$\left(\prod_i \lambda_i\right)^{\frac{1}{n}} \leq \frac{1}{n}\sum_i \lambda_i.$$

Notice that

$$\sum_i \lambda_i = \operatorname{trace}(J^{-1}\mathbf{M}^{-1}J^{-T}) = \sum_i (\boldsymbol{\nabla}\xi_i)^T \mathbf{M}^{-1}\boldsymbol{\nabla}\xi_i,$$

$$\prod_i \lambda_i = \det(J^{-1}\mathbf{M}^{-1}J^{-T}) = \frac{1}{(|J|\sqrt{\det(\mathbf{M})})^2}.$$

Then we have

$$\left(\frac{1}{(|J|\sqrt{\det(\mathbf{M})})^2}\right)^{\frac{1}{n}} \leq \frac{1}{n}\sum_i (\boldsymbol{\nabla}\xi_i)^T \mathbf{M}^{-1}\boldsymbol{\nabla}\xi_i,$$

or equivalently

$$\frac{n^{\frac{n}{2}}}{|J|} \leq \sqrt{\det(\mathbf{M})}\left(\sum_i (\boldsymbol{\nabla}\xi_i)^T \mathbf{M}^{-1}\boldsymbol{\nabla}\xi_i\right)^{\frac{n}{2}}. \tag{2.36}$$

Integrating the above inequality over the physical domain yields

$$n^{\frac{n}{2}} \int_{\Omega_C} \mathrm{d}\boldsymbol{\xi} \leq \int_{\Omega_P} \sqrt{\det(\mathbf{M})}\left(\sum_i (\boldsymbol{\nabla}\xi_i)^T \mathbf{M}^{-1}\boldsymbol{\nabla}\xi_i\right)^{\frac{n}{2}} \mathrm{d}\mathbf{x}.$$

Hence, the adaptation functional associated with mesh alignment for the inverse coordinate transformation $\boldsymbol{\xi} = \boldsymbol{\xi}(\mathbf{x})$ can be defined as

$$I_{\mathrm{ali}}(\boldsymbol{\xi}) = \frac{1}{2}\int_{\Omega} \sqrt{\det(\mathbf{M})}\left(\sum_i (\boldsymbol{\nabla}\xi_i)^T \mathbf{M}^{-1}\boldsymbol{\nabla}\xi_i\right)^{\frac{n}{2}} \mathrm{d}\mathbf{x}. \tag{2.37}$$

https://doi.org/10.1017/S0962492906400015 Published online by Cambridge University Press

We remark that the functional (2.37) can also be derived from the concept of conformal norm in the context of differential geometry (Huang 2001*b*). Moreover, in two dimensions ($n = 2$), (2.37) gives the energy of a harmonic mapping (Dvinsky 1991). In this sense, the harmonic map method can be understood as a functional associated with alignment. Similarly, we can take squares on both sides of (2.36) and integrate the resulting inequality over Ω_P. We get

$$n^n \int_{\Omega_P} \frac{\sqrt{\det(\mathbf{M})}}{(|J|\sqrt{\det(\mathbf{M})})^2}\,\mathrm{d}\mathbf{x} \le \int_{\Omega_P} \sqrt{\det(\mathbf{M})}\left(\sum_i (\boldsymbol{\nabla}\xi_i)^T \mathbf{M}^{-1}\boldsymbol{\nabla}\xi_i\right)^2 \mathrm{d}\mathbf{x}.$$

The resulting functional for alignment then takes the form

$$\begin{aligned}\tilde{I}_{\mathrm{ali}}(\boldsymbol{\xi}) = &\int_{\Omega_P} \sqrt{\det(\mathbf{M})}\left(\sum_i (\boldsymbol{\nabla}\xi_i)^T \mathbf{M}^{-1}\boldsymbol{\nabla}\xi_i\right)^2 \mathrm{d}\mathbf{x} \\ &- n^n \int_{\Omega_P} \frac{\sqrt{\det(\mathbf{M})}}{(|J|\sqrt{\det(\mathbf{M})})^2}\,\mathrm{d}\mathbf{x}. \end{aligned} \tag{2.38}$$

2.7.2. A functional for equidistribution

We now consider the equidistribution condition (2.22). From Hölder's inequality we have

$$\left(\int_{\Omega_P} \frac{\sqrt{\det(\mathbf{M})}}{|J|\sqrt{\det(\mathbf{M})}}\,\mathrm{d}\mathbf{x}\right)^2 = \left(\int_{\Omega_C} \mathrm{d}\boldsymbol{\xi}\right)^2 \le \int_{\Omega_P} \frac{\sqrt{\det(\mathbf{M})}}{(|J|\sqrt{\det(\mathbf{M})})^2}\,\mathrm{d}\mathbf{x},$$

which leads to the functional for equidistribution given by

$$I_{\mathrm{eq}}(\boldsymbol{\xi}) = \int_{\Omega_P} \frac{\sqrt{\det(\mathbf{M})}}{(|J|\sqrt{\det(\mathbf{M})})^2}\,\mathrm{d}\mathbf{x}. \tag{2.39}$$

2.7.3. An adaptation functional based on equidistribution and alignment

We note that neither of the adaptation functionals defined in the previous subsections can alone lead to a robust mesh adaptation method because each of them represents only one of the mesh control conditions (2.23) and (2.22). It is necessary and natural to combine them. A way to achieve this goal is to take an average of the functionals (2.38) and (2.39), *i.e.*,

$$\begin{aligned} I(\boldsymbol{\xi}) = &\theta \int_{\Omega_P} \sqrt{\det(\mathbf{M})}\left(\sum_i (\boldsymbol{\nabla}\xi_i)^T \mathbf{M}^{-1}\boldsymbol{\nabla}\xi_i\right)^n \mathrm{d}\mathbf{x} \\ &+ (1-2\theta)n^n \int_{\Omega_P} \frac{\sqrt{\det(\mathbf{M})}}{(|J|\sqrt{\det(\mathbf{M})})^2}\,\mathrm{d}\mathbf{x}, \end{aligned} \tag{2.40}$$

where $\theta \in [0, 1]$ is a parameter. Notice that the two terms in the functional have the same dimension. The balance between them is controlled by a

https://doi.org/10.1017/S0962492906400015 Published online by Cambridge University Press

dimensionless parameter θ. When $\theta = 1/2$, only the first term remains. Regarding well-posedness, it is noted that the first term of the functional is convex, and the existence, uniqueness, and the maximal principle for its minimizer are guaranteed; *e.g.*, see Reshetnyak (1989). It is unclear if this result can apply to the whole functional.

2.7.4. Mesh quality measures: alignment and equidistribution

Mesh quality measures can also be developed based on the alignment and equidistribution conditions (2.23) and (2.22). Indeed, for a given matrix-valued monitor function $\mathbf{M} = \mathbf{M}(\mathbf{x})$ and a coordinate transformation $\mathbf{x} = \mathbf{x}(\boldsymbol{\xi})$ (or its inverse), we can use

$$Q_{\text{ali}} = \left[\frac{\text{trace}(J^T\mathbf{M}J)}{n\,\det(J^T\mathbf{M}J)^{\frac{1}{n}}}\right]^{\frac{n}{2(n-1)}}, \tag{2.41}$$

$$Q_{\text{eq}} = \frac{|J|\,\sqrt{\det(\mathbf{M})}|\Omega_C|}{\int_{\Omega_P}\sqrt{\det(\mathbf{M})}\,\mathrm{d}y} \tag{2.42}$$

to measure how closely the coordinate transformation (*i.e.*, mesh) satisfies the alignment and equidistribution conditions (2.23) and (2.22), respectively. We note that Q_{ali} is equivalent to

$$\hat{Q}_{\text{ali}} = \left[\frac{\text{trace}(J^{-1}\mathbf{M}^{-1}J^{-T})}{n\,\det(J^{-1}\mathbf{M}^{-1}J^{-T})^{\frac{1}{n}}}\right]^{\frac{n}{2(n-1)}}. \tag{2.43}$$

The quantity Q_{ali} ranges from 1 to ∞, with $Q_{\text{ali}} \equiv 1$ for the identity mapping, while Q_{eq} takes values in $(0, \infty)$, with $\max_x Q_{\text{eq}} = 1$ implying an equidistributing mesh. Interestingly, Q_{ali} reduces to an equivalence of Q_{geo} when $M = \text{Id}$. In this sense, Q_{ali} can be viewed as a geometric quality measure in the metric specified by $\mathbf{M}$.

2.8. Error control and associated monitor functions

The measures for mesh quality and geometry described in Section 2.7 have largely been constructed in the absence of a clear application. For the majority of this article we are considering the effectiveness of a mesh for computing the solution of a partial differential equation. In this case we are expecting to impose some form of discretization of the system on the mesh. From this discretization we hope to solve a (typically rapidly evolving) partial differential equation. The mesh so constructed should attempt to minimize error (such as the truncation or the interpolation error) in some way. In this subsection we consider three forms of error, namely static truncation error, static interpolation error and dynamic errors, and in the first two cases look at monitor functions which lead to reduced errors. The difficulty in implementing such a procedures is, of course, that not only is

https://doi.org/10.1017/S0962492906400015 Published online by Cambridge University Press

it difficult to measure (or indeed to precisely define) the error during the calculation and adapting the mesh accordingly, but also some of the 'best' adaptive meshes for solving time-dependent problems lead to very stiff differential equations, thus significantly increasing the computational cost of the process and in some cases making the whole calculation significantly unstable. However, it is intuitively reasonable that for solutions with small length scales over part of the domain, and larger length scales elsewhere, we might expect to gain significant efficiency by using a smaller mesh in the region of high variation. Exactly this observation motivated the important early work of Dorfi and Drury (1987).

2.8.1. Static truncation error and 'optimal' meshes

The most natural reason for using an adaptive mesh in the context of solving a PDE is to control the overall error in any discretization. It is a surprisingly difficult problem to obtain such an estimate in the context of a (non-uniform) moving mesh. Typically there are contributions to the local truncation error from the local mesh scale, the variation of the mesh from one element to the next, and also the effects of the mesh motion, which all need to be taken into consideration. It is also difficult to then extrapolate from a local to a global error estimate in such cases. Accordingly, we will confine ourselves to giving a flavour of this analysis by looking at some simple one-dimensional problems for which we can perform the technical calculations needed to analyse the error. Following this we will return to more general ideas shortly. Accordingly, as examples of two *steady-state* problems for which adaptivity may be required, we may wish to solve the Poisson equation

$$-\Delta u = f(x, y, z, \dots) \tag{2.44}$$

for a potentially singular right-hand side f. Alternatively we may seek to solve the singular diffusion equation

$$-\epsilon u'' - c(x)u' = f(x), \quad \epsilon \ll 1. \tag{2.45}$$

An ideal mesh with N points, used to compute the function u, is one which leads to low errors – ideally, in the case of (2.45), to errors which are ϵ-independent and depend only upon N. Such a mesh should also keep computational costs low. Essentially we can consider two types of non-uniform mesh for the computation. One type is an *optimal, fitted or a priori mesh*, which is prescribed in advance of the calculation and gives best possible errors for that computation in some appropriate norm. Important examples of this class are the *Shishkin and Bakhvalov meshes* for the singularly perturbed problems (2.45) and optimal meshes for Poisson-type problems. In Babuška and Rheinboldt (1979), a general analysis of such meshes is made in the context of finite element calculations in one dimension. An adaptive mesh, on the other hand, attempts to approximate an optimal mesh

https://doi.org/10.1017/S0962492906400015 Published online by Cambridge University Press

through equidistributing a suitable monitor function determined during the computation.

It is important to note at this stage that the error in discretizing a differential equation (or indeed in interpolating the solution to that equation or a function in general) is a combination of the error that would occur on a uniform mesh together with further errors that arise from the non-uniformity of the mesh (variation in the size of the elements) and (in more than one dimension) the mesh skewness. The latter errors have to be treated with great care as they can easily dominate the truncation error on the uniform mesh and make an adapted mesh worse than useless in solving the underlying problem. However, in contrast, a common error in many numerical analysis texts is to assume either that these errors add together to give a larger error, or that, for example, the error due to the non-uniformity of the mesh is always at a lower order than the error on the uniform mesh and thus dominates the overall calculation. In fact, provided that the mesh function is *suitably smooth*, for example if (in one dimension) the mesh is quasi-uniform and obeys the condition (2.9), then the three errors can be *at the same order* when expressed in terms of $1/N^p$. In an 'optimal' mesh it may be possible for the errors to cancel each other out to leading order. However, such meshes are usually very hard to construct and require a lot of *a priori* information about the solution. Adaptive meshes generally work by bounding the leading order error (regardless of the behaviour of the underlying solution).

We start by looking at both optimal and adaptive non-uniform meshes on which we can pose finite difference discretization of the Poisson equation:

$$-\frac{\mathrm{d}^2 u}{\mathrm{d}x^2} = f(x). \tag{2.46}$$

If the mesh is a function $x(\xi)$ of the computational variable, then in the computational domain we have

$$-\frac{1}{J}\left(\frac{u_\xi}{J}\right)_\xi = f(x(\xi)), \quad J = x_\xi. \tag{2.47}$$

The equation (2.47) can then be discretized in the computational domain for which we use the approximations

$$U_j \approx u(X_j), \quad X_j = x(j\Delta_\xi), \quad f_j = f(X_j).$$

A natural centred difference approximation to (2.47) then takes the form

$$-\frac{2}{(\Delta\xi)^2}\frac{\left(\frac{U_{j+1}-U_j}{X_{j+1}-X_j} - \frac{U_j-U_{j-1}}{X_j-X_{j-1}}\right)}{X_{j+1}-X_{j-1}} = f_j, \tag{2.48}$$

with

$$\Delta_i = X_{i+1} - X_i.$$

https://doi.org/10.1017/S0962492906400015 Published online by Cambridge University Press

We now assume that the mesh function $x(\xi)$ has regularity C^2 and exactly equidistributes a scalar monitor function M.

Lemma 2.3.

(i) The local truncation error T of the above discretization is given in the original variables by

$$T = \frac{\Delta_i^2}{3}\left[\frac{x_{\xi\xi}}{x_\xi^2}u_{xxx} + \frac{u_{xxxx}}{4}\right] + \mathcal{O}(\Delta_i^3), \tag{2.49}$$

and in the computational variables by

$$T = \frac{\Delta\xi^2 x_\xi^2}{3}\left[-\frac{M_\xi u_{xxx}}{M x_\xi} + \frac{u_{xxxx}}{4}\right] + \mathcal{O}(\Delta\xi^3). \tag{2.50}$$

(ii) The truncation error is of second order if the mesh is quasi-uniform so that condition (2.10) is satisfied.

(iii) The truncation error is *zero to leading order* if the mesh equidistributes the monitor function

$$M_{\text{opt}} = (u_{xxx})^{1/4} = (-f_x)^{1/4}. \tag{2.51}$$

Proof. Let $\Delta_j = X_{j+1} - X_j$. A simple Taylor expansion gives

$$U_{j+1} = U_j + \Delta_j u' + \frac{\Delta_j^2}{2}u'' + \frac{\Delta_j^3}{6}u''' + \frac{\Delta_j^4}{24}u'''' + \mathcal{O}(5),$$
$$U_{j-1} = U_j - \Delta_{j-1} u' + \frac{\Delta_{j-1}^2}{2}u'' - \frac{\Delta_{j-1}^3}{6}u''' + \frac{\Delta_j^4}{24}u'''' + \mathcal{O}(5),$$

where all derivatives of u are expressed in terms of x. Hence, expanding the left-hand side of (2.48), we obtain (after some manipulation) that the truncation error is given by

$$T = \frac{1}{3}(\Delta_j - \Delta_{j-1})u''' + \frac{1}{12}\frac{\Delta_j^3 + \Delta_{j-1}^3}{\Delta_j + \Delta_{j-1}}u'''' + \mathcal{O}(3).$$

This error has two components. The second is the usual component (of order Δ_j^2) which is seen on a uniform mesh. The first is an additional error due to the variation in the size of the mesh. In many texts this is considered to be large (as it is apparently of higher order); however, if Δ_j varies smoothly over the domain then it is actually of the same order as the second error. Since, to leading order,

$$\Delta_j = \Delta\xi x_\xi,$$

we have, to leading order,

$$T = (\Delta\xi)^2\left(\frac{1}{3}x_{\xi\xi}u''' + \frac{1}{12}x_\xi^2 u''''\right) + \mathcal{O}(\Delta\xi^3).$$

https://doi.org/10.1017/S0962492906400015 Published online by Cambridge University Press

Setting (to leading order) $\Delta_j = \Delta\xi x_\xi$ gives (2.49). Now, from the equidistribution equation we have

$$x_\xi = \frac{\theta}{M}.$$

Hence $M_\xi x_\xi + M x_{\xi\xi} = 0$. Substituting for M in the above gives (2.50).

Result (ii) follows immediately from the expression (2.49)

The optimal form of M in (iii) arises from setting the leading-order term to zero and integrating. Note that this latter calculation can break down if u_{xxx} vanishes at some point. □

An almost identical calculation to the above leads to the following result.

Lemma 2.4.

(i) If we consider using the standard central difference approximation to u_x given by

$$u_x = \frac{U_{i+1} - U_{i-1}}{X_{i+1} - X_{i-1}},$$

then the truncation error is given in the physical coordinates by

$$T = \frac{\Delta_i^2}{2}\left[\frac{x_{\xi\xi}}{x_\xi^2}u_{xx} + \frac{1}{3}u_{xxx}\right] + \mathcal{O}(\Delta_i^3), \tag{2.52}$$

or in the computational coordinates by

$$T = \frac{\Delta\xi^2 x_\xi^2}{2}\left[-\frac{M_\xi u_{xx}}{M x_\xi} + \frac{1}{3}u_{xxx}\right] + \mathcal{O}(\Delta\xi^3). \tag{2.53}$$

(ii) This error is of second order on a quasi-uniform mesh, and is zero to leading order on an 'optimal mesh' given when

$$M = \left(u_{xx}\right)^{1/3}. \tag{2.54}$$

These calculations, both of the errors in approximating u_x and u_{xx} and of the possible optimal meshes, are revealing in a number of ways. Firstly, they show that in all such calculations there is a subtle interplay between the mesh variability and the mesh size. This is even more marked in the case of singular perturbation problems. By choosing M very carefully we can exploit this to give very high accuracy and an *optimal mesh*. In general this is not usually possible. Indeed this calculation requires an accurate knowledge of the third derivative of the function u.

Secondly, we can also see from (2.50) the effect of choosing other types of monitor function as part of an adaptive calculation. The optimal mesh eliminates the truncation error to leading order. However, the truncation error is actually an estimate for the second derivative (with respect to x) of the solution error between the calculated solution U_j and $u(X_j)$. To obtain

https://doi.org/10.1017/S0962492906400015 Published online by Cambridge University Press

a true estimate, this expression needs to be integrated. A useful expression for the error for both (2.46) and (2.45) (see Andreev and Kopteva (1998)) is then given by the next lemma.

Lemma 2.5.

$$\|U_j - u(X_j)\|_\infty \leq C \max\Big[\Delta_i^2 \max_{[X_i, X_{i+1}]} |u''| + \Delta_i^2\Big]. \tag{2.55}$$

Given suitable *a priori* estimates, this error can be bounded by using a monitor function M which controls this via the expression

$$\begin{aligned}\Delta_i^2\Big(\max_{[X_i,X_{i+1}]} |u''| + 1\Big) &= \Delta\xi^2 x_\xi^2\Big(\max_{[X_i,X_{i+1}]} |u''| + 1\Big)\\ &= \Delta\xi^2\Big(\max_{[X_i,X_{i+1}]} |u''| + 1\Big)\theta^2/M^2.\end{aligned}$$

This motivates the choice of the curvature-dependent monitor function given by

$$M = \sqrt{1 + |u''|^2}.$$

Such a function has been used by Blom and Verwer (1989); see also Mackenzie and Robertson (2002), Chen (1994), Huang and Sun (2003) and Kopteva (2007). In this case the error *becomes a function of* $\Delta\xi$ *only* and does not depend upon the solution. Hence it has the great advantage of yielding a mesh for which large variations in u'' (for example at boundary layers) do not affect accuracy. This is good enough for most calculations. Observe, however, the difference between using the curvature-based monitor function to bound the error, and the optimal monitor function for the Poisson equation which eliminates this error to leading order.

Similar issues arise in the case of the singularly perturbed problems (2.45). For example, it is possible to get very sharp estimates on the solution in certain cases (such as when $c(x) = 1$). In the latter case (Andreev and Kopteva 1998) we have the following result.

Lemma 2.6.

$$\|U_j - u(X_j)\|_\infty \leq C\big[\|\min\{\Delta_i^2/\epsilon^2, 1\}\, \mathrm{e}^{-x_{i-1}/\epsilon}\|_\infty + \max \Delta_i^2\big]. \tag{2.56}$$

This error can be completely controlled to be proportional only to $\Delta\xi^2$ using a Bakhvalov mesh. For such problems it can also be shown (Kopteva 2007) that, if the monitor function is chosen to be a discrete arclength of the form

$$M = \sqrt{1 + u_x^2},$$

then, provided that the solution has converged closely to an equidistributed one, the computed solution is first-order accurate with errors $\mathcal{O}(\Delta\xi)$, independent of the value of ϵ.

https://doi.org/10.1017/S0962492906400015 Published online by Cambridge University Press

It is interesting to point out that uniform convergence has been obtained by a number of researchers for equidistributing meshes determined *a priori* by the exact solution or the singularity information of the exact solution for singularly perturbed differential equations: *e.g.*, see Sloan *et al.* (Qiu and Sloan 1999, Qiu, Sloan and Tang 2000), Mackenzie *et al.* (Mackenzie 1999, Beckett and Mackenzie 2000, Beckett, Mackenzie, Ramage and Sloan 2001*b*, Beckett and Mackenzie 2001*a*, 2001*b*, Mackenzie and Mekwi 2007*b*), and Huang (2005*c*). Convergence results are also obtained for *a posteriori* equidistributing meshes determined by computational solutions for differential equations in Babuška and Rheinboldt (1979), Kopteva and Stynes (2001), He and Huang (2009) and Huang, Kamenski and Lang (2009).

2.8.2. Static interpolation error

In higher dimensions it is very hard to obtain reliable estimates for the truncation error when solving a general PDE. A somewhat easier, but still very important, question to address is whether a mesh is suitable to approximate the solution of the PDE, in particular to interpolate the solution. We now consider this question.

Suppose that the solution of the differential equation (or indeed any appropriate function defined in the physical domain) is given by $u(x, y, \ldots)$. For the case of a problem in two dimensions we can define the point values of u on the non-uniform mesh by

$$U_{i,j} = u\big(X_{i,j}, Y_{i,j}\big).$$

A natural measure of error is the *interpolation error* obtained by approximating u on the mesh with suitable functions using the above point values. Significant progress in finding meshes with good properties in reducing the interpolation error of a solution has been made in this direction in the past decade. Formulae giving the optimal monitor function to minimize this error over a suitable mesh have been developed based on interpolation error estimates by Huang and Sun (2003) in the H^m-norm, Chen *et al.* (2007) in the L^q-norm, Huang (2005*a*, 2005*b*) in the $W^{m,q}$-norm, and Cao (2005, 2007*a*, 2007*b*, 2008) for higher-order interpolation in two dimensions. Formulae have also been developed based on an *a posteriori* error estimate for one dimension (He and Huang 2009), a hierarchical basis *a posteriori* error estimate (Huang *et al.* 2009), and semi *a posteriori* error estimates for variational problems (Huang and Li 2009). Formulae for the monitor functions in these cases can be obtained as follows (Huang and Sun 2003, Huang 2005*a*). A so-called anisotropic error bound, taking into consideration the directional effect of the error or solution derivatives, is first developed. This error bound can be regarded as a function of the monitor function M when only meshes satisfying the alignment and equidistribution

https://doi.org/10.1017/S0962492906400015 Published online by Cambridge University Press

conditions (2.23) and (2.22) are concerned. Then the optimal monitor function is obtained by minimizing the bound among all possible matrix-valued functions $\mathbf{M}$. Consider a simple situation where a function $u \in H^2(\Omega_P)$ is interpolated by piecewise linear polynomials on a simplicial mesh (of N elements) and the error is measured in L^2-norm. Then an anisotropic asymptotic bound (as $N \to \infty$) can be obtained from the interpolation theory of Sobolev spaces (Huang and Sun 2003), namely

$$\|e_h\|^2_{L^2(\Omega_P)} \leq C\alpha^2 N^{-\frac{4}{n}} \int_{\Omega_P} \big(\mathrm{trace}\big(J^T[I+\alpha^{-1}|H(u)|]J\big)\big)^2 \,\mathrm{d}\mathbf{x} + \text{h.o.t.}, \quad (2.57)$$

where $H(u)$ denotes the Hessian of the function u, $|H(u)| = \sqrt{H(u)^T H(u)}$, and $\alpha > 0$ is an arbitrary number which serves as a regularization parameter, whose value will be determined later. Note that a rigorous bound can be obtained. But in this situation the derivation has to be associated with a discrete form; *e.g.*, see Huang (2007). Since the procedure is the same for both, for simplicity we use the non-rigorous continuous form. Noticing that a mesh satisfying (2.23) and (2.22) (and a proper boundary correspondence) is a function of $\mathbf{M}$, we can regard the integral on the right-hand side of (2.57) as a function of $\mathbf{M}$, namely

$$B(\mathbf{M}) = \int_{\Omega_P} \big(\mathrm{trace}\big(J^T[I+\alpha^{-1}|H(u)|]J\big)\big)^2 \,\mathrm{d}\mathbf{x}. \quad (2.58)$$

In the following analysis, we consider only meshes satisfying (2.22) and (2.23) and derive the optimal monitor function by minimizing $B(\mathbf{M})$ among all possible matrix-valued functions $\mathbf{M}$. First we notice that (2.23) is mathematically equivalent to

$$\frac{1}{n}\mathrm{trace}(J^T\mathbf{M}J) = \det(J^T\mathbf{M}J)^{\frac{1}{n}}. \quad (2.59)$$

A direct comparison of (2.59) suggests that $\mathbf{M}$ can be chosen in the form

$$\mathbf{M} = \theta(\mathbf{x})[I+\alpha^{-1}|H(u)|], \quad (2.60)$$

where $\theta = \theta(\mathbf{x})$ is a scalar function. For matrix-valued monitor functions in this form, (2.59) reduces to

$$\frac{1}{n}\mathrm{trace}(J^T[I+\alpha^{-1}|H(u)|]J) = \det(J^T[I+\alpha^{-1}|H(u)|]J)^{\frac{1}{n}}.$$

Inserting this into (2.58) and using Hölder's inequality, we have

$$\begin{aligned} B(\mathbf{M}) &= n^2 \int_{\Omega_P} |J|^{\frac{4}{n}} \det(I+\alpha^{-1}|H(u)|)^{\frac{2}{n}} \,\mathrm{d}\mathbf{x} \\ &= n^2 \int_{\Omega_C} \big[|J|\det(I+\alpha^{-1}|H(u)|)^{\frac{2}{n+4}}\big]^{\frac{n+4}{n}} \,\mathrm{d}\boldsymbol{\xi} \end{aligned}$$

https://doi.org/10.1017/S0962492906400015 Published online by Cambridge University Press

$$\geq n^2|\Omega_C|^{-\frac{4}{n}}\left[\int_{\Omega_C}|J|\det(I+\alpha^{-1}|H(u)|)^{\frac{2}{n+4}}\,\mathrm{d}\boldsymbol{\xi}\right]^{\frac{n+4}{n}} \tag{2.61}$$

$$= n^2|\Omega_C|^{-\frac{4}{n}}\left[\int_{\Omega_P}\det(I+\alpha^{-1}|H(u)|)^{\frac{2}{n+4}}\,\mathrm{d}\mathbf{x}\right]^{\frac{n+4}{n}}. \tag{2.62}$$

We note that equality in (2.61) holds when the mesh satisfies

$$|J|\det(I+\alpha^{-1}|H(u)|)^{\frac{2}{n+4}} = \frac{1}{|\Omega_C|}\int_{\Omega_P}\det(I+\alpha^{-1}|H(u)|)^{\frac{2}{n+4}}\,\mathrm{d}\mathbf{y}.$$

Comparing this with the equidistribution condition (2.22), we have

$$\sqrt{\det(\mathbf{M})} = \det(I+\alpha^{-1}|H(u)|)^{\frac{2}{n+4}}.$$

From this and (2.60), the optimal matrix-valued monitor function to minimize the interpolation error is given by

$$\mathbf{M} = \det(I+\alpha^{-1}|H(u)|)^{-\frac{1}{n+4}}\ \ [I+\alpha^{-1}|H(u)|]. \tag{2.63}$$

Inserting (2.62) into (2.57), the interpolation error bound for a mesh satisfying (2.23) and (2.22) with optimal $\mathbf{M}$ given in (2.63) is then

$$\|e_h\|^2_{L^2(\Omega_P)} \leq C\alpha^2 N^{-\frac{4}{n}}\left[\int_{\Omega_P}\det(I+\alpha^{-1}|H(u)|)^{\frac{2}{n+4}}\,\mathrm{d}\mathbf{x}\right]^{\frac{n+4}{n}} + \text{h.o.t.} \tag{2.64}$$

We now discuss how to choose α. We first notice that conditions (2.57) and (2.62) are invariant under scaling transformations of $\mathbf{M}$ of the form $\mathbf{M}\to c\mathbf{M}$, for any positive constant c. Thus, if $|H(u)|$ is strictly positive definite on Ω_P, we can take $\alpha\to 0$ in (2.63) and (2.64). This gives

$$\mathbf{M} = \det(|H(u)|)^{-\frac{1}{n+4}}\ \ |H(u)|, \tag{2.65}$$

$$\|e_h\|^2_{L^2(\Omega_P)} \leq CN^{-\frac{4}{n}}\left[\int_{\Omega_P}\det(|H(u)|)^{\frac{2}{n+4}}\,\mathrm{d}\mathbf{x}\right]^{\frac{n+4}{n}} + \text{h.o.t.} \tag{2.66}$$

When $|H(u)|$ vanishes locally, the monitor function cannot be defined by (2.65) since the right-hand side is not positive definite. In this case, a positive α should be used. Huang (2001*b*) suggests that α be defined implicitly via

$$\int_{\Omega_P}\det(I+\alpha^{-1}|H(u)|)^{\frac{2}{n+4}}\,\mathrm{d}\mathbf{x} = 2|\Omega_P|. \tag{2.67}$$

It is easy to show that (2.67) has a unique solution for α. A simple iteration method such as the bisection method can be used for solving this equation. Moreover, when α is defined in this way, $\mathbf{M}$ is invariant for scaling transformation of $|H(u)|$. Furthermore, it is shown in Huang (2001*b*) that about fifty per cent of the mesh points are then concentrated in regions where

https://doi.org/10.1017/S0962492906400015 Published online by Cambridge University Press

$\det(I + \alpha^{-1}|H(u)|)^{\frac{2}{n+4}}$ is large. Finally, the error bound reads as

$$\|e_h\|^2_{L^2(\Omega_P)} \leq C\alpha^2 N^{-\frac{4}{n}}. \tag{2.68}$$

From (2.67) it is not difficult to show that, for $n \leq 4$, α is bounded as

$$\left[\frac{1}{2|\Omega_P|}\int_{\Omega_P} \det(|H(u)|)^{\frac{2}{n+4}}\,\mathrm{d}\mathbf{x}\right]^{\frac{n+4}{2n}} \leq \alpha \leq \left[\frac{1}{n^{\frac{2n}{n+4}}|\Omega_P|}\int_{\Omega_P} \big(\mathrm{trace}(|H(u)|)\big)^{\frac{2n}{n+4}}\,\mathrm{d}\mathbf{x}\right]^{\frac{n+4}{2n}}. \tag{2.69}$$

2.8.3. Dynamic error

Usually when we apply a moving mesh method we are interested in solving a time-evolving PDE. This leads to additional dynamic errors (Li and Petzold 1997, Li *et al.* 1998) such as oscillations around rapidly evolving fronts or miscalculations of the front speed. These depend significantly on the way in which the mesh is updated and coupled to the PDE. We consider these in more detail in the next section when we look at how the moving mesh equations are coupled to the underlying PDE.

2.9. Monitor function smoothing and regularization

Having considered the mesh quality, we now return to further considerations of the monitor function and of mesh smoothness. Recall that for one-dimensional problems it is essential that the mesh should be quasi-uniform in order to have a low truncation error. Smoothing a mesh either directly or indirectly through smoothing/averaging aims to achieve this.

2.9.1. The Dorfi and Drury method

A direct approach to smoothing a one-dimensional mesh derived from an equidistribution principle is proposed in Dorfi and Drury (1987), and is often called the Dorfi and Drury method. In this method, if

$$n_i = (\Delta X_i)^{-1} \equiv \big(X_{i+1} - X_i\big)^{-1},$$

then a smoother mesh is given by computing $\hat{n}_i$ where

$$\hat{n}_i = n_i - \gamma\big(n_{i+1} - 2n_i + n_{i-1}\big) \tag{2.70}$$

for a suitable constant γ. A variant of this, considered in Li and Petzold (1997), is given by updating the mesh differences by

$$\Delta\hat{X}_i = \sum_{j=i-p}^{i+p} \theta^{|i-j|}\Delta X_i$$

https://doi.org/10.1017/S0962492906400015 Published online by Cambridge University Press

for a suitable constant $0 < \theta < 1$. There are many other strategies for direct mesh smoothing. For example it is possible to use *a posteriori* estimates of the solution on the mesh to do this (Bank and Smith 1997).

2.9.2. Monitor function smoothing

Alternatively we can generate a smoother mesh by averaging the monitor function prior to the mesh calculation. Suppose that point values of (a scalar or matrix-valued) monitor function $M_{i,j}$ are given. A Jacobian-type strategy, also referred to as averaging or low-pass filtering in the literature, is commonly used, *e.g.*, see Dorfi and Drury (1987), Verwer *et al.* (1989) and Huang and Sloan (1994). When a rectangular computational mesh is used, this smoothing can be conveniently expressed as

$$\hat{M}_{i,j} = \frac{\sum_{k=-1}^{1}\sum_{l=-1}^{1} M_{i+k,j+l}\gamma^{|k|+|l|}}{\sum_{k=-1}^{1}\sum_{l=-1}^{1}\gamma^{|k|+|l|}},$$

where $\gamma \in (0,1)$ is a parameter. This type of local smoothing of the monitor function can be viewed as an approximation of Laplace-operator-based smoothing:

$$(I - \lambda^{-2}\Delta_\xi)\hat{M} = M,$$

where λ is a parameter. In one dimension, Huang and Russell (1997*a*) show that, when λ is chosen as a value of order $\mathcal{O}(N)$, where N is the number of sub-intervals, a mesh equidistributing $\hat{M}$ is *locally quasi-uniform*, indeed there exists a reasonably small constant $\nu \geq 1$ such that

$$\frac{1}{\nu} \leq \frac{X_{j+1} - X_j}{X_j - X_{j-1}} \leq \nu \quad \forall j.$$

Another interesting strategy is to use a reference Jacobian matrix (Knupp 1996, Knupp, Margolin and Shashkov 2002) where a new mesh is generated to have a close Jacobian matrix to the reference one that is typically obtained from a reference, often non-smooth mesh.

2.9.3. 50:50 meshes and the Mackenzie regularization

A recurring problem with r-adaptive meshes which equidistribute a poorly chosen monitor function is that they can concentrate points in areas of particular identified interest where high resolution is needed, but leave other regions sparse of points. This can lead not only to low resolution in such areas, but also to a severe lack of mesh regularity and consequent large errors caused by a too rapid mesh variation. An example of such would be the calculation of the solution of a system which is blowing up in finite time with a large peak, in which all of the mesh points are concentrated in the peak alone. Such problems can be significantly reduced if the mesh is designed so that roughly half of the points are concentrated in the areas

https://doi.org/10.1017/S0962492906400015 Published online by Cambridge University Press

where high resolution is required, and half where it is not. Such meshes are called 50:50 meshes (see Budd *et al.* (2005), Huang (2001*a*), Huang *et al.* (2002)) and a regularization of M to ensure that such meshes arise in practice has been proposed by Beckett and Mackenzie (2000). To show how such problems arise in a calculation in n dimensions, suppose that we have a scalar monitor function M for which $\int_{\Omega_P} M\,\mathrm{d}x = \theta$. Consider now the situation in which there are two subsets A and B of Ω_P, with $\Omega_P = A \cup B$ so that the monitor function is designed to concentrate points in a small region A (so that A may be the support of a singularity or of a front). The preimage $A' = F^{-1}(A) \subset \Omega_C$ represents those points in the computational domain which are mapped to A, with a similar set B'. Suppose now that $|A'|$ and $|B'|$ are the areas of these sets in Ω_C, with respective areas $|A|$ and $|B|$ in Ω_P. These areas measure the proportion of mesh points allocated to the corresponding sets A and B. Note that in most applications of an adaptive method, where mesh points have to be concentrated into a small region we would expect that

$$|A'| = \mathcal{O}(1), \quad |A| = \mathbf{o}(1), \quad |B'| = \mathcal{O}(1), \quad |B| \approx |\Omega_P|. \tag{2.71}$$

Problems arise with mesh regularity and solution resolution away from the set A if $|B'| \ll |A'|$. It follows immediately from the equidistribution principle that if $\theta = \int_{\Omega_P \equiv A \cup B} M\,\mathrm{d}\mathbf{x}$ then

$$\Lambda = \frac{|A'|}{|B'|} = \frac{\int_A M\,\mathrm{d}\mathbf{x}}{\int_B M\,\mathrm{d}\mathbf{x}} = \frac{\theta}{\int_B M\,\mathrm{d}\mathbf{x}} - 1.$$

Furthermore,

$$|A'| = \frac{\int_A M\,\mathrm{d}\mathbf{x}}{\theta}.$$

It follows from the conditions on A' and A in (2.71) that over the set A we have $M \gg \theta$. However, if the monitor function is so constructed such that over the set B we have $M \ll \theta$ and hence $\int_B M\,\mathrm{d}x \ll \theta$ (so that the integral of M is concentrated in A), then Λ will be very large and the mesh will lose regularity. Indeed, we will have $|A'| \approx 1$. Exactly such problems arose in some of the blow-up calculations reported in Budd *et al.* (1996). In such cases we must replace M by the regularized function introduced by Beckett and Mackenzie (2000) and given by

$$\hat{M} = M + \frac{\theta}{|\Omega_P|}. \tag{2.72}$$

Observe that over the set A we have $\hat{M} \approx M$, and over B we have $\hat{M} \approx \theta/|\Omega_P|$, and trivially

$$\int_{\Omega_P} \hat{M}\,\mathrm{d}\mathbf{x} = 2\theta.$$

https://doi.org/10.1017/S0962492906400015 Published online by Cambridge University Press

Consequently, when we make use of the regularized monitor function $\hat{M}$ to define the mesh we have

$$|A'| = \frac{\int_A \hat{M}\,\mathrm{d}\mathbf{x}}{2\theta} \approx \frac{\int_A M\,\mathrm{d}\mathbf{x}}{2\theta} \approx \frac{1}{2},$$

and

$$\Lambda \approx \frac{2|\Omega_P|}{|B|} - 1 \approx 1.$$

This gives the desired 50:50 quality to the mesh.

3. Location-based moving mesh methods

In this section we will look in greater detail at the various methods described in Section 2 under the general heading of *location-based methods*. These are those methods which determine the *location* (or more precisely the density) of the mesh points, typically through solving some form of nonlinear differential equation through some form of gradient flow method. The latter can be hard to solve. However, the advantage of these methods is that they tend to give meshes with good global properties, avoiding excessive skewness. We will consider in detail the various methods outlined in the previous section, such as MMPDE-based methods, variational methods and optimal transport methods.

3.1. MMPDE methods in one dimension

Methods based on moving mesh partial differential equations (MMPDEs) are now universally used as a means of r-adaptivity in one dimension, and have been incorporated into codes such as MOVCOL and AUTO. There are many different MMPDEs, which together encapsulate most of the methods used to derive adaptive meshes in one dimension.

We consider a one-dimensional map $x(\xi, t)$ from $[0, 1]$ to $[a, b]$ with associated mesh points $X_i = x(i\Delta\xi, t)$, which equidistributes the monitor function M. This map satisfies the equidistribution equation

$$Mx_\xi = \theta, \quad x(0,t) = a,\ x(1,t) = b, \quad \theta = \int_a^b M\,\mathrm{d}x. \tag{3.1}$$

Lemma 3.1. The equidistribution equation (3.1) has a unique monotone increasing solution $x(\xi, t)$ for all $M > 0$.

Proof. Integrating (3.1) with respect to ξ and changing variables gives

$$\int_a^x M\,\mathrm{d}x' = \theta\xi \quad \text{or} \quad \int_{X_{i-1}}^{X_i} M\,\mathrm{d}x = \frac{1}{N}\int_a^b M\,\mathrm{d}x. \tag{3.2}$$

Now, as $M > 0$ the left-hand side of this expression is a *monotone increasing*

https://doi.org/10.1017/S0962492906400015 Published online by Cambridge University Press

function of x. It immediately follows that x is a unique monotone increasing function of ξ. Observe further that this function is as smooth as the function M. □

This simple observation makes equidistribution relatively easy in one dimension.

The most direct way to enforce equidistribution is to solve (3.1) directly. However, this has the disadvantage that it requires the calculation of the integral θ. This can be avoided by a further differentiation with respect to ξ, and thus solving the moving mesh equation (together with boundary conditions) given by

$$(Mx_\xi)_\xi = 0, \quad x(0,t) = a,\ x(1,t) = b. \tag{3.3}$$

To determine an equidistributed mesh, the equation (3.3) can be discretized over the computational domain and then solved. This discretization does not have be done to high accuracy in order to obtain a regular mesh suitable for solving the underlying PDE. A typical such discretization takes the form

$$E_i \equiv \frac{2}{\Delta\xi^2}\big(M_{i+1/2}(X_{i+1} - X_i) - M_{i-1/2}(X_i - X_{i-1})\big) = 0,$$
$$M_{i+1/2} = \frac{1}{2}(M_i + M_{i+1}). \tag{3.4}$$

However, the solution of the system (3.4) requires solving a system of nonlinear equations, which is usually difficult and requires the use of some form of iterative procedure. See Pryce (1989), Xu, Huang, Russell and Williams (2009), He and Huang (2009), Kopteva and Stynes (2001) and Kopteva (2007) for a discussion of such methods, and conditions for them to converge to a solution.

This problem can be avoided by instead introducing a natural time evolution into the mesh equations. Differentiating the equidistribution equation (3.3) with respect to time gives the (so-called) MMPDE0 (Huang *et al.* 1994):

$$\frac{\mathrm{d}}{\mathrm{d}t}\big((Mx_\xi)_\xi\big) = 0. \tag{3.5}$$

Instead we may also differentiate (3.1) with respect to time (Adjerid and Flaherty 1986). This leads directly to the GCL method described in the next section. The resulting equation then takes the form

$$\frac{\partial}{\partial\xi}(Mx_t) + M_t x_\xi = \theta_t. \tag{3.6}$$

This equation can then also be differentiated with respect to ξ to eliminate the θ contribution, giving MMPDE1 (Huang *et al.* 1994), where it is assumed that we can find M_t, although in practice this may not be easy.

https://doi.org/10.1017/S0962492906400015 Published online by Cambridge University Press

Starting from any mesh (uniform or otherwise), we can evolve the mesh by solving MMPDE0 (3.5) or MMPDE1. Unfortunately, a uniform mesh does not necessarily satisfy the equidistribution equation (3.1). Furthermore, even if a mesh does exactly satisfy it at some time, solving a discretized form of (3.5) inevitably leads to meshes that drift away from an equidistributed state. Both of these can lead to problems with mesh crossing (the one-dimensional version of mesh tangling) which occurs when $x_\xi = 0$.

As an example of this, which also demonstrates the general applicability of the method, we consider solving (3.5) starting from an initially *uniform mesh* on $[0, 1]$ for which $x_\xi = 1$. In this calculation we will assume that we have a time-evolving monitor function $M(x, t)$ with $M(x, 0) \equiv M^0(x)$. It follows from integrating (3.5) with respect to t and applying the initial conditions that, for all time, we have

$$(Mx_\xi)_\xi = M^0_\xi.$$

Hence, integrating again we have

$$Mx_\xi = M^0 + B(t),$$

for some function $B(t)$. This can be determined by integrating this expression with respect to ξ to give

$$Mx_\xi = M^0 + \theta(t) - \theta(0).$$

As $M^0 > 0$ it follows that if θ is increasing in time then $x_\xi > 0$. However, if θ decreases with t then it is quite possible for x_t to vanish (initially at the point where M^0 takes its minimum value) and for mesh crossing (tangling) to result.

Such problems can be avoided (both in one and in higher dimensions) by introducing a relaxation time into the solution of (3.3). The philosophy behind doing this is that the equation (3.3) need not be solved exactly to obtain a mesh which is perfectly reasonable for any computation. What is more important is that the mesh evolves *at least as fast as any significant features of the solution*. Exactly the same philosophy applies to moving meshes in any number of dimensions. Thus it is possible to consider meshes which relax towards an equidistributed mesh, provided *the relaxation time is smaller than the natural time scale of the solution*. Ideally the relaxation time should be of a similar order to that of the solution evolution. This prevents the mesh equations becoming unnecessarily stiff. Various different forms of mesh relaxation are possible.

The most obvious way of relaxing towards an equidistributed state was proposed by Anderson and Rai (1983), who computed the mesh through a relaxation equation, based on considering pseudo-forces between the mesh points, given by

$$\epsilon \dot{x} = (Mx_\xi)_\xi, \tag{3.7}$$

https://doi.org/10.1017/S0962492906400015 Published online by Cambridge University Press

where $\epsilon > 0$ is presumed to be small. Alternatively, we can consider the original equidistribution equation in integral form. If a mesh is not exactly equidistributed then we can determine the residual

$$R = \int_a^x M \, \mathrm{d}x - \xi \int_a^b M \, \mathrm{d}x.$$

If we then set $\epsilon \dot{x} = -R$ and differentiate this expression twice with respect to ξ, we obtain

$$\epsilon(\dot{x})_{\xi\xi} = -(M x_\xi)_\xi. \tag{3.8}$$

This equation was originally derived in Adjerid and Flaherty (1986). The equations (3.7) and (3.8) are known respectively (Huang *et al.* 1994) as MMPDE5 and MMPDE6. We can combine them to give the (smoothed) moving mesh equation considered in Huang and Russell (1997*a*) (see also the discussion in Section 2), which takes the form

$$\epsilon\left(1 - \gamma \frac{\partial^2}{\partial \xi^2}\right)\dot{x} = (M x_\xi)_\xi. \tag{3.9}$$

Here $\gamma > 0$ can be chosen to give some control over the smoothness of the mesh. The equation (3.9) (and its various discretizations) is very dissipative, and leads to extremely stable meshes under most discretizations. The equation (3.9) also has natural extensions to higher dimensions, both in the context of the methods described in Huang and Russell (1997*a*) and Ceniceros and Hou (2001) and also in the optimal transport methods we consider later in this section. Other smoothed versions of the MMPDEs have also been considered by Huang and Russell (1997*a*). One of them is given by

$$\epsilon\left(1 - \gamma \frac{\partial^2}{\partial \xi^2}\right)\frac{\partial}{\partial \xi}\left(-\left(\frac{\partial x}{\partial \xi}\right)^{-2}\frac{\partial \dot{x}}{\partial \xi}\right) = -\left(1 - \gamma \frac{\partial^2}{\partial \xi^2}\right)\frac{\partial}{\partial \xi}\left(\frac{\partial x}{\partial \xi}\right). \tag{3.10}$$

Huang and Russell (1997*a*) have proved that the solutions (*i.e.*, the coordinate transformation and the mesh) to the continuous equation (3.10) using a central finite difference discretization have the properties both of local quasi-uniformity and no node-crossing.

Note. Many other MMPDEs have been derived, such as MMPDE2, given by

$$(M\dot{x})_{\xi\xi} = -(M_t x_\xi)_\xi - \frac{1}{\epsilon}(M x_\xi)_\xi.$$

However, we will focus our discussion on the more widely used (3.9).

The moving mesh equation evolves a mesh towards an equidistributed state satisfying (3.3). When implementing the MMPDE method, the equation (3.9) is typically discretized over the computational space, leading to a set of ordinary differential equations for the location of the mesh points X_i.

https://doi.org/10.1017/S0962492906400015 Published online by Cambridge University Press

These can then be solved using standard stiff ODE software, *e.g.*, by using an SDIRK (singly diagonally implicit Runge–Kutta) method. A simple such semi-discretization of (3.9) is given by

$$\epsilon\left(\dot{X}_i - \gamma\frac{\dot{X}_{i+1} - 2\dot{X}_i + \dot{X}_{i-1}}{(\Delta\xi)^2}\right) = E_i(t), \tag{3.11}$$

where the equidistribution measure $E_i(t)$ is as given in (3.4). This leads (on inversion of the simple tri-diagonal system on the right-hand side of this equation) to a simple set of ODEs for the location of the mesh points. Alternatively, a simple full discretization of (3.9) for a mesh X_i^n evaluated at the time $t_n = n\Delta t$ is proposed in Ceniceros and Hou (2001), and takes the form

$$\epsilon\left(X_i^{n+1} - \gamma\frac{X_{i+1}^{n+1} - 2X_i^{n+1} + X_{i-1}^{n+1}}{(\Delta\xi)^2}\right) = \epsilon\left(X_i^n - \gamma\frac{X_{i+1}^n - 2X_i^n + X_{i-1}^n}{(\Delta\xi)^2}\right) + \Delta t E_i^n. \tag{3.12}$$

These equations for the mesh can then be solved together with a suitable discretization of the underlying PDE, either simultaneously or alternately. We will give more details of this procedure later in this section in the context of moving meshes in higher dimensions, but we note at this stage that the simultaneous solution method is both possible and effective in such one-dimensional problems.

The method for evolving the mesh is typically implemented in two stages.

(1) Starting from an *initially uniform mesh* in the physical space, we evolve this to equidistribute the monitor function *at the initial time* over Ω_P. To do this we set $M_0(x) \equiv M(x, 0)$, with $x_\xi = a + (b - a)\xi$, and solve (3.46) with M fixed to equal the function M_0, with $\epsilon = 1$ for $0 < t < T$, where T is a fixed time. In this first calculation t is an *artificial time* during which the uniform mesh evolves toward an equidistributed mesh for which the right-hand side of (3.9) is zero. It follows from the earlier results that, provided $M_0 > 0$, such a mesh exists, and we show presently that it is stable. In this initial calculation the right-hand side of (3.9) is initially relatively large, and taking $\epsilon = 1$ prevents the numerical calculation of the solution of the ODEs for the mesh point locations from being unnecessarily stiff. The value of T is chosen large enough to allow the mesh to relax toward the equidistributed state.

(2) We then solve (3.9) with the true *time-dependent* monitor function $M(x, t)$, with t now *actual time*. For this calculation we typically set $\epsilon = 0.01$. We show presently that the resulting mesh is then ϵ-close to a mesh which exactly equidistributes $M(x, t)$, provided that M does not

https://doi.org/10.1017/S0962492906400015 Published online by Cambridge University Press

change too rapidly with time. As this procedure starts from a mesh which exactly equidistributes $M(\mathbf{X}, 0)$, the right-hand side of (3.9) is always close to zero and the resulting differential equations are not especially stiff.

Observe that this algorithm has the convenience of *starting from a uniform mesh*. This is a significant advantage over methods based on (3.5), or related methods such as the GCL method described in Section 4.

We will discuss later in this section the exact mechanism by which this algorithm for moving the mesh is coupled to the solution method for the underlying PDE.

This procedure has been criticized (for example, see Tang (2005)) for being imprecise about the way that ϵ is defined and the possibility of having to solve a very stiff system of equations. However, it can be given a very precise meaning. In the second stage of this calculation we are trying to find a mesh which is close to an equidistributed mesh. The natural time scale τ over which this mesh evolves is given simply by

$$\tau \approx \frac{\epsilon}{M}. \tag{3.13}$$

The key factor governing the choices of both ϵ and M is then to *ensure that τ is smaller than but of the same order as* the natural evolutionary time scale of the underlying PDE. In Section 5 we will show that in the context of PDEs with a strong scaling structure, this allows a natural choice to be made for both ϵ and M.

We now substantiate some of the claims made above, as well as stating another important property of the solutions of the moving mesh PDE (3.9).

Theorem 3.2.

(i) If $M_t = 0$, then the equidistributed mesh is a solution of (3.9) and is *linearly stable*.

(ii) If $M_t = \mathcal{O}(1)$, then an initially ϵ-close to equidistributed solution of (3.9) remains ϵ-close for all subsequent times.

(iii) At all times the solution of (3.9) satisfies $x_\xi > 0$, so that mesh crossing (tangling) does not occur.

Note. This applies for exact solutions of (3.9). If an overly coarse discretization is used to approximate these solutions then (iii) above may be violated (Smith 1996).

Proof. **(i)** Let $\hat{x}$ be an equidistributed mesh satisfying $(M(\hat{x})\hat{x}_\xi)_\xi = 0$, with $\hat{x}_t = M_t = 0$. It follows immediately that $\epsilon(\dot{\hat{x}} - \gamma\dot{\hat{x}}_{\xi\xi}) = (M\hat{x}_\xi)_\xi$ so that $\hat{x}$ satisfies the equidistribution equation. Now set $x = \hat{x} + R(\xi, t)$ with

https://doi.org/10.1017/S0962492906400015 Published online by Cambridge University Press

$R \ll 1$ and $R(a) = R(b) = 0$. To leading order, R satisfies the equation

$$\epsilon(\dot{R} - \gamma R_{\xi\xi}) = (MR_\xi)_\xi + (M_x x_\xi R)_\xi = (MR_\xi + M_\xi R)_\xi = (MR)_{\xi\xi}.$$

Therefore

$$\epsilon\dot{R} = (1 - \gamma\partial_\xi^2)^{-1}(MR)_{\xi\xi} \equiv G(MR)_{\xi\xi}. \tag{3.14}$$

Here G is a *positive compact operator* and, as $M > 0$, $ER \equiv (MR_{\xi\xi})$ is a uniformly elliptic operator with a negative real spectrum. It follows that R must decay to zero. Hence the equidistributed solution is locally stable.

(ii) To prove this result, consider a slowly varying monitor function $M(x,t)$ and an exact solution $\hat{x}$ of the equidistribution equation $(M\hat{x}_\xi)_\xi = 0$. If $x = \hat{x} + \epsilon R$ is a solution of (3.9) then, extending the calculation in (3.14), we see that R satisfies the equation

$$\epsilon(\dot{x} - \gamma\dot{x}_{\xi\xi}) + \mathcal{O}(\epsilon^2) = \epsilon(MR)_{\xi\xi} + \mathcal{O}(\epsilon^2).$$

Hence, we have

$$(MR)_{\xi\xi} = \dot{\hat{x}} - \gamma\dot{\hat{x}}_{\xi\xi} + \mathcal{O}(\epsilon).$$

But as $(M\hat{x}_\xi)_\xi = 0$, we have

$$(M\dot{\hat{x}}_\xi)_\xi = -(M_t\hat{x}_\xi)_\xi.$$

As the operator $E\phi \equiv (M\phi)_{\xi\xi}$ is uniformly elliptic, it follows that provided $\dot{M}$ is of order one, then $\dot{\hat{x}}$ and hence R and its derivatives are also of order one. Consequently, the solution x of (3.9) stays ϵ-close to the solution of the equidistribution equation.

(iii) To show this we need to show that x_ξ cannot vanish. This result is a consequence of the maximum principle. In the case when $\gamma = 0$, we have, on differentiating (3.9), that

$$\dot{x}_\xi = M_{\xi\xi}x_\xi + 2M_\xi x_{\xi\xi} + Mx_{\xi\xi\xi}.$$

Suppose that x_ξ is initially positive everywhere, and as x evolves it vanishes for a first time at (without loss of generality) the point $\xi = 0$. Then locally close to this point we have $x_\xi = a\xi^2 + \mathcal{O}(\xi^3)$ for some $a > 0$. Hence

$$\dot{x}_\xi = a\xi^2 M_{\xi\xi} + 2a\xi M_\xi + aM + \mathcal{O}(\xi).$$

Thus $\dot{x}_\xi > 0$ at this point and time. Hence x_ξ must remain positive. The more general result follows from the positivity of the compact operator G. □

3.1.1. Coupling a one-dimensional MMPDE method to a PDE

In one dimension, MMPDE methods can be very effectively coupled to an underlying PDE system by using a variety of different methods, including finite difference, finite element, collocation and spectral methods. The

https://doi.org/10.1017/S0962492906400015 Published online by Cambridge University Press

mesh equations and the PDE equations can then be solved together or alternately. We will discuss this in more detail presently in the context of moving mesh methods in higher dimensions, but it is appropriate to make some preliminary remarks here.

3.1.2. Finite difference methods

To motivate the discussion of appropriate discretizations, we assume that the underlying PDE system takes the form

$$\mathbf{u}_t = f(t, x, \mathbf{u}, \mathbf{u}_x, \mathbf{u}_{xx}). \tag{3.15}$$

If $x(\xi, t)$ is itself a time-dependent function of a computational variable ξ then (3.15) can be cast into the Lagrangian form in the moving coordinate system given by

$$\frac{\mathrm{d}\mathbf{u}}{\mathrm{d}t} = \mathbf{f}(t, x, \mathbf{u}, \mathbf{u}_x, \mathbf{u}_{xx}) + \mathbf{u}_x x_t. \tag{3.16}$$

The MMPDE governing the mesh motion gives a direct value for x_t. A method effective for solving (3.16) (in one-dimensional problems) is to use a semi-discretization. In this approach we discretize the differential equation (3.16) in the computational coordinates together with a similar discretization of the MMPDE (3.9). In such a semi-discretization we set

$$X_i(t) \approx x(i\Delta\xi, t) \quad \text{and} \quad U_i(t) \approx u(X_i(t), t).$$

As a simple example of the use of a finite difference method we can then take

$$u_x \approx \frac{U_{i+1} - U_{i-1}}{X_{i+1} - X_{i-1}} \quad \text{and} \quad u_{xx} \approx \frac{\frac{U_{i+1}-U_i}{X_{i+1}-X_i} - \frac{U_i - U_{i-1}}{X_i - X_{i-1}}}{\frac{X_{i+1}-X_{i-1}}{2}}. \tag{3.17}$$

These discretizations can then be substituted into (3.16) and the resulting set of ODEs for X_i and U_i solved along with one of the discretizations of (3.9). We discuss presently, and in more detail, the various alternating and simultaneous approaches for discretizing in time and then solving the resulting combined system.

On a static mesh, the truncation errors in calculating these finite difference approximations were given in the expressions (2.49) and (2.52). Provided that the stretching condition (2.10) is satisfied, then these errors are of second order.

We note, however, that additional errors may arise from the additional convective terms arising from the mesh movement, in particular the term

$$\mathbf{u}_x x_t \tag{3.18}$$

arising in (3.16). This additional term leads to both theoretical and practical difficulties in applying the moving mesh methods. From a theoretical

https://doi.org/10.1017/S0962492906400015 Published online by Cambridge University Press

perspective it is very possible that certain desirable properties of the equation (3.15) (such as symmetries, Hamiltonian structure and/or conservation laws) may not be inherited by the Lagrangian form (3.16). A practical difficulty, observed by Li *et al.* (1998), arises from certain discretizations of (3.18). In particular it was shown in this paper that it is possible that these can lead to instabilities and degrade the accuracy of the calculation. For example, if a centred finite difference approximation is used to discretize u_x, then from the expression (2.52) we have an additional truncation error given to leading order by (Li *et al.* 1998)

$$\dot{x}\frac{\Delta_i^2}{2}\left[\frac{x_{\xi\xi}}{x_\xi^2}u_{xx}+\frac{1}{3}u_{xxx}\right]. \tag{3.19}$$

It was observed in Li *et al.* (1998) that as $x_{\xi\xi}$ can be negative and $\dot{X}$ large, then the term $X_{\xi\xi}u_{xx}/x_{\xi^2}$ can be anti-diffusive (even dominating the diffusive terms in the underlying PDE), and hence destabilizing, and also potentially quite large. It was considered in Li *et al.* (1998) that this contributed to some large errors and instabilities arising in their calculation of the front solutions to Fisher's equation. Such problems were also observed in calculations of the nonlinear Schrödinger equation reported in Ceniceros (2002). Various strategies can be used to overcome such problems. These include increasing the mesh density in the unstable (wave front) region (Qiu and Sloan 1998), using a higher-order upwind strategy such as an ENO or Roe scheme (Li and Petzold 1997, Li *et al.* 1998) or a higher-order (fourth-order) centred difference scheme (Ceniceros 2002). (Alternatively, a static rezoning method can be used, as discussed in the next subsections.) An alternative strategy in one dimension is to use collocation, which deals with errors on non-uniform meshes very effectively, and we now describe this.

3.1.3. Collocation methods

Spline collocation gives a powerful method of discretizing the underlying partial differential equation in the physical domain, which has significant advantages over finite difference and finite element methods. In particular, it affords a continuous representation of the solution and its derivatives, provides a higher order of convergence, easily handles boundary conditions, and gives errors independent of local mesh grading, so that by using collocation we are able to avoid the problem of approximating high-order derivatives over a widely non-uniform mesh (Saucez, Vande Vouwer and Zegeling 2005). It also discretizes the PDE in the physical domain Ω_P and avoids the problems with the additional advective terms for the mesh movement described in Section 3.1.2. A very effective spline collocation discretization procedure coupled to various possible MMPDEs is adopted in the moving mesh collocation code MOVCOL, described in Huang and Russell (1996) (with

https://doi.org/10.1017/S0962492906400015 Published online by Cambridge University Press

extensions to higher-order systems using higher-degree Hermite polynomials, given in the code MOVCOL4 (Russell *et al.* 2007)) and this package has been used in many tests of adaptive methods in one dimension: see, for example, Huang and Russell (1996) and Budd *et al.* (1999*a*). Spline collocation methods for second-order PDEs (see Ascher, Christiansen and Russell (1981)) typically use a basis of third-degree cubic Hermite polynomials to give a piecewise smooth approximation $\mathbf{U}(x,t)$ over a series of N intervals $x \in [X_i(t), X_{i+1}(t)]$ to the solution $\mathbf{u}(x,t)$ of the underlying partial differential equation and its associated boundary conditions The collocation points are then chosen to be the Gauss points within the intervals. The interval points are precisely the mesh points moved by solving the MMPDE. The physical solution $u(x,t)$ is approximated on the moving mesh by the piecewise cubic Hermite polynomial

$$\begin{aligned}\mathbf{U}(x,t) = {} & \mathbf{U}_i(t)\phi_1(s^{(i)}) + \mathbf{U}_{x,i}(t)H_i(t)\phi_2(s^{(i)}) \\ & + \mathbf{U}_{i+1}(t)\phi_3(s^{(i)}) + \mathbf{U}_{x,i+1}(t)H_i(t)\phi_4(s^{(i)}),\end{aligned} \tag{3.20}$$

for $x \in [X_i(t), X_{i+1}(t)],\ i = 1, 2, \ldots,\ N-1$, where $\mathbf{U}_i(t)$ and $\mathbf{U}_{x,i}(t)$ denote the approximations to $\mathbf{u}(X_i(t),t)$ and $\mathbf{u}_x(X_i(t),t)$, respectively. The local coordinate $s^{(i)}$ is defined by

$$s^{(i)} := (x - X_i(t))/H_i(t), \quad H_i(t) := X_{i+1}(t) - X_i(t), \tag{3.21}$$

and the piecewise cubic shape functions are defined by

$$\begin{aligned}\phi_1(s) &:= (1+2s)(1-s)^2, & \phi_2(s) &:= s(1-s)^2, \\ \phi_3(s) &:= (3-2s)s^2, & \phi_4(s) &:= (s-1)s^2.\end{aligned} \tag{3.22}$$

For $x \in [X_i(t), X_{i+1}(t)],\ i = 1, \ldots, N-1$, we then have

$$\mathbf{U}_x(x,t) = \frac{1}{H_i}\left(\mathbf{U}_i\frac{\mathrm{d}\phi_1}{\mathrm{d}s} + \mathbf{U}_{x,i}H_i\frac{\mathrm{d}\phi_2}{\mathrm{d}s} + \mathbf{U}_{i+1}\frac{\mathrm{d}\phi_3}{\mathrm{d}s} + \mathbf{U}_{x,i+1}H_i\frac{\mathrm{d}\phi_4}{\mathrm{d}s}\right), \tag{3.23}$$

$$\mathbf{U}_{xx}(x,t) = \frac{1}{H_i^2}\left(\mathbf{U}_i\frac{\mathrm{d}^2\phi_1}{\mathrm{d}s^2} + \mathbf{U}_{x,i}H_i\frac{\mathrm{d}^2\phi_2}{\mathrm{d}s^2} + \mathbf{U}_{i+1}\frac{\mathrm{d}^2\phi_3}{\mathrm{d}s^2} + \mathbf{U}_{x,i+1}H_i\frac{\mathrm{d}^2\phi_4}{\mathrm{d}^2 s}\right), \tag{3.24}$$

$$\begin{aligned}\mathbf{U}_t(x,t) = {} & \frac{\mathrm{d}\mathbf{U}_i}{\mathrm{d}t}\phi_1 + \left(\frac{\mathrm{d}\mathbf{U}_{x,i}}{\mathrm{d}t}H_i + \mathbf{U}_{x,i}\frac{\mathrm{d}H_i}{\mathrm{d}t}\right)\phi_2 \\ & + \frac{\mathrm{d}\mathbf{U}_{i+1}}{\mathrm{d}t}\phi_3 + \left(\frac{\mathrm{d}\mathbf{U}_{x,i+1}}{\mathrm{d}t}H_i + \mathbf{U}_{x,i+1}\frac{\mathrm{d}H_i}{\mathrm{d}t}\right)\phi_4 \\ & - \mathbf{U}_x(x,t)\left(\frac{\mathrm{d}X_i}{\mathrm{d}t} + s^{(i)}\frac{\mathrm{d}H_i}{\mathrm{d}t}\right),\end{aligned} \tag{3.25}$$

https://doi.org/10.1017/S0962492906400015 Published online by Cambridge University Press

where ϕ_j, $(\mathrm{d}\phi_j/\mathrm{d}s)$ and $(\mathrm{d}^2\phi_j/\mathrm{d}^2 s)$, $j = 1, \ldots, 4$, are functions of $s^{(i)}$. These expressions for U and its derivatives can then be directly substituted into (3.15), and the expression

$$\mathbf{U}_t = \mathbf{f}(t, x, \mathbf{U}, \mathbf{U}_x, \mathbf{U}_{xx})$$

evaluated at the two Gauss points $X_{ij} = X_i + s_j H_i, j = 1, 2$, where

$$s_1 = \frac{1}{2}\left(1 - \frac{1}{\sqrt{3}}\right), \quad s_2 = \frac{1}{2}\left(1 + \frac{1}{\sqrt{3}}\right).$$

This, when coupled to the boundary conditions of the underlying PDE, leads to a set of ordinary differential equations for $\mathbf{U}_i, \mathbf{U}_{i,x}$ which can then be coupled directly to the ODEs for the moving mesh given, for example, by (3.11). In certain circumstances, such as when the underlying PDE has a conservation form, it is also possible for the collocation scheme to satisfy an analogous discrete conservation law. This procedure is implemented in MOVCOL and is described in detail in Huang and Russell (1996) The resulting ODEs are somewhat stiff, and are typically solved using an appropriate stiff solver such as an SDIRK (singly diagonally implicit Runge–Kutta) or a BDF (backward differentiation formula) method. In MOVCOL they are solved using a BDF method in the code dassl (Petzold 1982).

3.1.4. Spectral methods

Spectral methods provide an attractive alternative to finite difference and finite element methods for numerical solution of PDEs. They involve approximation by global basis functions, such as trigonometric or algebraic polynomials. For problems with smooth solutions the convergence rate of spectral methods is faster than algebraic, as the number of grid points increases, and the significance of this so-called spectral convergence is that a specified accuracy can usually be achieved using fewer grid points than would be required by the algebraically convergent finite difference or finite element approaches. However, if a solution has a steep region such as a boundary layer or an interior layer, spectral methods will achieve high accuracy only if the number of grid points is sufficiently high to permit resolution of the localized phenomena. To overcome this difficulty, a common approach is to apply a coordinate transformation that is designed to smooth out regions of high gradient. Such a transformation can be generated numerically and adaptively through a moving mesh method. Another benefit of using a moving mesh method is that PDEs can be conveniently discretized on the computational domain where a rectangular or cubic mesh is often used. Adaptivity of this type has proved successful, producing highly accurate solutions to problems that have steep, smooth solutions using a reasonably small number of grid points, although some care must be taken that the numerically generated coordinate transformation should be made sufficiently

https://doi.org/10.1017/S0962492906400015 Published online by Cambridge University Press

smooth to avoid possible deterioration of accuracy: see, *e.g.*, Mulholland, Huang and Sloan (1998), Wang and Shen (2005), Feng, Yu, Hu, Liu, Du and Chen (2006) and Tee and Trefethen (2006). While preliminary results are promising, much further investigation is needed to determine the full potential of these adaptive spectral methods.

3.2. MMPDEs and variational methods in n dimensions

3.2.1. Description of some variational-based methods

In the variational and MMPDE approaches of mesh adaptation in n dimensions, briefly described in Section 2, adaptive meshes are also generated as images of a computational mesh under a coordinate transformation from the computational domain to the physical domain. Such a coordinate transformation is determined by an adaptation functional, which is commonly designed to measure the difficulty in the numerical approximation of the physical solution. The functional often involves mesh properties and employs a monitor function to control mesh quality and mesh concentration. The key to the development of variational and MMPDE methods is the formulation of the adaptation functional. Direct-use standard-error estimates are often not appropriate since they often lead to non-convex functionals in two and higher dimensions. Instead, most of the existing methods have been developed based on physical, geometric, mesh quality control, and/or other considerations.

The functional can be formulated in terms of either the coordinate transformation $\mathbf{x} = \mathbf{F}(\boldsymbol{\xi}, t)$ or its inverse transformation $\boldsymbol{\xi} = \mathbf{F}^{-1}(\mathbf{x}, t)$. The latter has been used more commonly than the former because it is less likely to produce mesh tangling for non-convex domains (*e.g.*, see Dvinsky (1991)). In the latter case, the adaptation functional takes the general form

$$I(\boldsymbol{\xi}) = \int_{\Omega_P} G(\mathbf{M}, \boldsymbol{\xi}, \boldsymbol{\nabla}\xi_i)\,\mathrm{d}\mathbf{x}, \quad i = 1, \ldots, n, \tag{3.26}$$

where G is a continuous function of its arguments, $\mathbf{M}$ is the (scalar or matrix-valued) monitor function, and $\boldsymbol{\nabla}$ is the gradient operator with respect to the physical coordinate $\mathbf{x}$. Once a functional has been defined, an MMPDE can be obtained as described in (2.26) as the gradient flow equation of the functional (Huang and Russell 1997*b*, 1999), *i.e.*,

$$\frac{\partial \xi_i}{\partial t} = -\frac{P}{\epsilon}\frac{\partial I}{\partial \xi_i}, \quad i = 1, \ldots, n, \tag{3.27}$$

where P is a positive differential operator and $\epsilon > 0$ is a parameter for adjusting the time scale of mesh movement. For the general form (3.26), this becomes

$$\frac{\partial \xi_i}{\partial t} = \frac{P}{\epsilon}\left(\boldsymbol{\nabla} \cdot \frac{\partial G}{\partial(\boldsymbol{\nabla}\xi_i)} - \frac{\partial G}{\partial \xi_i}\right), \quad i = 1, \ldots, n. \tag{3.28}$$

https://doi.org/10.1017/S0962492906400015 Published online by Cambridge University Press

For example, Winslow's variable diffusion method (Winslow 1981), as described in Section 2, takes this form with

$$I(\boldsymbol{\xi}) = \frac{1}{2}\int_{\Omega_P} \frac{1}{w}\sum_i (\boldsymbol{\nabla}\xi_i)^T \boldsymbol{\nabla}\xi_i \,\mathrm{d}\mathbf{x}, \tag{3.29}$$

where w is the weight function prescribed by the user. We can also consider the generalized version of this method described in Huang and Russell (1997*b*, 1999), given by

$$I(\boldsymbol{\xi}) = \frac{1}{2}\int_{\Omega_P} \sum_i (\boldsymbol{\nabla}\xi_i)^T \mathbf{M}^{-1}\boldsymbol{\nabla}\xi_i \,\mathrm{d}\mathbf{x}, \tag{3.30}$$

where $\mathbf{M}$ is a matrix-valued monitor function in d dimensions. (Obviously, (3.30) reduces to (3.29) when $\mathbf{M} = wI$.)

Since $\boldsymbol{\xi} = \boldsymbol{\xi}(\mathbf{x}, t)$ does not explicitly define the location of mesh points, a mesh equation for $\mathbf{x}(\boldsymbol{\xi}, t)$ is commonly used in actual computation. Such an equation can be obtained by interchanging the dependent and independent variables in (3.27) or (3.28) and in the case of the variational principle (3.30) in two dimensions, we obtain the following MMPDE:

$$\begin{aligned}\frac{\partial}{\partial t}\begin{pmatrix}x\\ y\end{pmatrix} = &-\frac{1}{\epsilon|J|\sqrt{\det(\mathbf{M})}}\begin{pmatrix}x_\xi\\ y_\xi\end{pmatrix}\left\{\frac{\partial}{\partial\xi}\left[\frac{1}{|J|\det(\mathbf{M})}\begin{pmatrix}x_\eta\\ y_\eta\end{pmatrix}^T\mathbf{M}\begin{pmatrix}x_\eta\\ y_\eta\end{pmatrix}\right]\right.\\ &\left.-\frac{\partial}{\partial\eta}\left[\frac{1}{|J|\det(\mathbf{M})}\begin{pmatrix}x_\eta\\ y_\eta\end{pmatrix}^T\mathbf{M}\begin{pmatrix}x_\xi\\ y_\xi\end{pmatrix}\right]\right\}\\ &-\frac{1}{\epsilon|J|\sqrt{\det(\mathbf{M})}}\begin{pmatrix}x_\eta\\ y_\eta\end{pmatrix}\left\{-\frac{\partial}{\partial\xi}\left[\frac{1}{|J|\det(\mathbf{M})}\begin{pmatrix}x_\xi\\ y_\xi\end{pmatrix}^T\mathbf{M}\begin{pmatrix}x_\eta\\ y_\eta\end{pmatrix}\right]\right.\\ &\left.+\frac{\partial}{\partial\eta}\left[\frac{1}{|J|\det(\mathbf{M})}\begin{pmatrix}x_\xi\\ y_\xi\end{pmatrix}^T\mathbf{M}\begin{pmatrix}x_\xi\\ y_\xi\end{pmatrix}\right]\right\}.\end{aligned} \tag{3.31}$$

This MMPDE can be easily discretized to move the mesh. For details of this derivation, and a series of computations using it, see Huang (2001*a*). Most of these variational methods can be straightforwardly extended from two dimensions to n dimensions.

A disadvantage of all of the above-mentioned methods, such as the MMPDEs given in (3.31), is that the computations have to be done on a highly nonlinear system. Ceniceros and Hou (2001) also consider a variational principle using a scalar monitor function, but this time in the *computational domain*. After certain further simplifications this leads (in two dimensions) to the equations

$$\boldsymbol{\nabla}_{\boldsymbol{\xi}}\cdot(M\boldsymbol{\nabla}_{\boldsymbol{\xi}}x) = 0, \quad \boldsymbol{\nabla}_{\boldsymbol{\xi}}\cdot(M\boldsymbol{\nabla}_{\boldsymbol{\xi}}y) = 0. \tag{3.32}$$

Now *all derivatives are expressed in terms of the computational variables* so that $\boldsymbol{\nabla}_{\boldsymbol{\xi}} = (\partial_\xi, \partial_\eta)^T$, and the monitor function is considered as a function

https://doi.org/10.1017/S0962492906400015 Published online by Cambridge University Press

of the computational coordinates, *i.e.*, $M = M(\xi, \eta)$. A relaxation method is proposed by Ceniceros and Hou (2001) to solve (3.32), which leads to a set of moving mesh PDEs of the form

$$x_\tau = \boldsymbol{\nabla}_{\boldsymbol{\xi}} \cdot (M \boldsymbol{\nabla}_{\boldsymbol{\xi}} x), \quad y_\tau = \boldsymbol{\nabla}_{\boldsymbol{\xi}} \cdot (M \boldsymbol{\nabla}_{\boldsymbol{\xi}} y). \tag{3.33}$$

This system is significantly simpler than (3.31) and can be easily discretized. The above equation, when discretized, is rather stiff and can also benefit from a degree of mesh smoothing. A low-pass filter smoothing is applied to the monitor function by Ceniceros and Hou (2001). Smoothing can also be applied directly to the mesh itself, *e.g.*,

$$(1 - \gamma \Delta_{\boldsymbol{\xi}}) x_\tau = \boldsymbol{\nabla}_{\boldsymbol{\xi}} \cdot (M \boldsymbol{\nabla}_{\boldsymbol{\xi}} x), \quad (1 - \gamma \Delta_{\boldsymbol{\xi}}) y_\tau = \boldsymbol{\nabla}_{\boldsymbol{\xi}} \cdot (M \boldsymbol{\nabla}_{\boldsymbol{\xi}} y), \tag{3.34}$$

where $\gamma > 0$ is related to M (typically, if a time step of Δt is used then $\gamma = \Delta t \max(M)$). We note that in one dimension this system is exactly that given by (3.9). The MMPDE method (3.34) in discretized form has been used with success in a number of different applications, including Tang (2005), Zegeling (2007), Ceniceros (2002) and some of the examples in Section 5.

The harmonic map method of Dvinsky (1991) given in (2.34) uses the functional

$$I(\boldsymbol{\xi}) = \frac{1}{2} \int_{\Omega_P} \sqrt{\det(\mathbf{M})} \sum_i (\boldsymbol{\nabla} \xi_i)^T \mathbf{M}^{-1} \boldsymbol{\nabla} \xi_i \, \mathrm{d}\mathbf{x}, \tag{3.35}$$

while the method of Brackbill and Saltzman (1982) (*cf.* (2.35)) takes the form

$$I(\boldsymbol{\xi}) = \theta_a \int_{\Omega_P} w|J| \, \mathrm{d}\mathbf{x} + \theta_s \int_{\Omega_P} \sum_i (\boldsymbol{\nabla} \xi_i)^T \boldsymbol{\nabla} \xi_i \, \mathrm{d}\mathbf{x} + \theta_o \int_{\Omega_P} \sum_{i \neq j} ((\boldsymbol{\nabla} \xi_i)^T \boldsymbol{\nabla} \xi_j)^2 \, \mathrm{d}\mathbf{x}. \tag{3.36}$$

Following Winslow (1967), Thompson *et al.* (1985) use a system of elliptic differential equations for generating body-fitted, adaptive meshes. They propose using the Poisson equations

$$\boldsymbol{\nabla}^2 \xi_i = P_i(\mathbf{x})$$

to control the mesh concentration and direction, where P_i, $1 \leq i \leq d$, are control functions. The system can be interpreted as the Euler–Lagrange equation of the quadratic functional

$$I(\boldsymbol{\xi}) = \int_{\Omega_P} \sum_i (|\boldsymbol{\nabla} \xi_i|^2 - P_i \xi_i) \, \mathrm{d}\mathbf{x}. \tag{3.37}$$

Knupp and his co-workers (Knupp 1995, Knupp 1996, Knupp and Robidoux 2000, Knupp *et al.* 2002) determine the coordinate transformation

https://doi.org/10.1017/S0962492906400015 Published online by Cambridge University Press

such that its Jacobian matrix is as close as possible to a reference Jacobian matrix in the least-squares sense. One of the functionals they use is

$$I(\xi) = \int_{\Omega_P} \left\| \frac{\partial \xi}{\partial x} - K \right\|_F^2 \mathrm{d}s, \tag{3.38}$$

where $\|\cdot\|_F$ is the Frobenius norm and $K = K(\mathbf{x})$ is the user-prescribed, reference Jacobian matrix. A detailed discussion on how to choose the matrix K is given in Knupp (1996); see also Knupp and Robidoux (2000) for a broader discussion on algebraic properties of the Jacobian matrix.

The method of Huang (2001*b*) given in Section 2 (*cf.* (2.40)) augments the above variational principles with an additional contribution based on mesh quality control of equidistribution alignment, and orientation. The choice of the monitor function $\mathbf{M}$ in this method, based on interpolation error estimates, was extensively studied in Huang and Sun (2003) and Huang (2005*a*). The idea of mesh quality control was also used by Branets and Carey (2003) in developing their grid-smoothing variational method.

3.2.2. Examples of meshes generated

We now consider using certain of these methods described above to generate a series of meshes. In Section 3.3 we compare these results to the meshes generated by using an optimal transport algorithm.

Example 1. This example is to generate adaptive meshes for a given weight function,

$$w(x,y) = 1 + 10\exp\left(-50\left(y - \frac{1}{2} - \frac{1}{4}\sin(2\pi x)\right)^2\right), \quad \text{in } \Omega \equiv (0,1)\times(0,1).$$

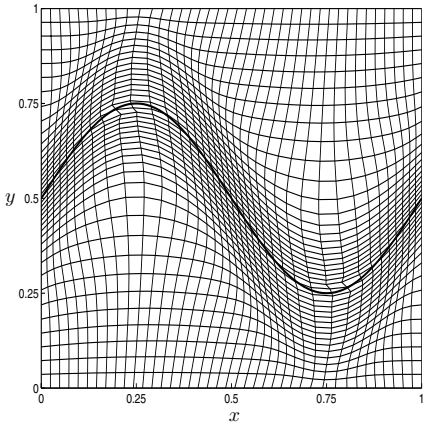
The monitor function is chosen to be $\mathbf{M} = wI$. Adaptive meshes are shown in Figure 3.1 using the harmonic mapping method, Winslow's method and the variational method with alignment control given in (2.40) with $\theta = 0.1$).

Example 2. In this example we generate adaptive moving meshes for the weight function

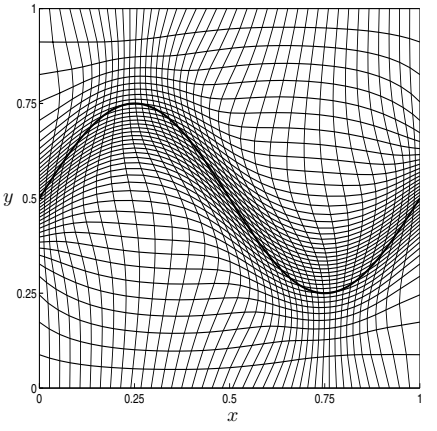
$$w(x,y,t) = 1 + 10\exp\left(-50\left|\left(x - \frac{1}{2} - \frac{1}{4}\cos(2\pi t)\right)^2 + \left(y - \frac{1}{2} - \frac{1}{4}\sin(2\pi t)\right)^2 - \left(\frac{1}{10}\right)^2\right|\right).$$

The monitor function is chosen as $\mathbf{M} = wI$. Adaptive meshes obtained using MMPDEs based on the methods in Example 1 are shown in Figures 3.2, 3.3, and 3.4.

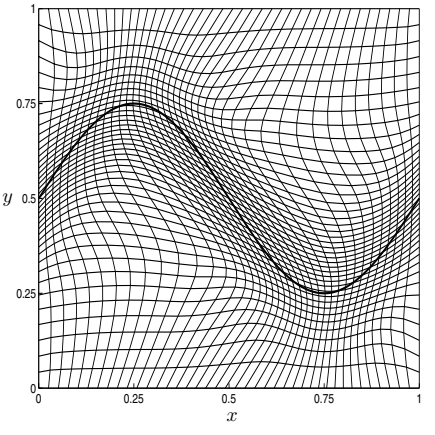
https://doi.org/10.1017/S0962492906400015 Published online by Cambridge University Press



(a) Harmonic mapping



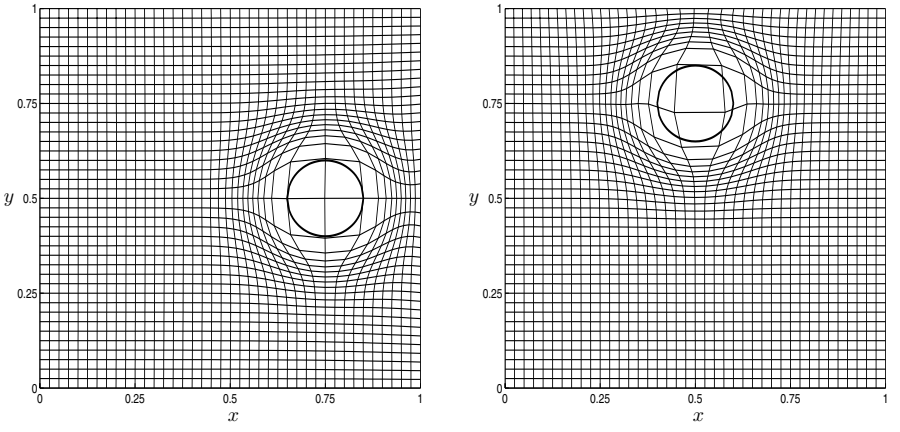
(b) Winslow's method



(c) New functional

Figure 3.1. *Example 1.* Adaptive moving meshes obtained by the harmonic mapping method, Winslow's method, and the method based on equidistribution and alignment control (2.40) ($\theta = 0.1$).

https://doi.org/10.1017/S0962492906400015 Published online by Cambridge University Press

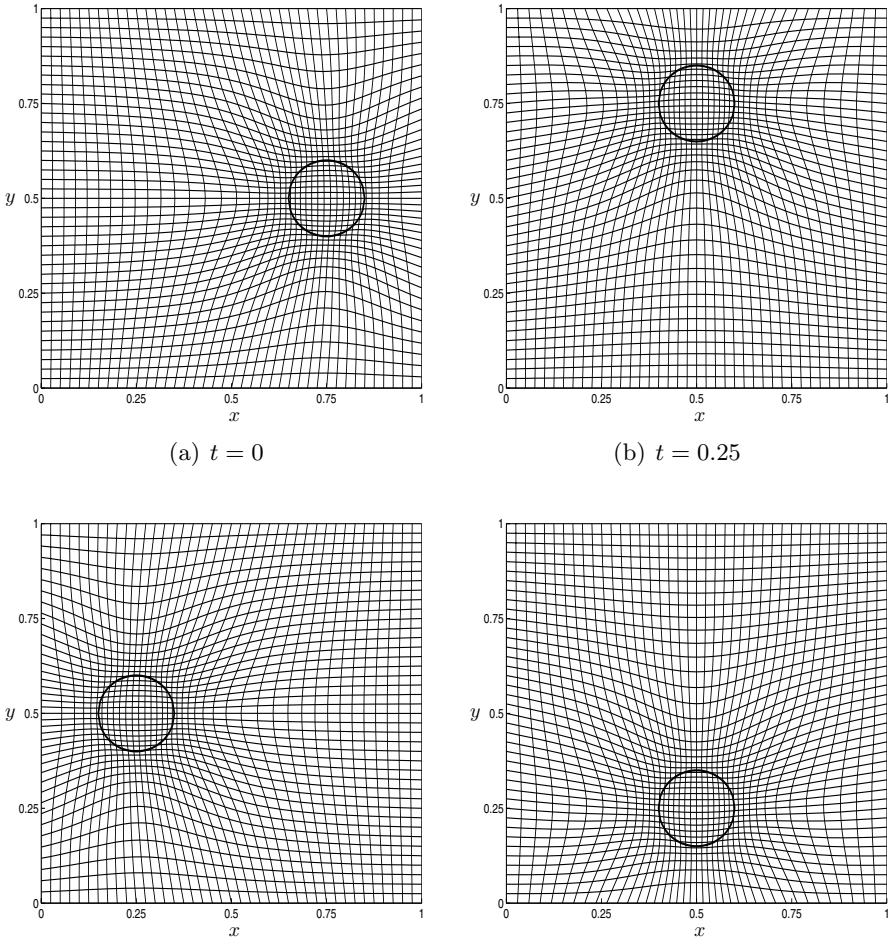


(a) $t = 0$ (b) $t = 0.25$

(c) $t = 0.5$ (d) $t = 0.75$

Figure 3.2. *Example 2.* Adaptive moving meshes obtained by MMPDEs based on the harmonic mapping method. The circles shown in this and the following figures indicate the locations where the mesh concentration is anticipated.

https://doi.org/10.1017/S0962492906400015 Published online by Cambridge University Press

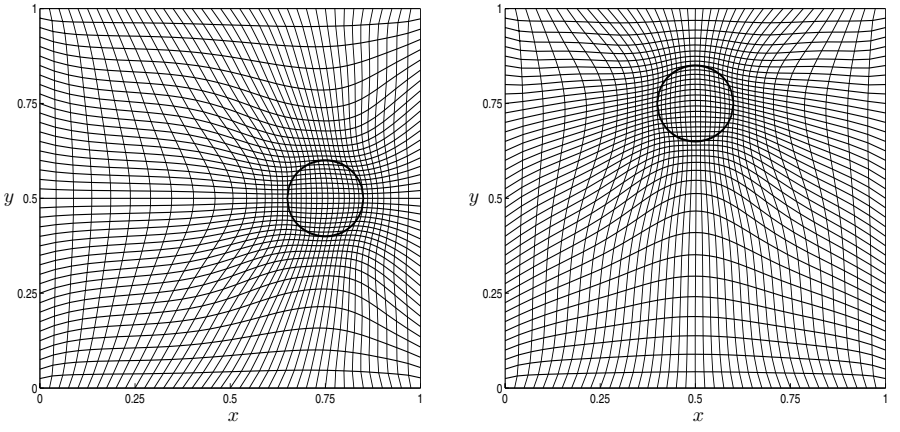


(a) $t = 0$ (b) $t = 0.25$

(c) $t = 0.5$ (d) $t = 0.75$

Figure 3.3. *Example 2.* Adaptive moving meshes obtained by MMPDEs based on Winslow's method.

https://doi.org/10.1017/S0962492906400015 Published online by Cambridge University Press



(a) $t = 0$ (b) $t = 0.25$

(c) $t = 0.5$ (d) $t = 0.75$

Figure 3.4. *Example 2.* Adaptive moving meshes obtained by MMPDEs based on the method with equidistribution and alignment control (2.40) ($\theta = 0.1$).

https://doi.org/10.1017/S0962492906400015 Published online by Cambridge University Press

Example 3. This example generates an adaptive mesh for a given analytical solution

$$\begin{aligned} u(x,y) = \tanh\left(30\left(x^2+y^2-\frac{1}{8}\right)\right) \\ + \tanh\left(30\left((x-0.5)^2+(y-0.5)^2-\frac{1}{8}\right)\right) \\ + \tanh\left(30\left((x-0.5)^2+(y+0.5)^2-\frac{1}{8}\right)\right) \\ + \tanh\left(30\left((x+0.5)^2+(y-0.5)^2-\frac{1}{8}\right)\right) \\ + \tanh\left(30\left((x+0.5)^2+(y+0.5)^2-\frac{1}{8}\right)\right) \end{aligned}$$

defined in $[-2,2]\times[-2,2]$. An adaptive mesh with a monitor function is based on isotropic and anisotropic estimates error in interpolating this function. This is expected to concentrate around five circles. Results are shown in Figure 3.5.

Example 4. This example generates a three-dimensional adaptive mesh for

$$u(x,y,z) = \tanh(100((x-0.5)^2+(y-0.5)^2+(z-0.5)^2)-0.0625)$$

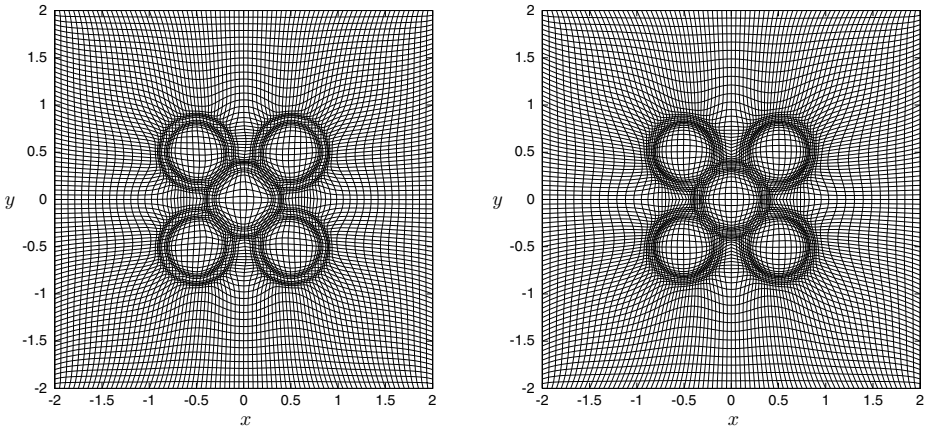
defined in the unit cube. An adaptive mesh with a monitor function is based on the error in interpolating this function. This is expected to concentrate near the sphere centred at $(0,0,0)$ with radius 0.25. Results are shown in Figure 3.6.

3.3. Optimal transport methods

3.3.1. Derivation of the optimal transport equations

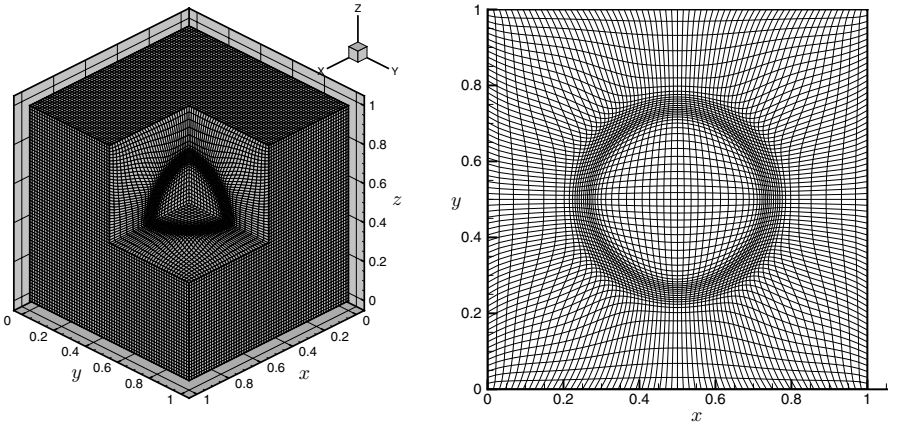
Optimal transport methods are a very natural generalization of MMPDE methods in one dimension, that retain much of the simplicity of the one-dimensional approach (such as always solving scalar equations and automatic calculation of the mesh on a boundary) whilst being general enough to deliver meshes of provable mesh quality (with many of the proofs following directly from the one-dimensional case). They have the disadvantage of being less flexible than some of the moving mesh methods described above. However, in practice they can give very regular meshes for a wide range of possible monitor functions. The key idea behind an optimal mesh is that it should be one which is closest to a uniform mesh in a suitable norm, consistent with satisfying the equidistribution principle. The simplest such

https://doi.org/10.1017/S0962492906400015 Published online by Cambridge University Press



(a) $M_{\text{iso}}, (l, m) = (2, 1)$ (b) $M_{\text{ani},2}, (l, m) = (2, 1)$

Figure 3.5. *Example 3.* Adaptive meshes of size $N = 81 \times 81$ obtained using the variational method (2.40) ($\theta = 0.1$) for different monitor functions based on isotropic and anisotropic interpolation error estimates.



(a) Winslow's type; $(k, m) = (1, 1)$ (b) Winslow's type; $(k, m) = (1, 1)$

Figure 3.6. *Example 4.* An adaptive mesh of size $N = 65 \times 65 \times 65$ obtained using the variational method (2.40) ($\theta = 0.1$) for a monitor function based on interpolation error. (a) Cut-away plot of the mesh. (b) Plane projection of slice at $K_z = 32$ of the mesh in (a).

https://doi.org/10.1017/S0962492906400015 Published online by Cambridge University Press

norm is the least-squares norm given by

$$I = \int_{\Omega_C} |\mathbf{F}(\boldsymbol{\xi}, t) - \boldsymbol{\xi}|^2 \, \mathrm{d}\boldsymbol{\xi}. \tag{3.39}$$

Minimizing I subject to the equidistribution principle is in fact the celebrated Monge–Kantorovich problem from differential geometry. This principle is often called optimum transport, as it leads to a transformation, the creation of which takes a minimum amount of work as a deviation from the identity. Intuitively, this is likely to deliver a regular mesh, as this mesh will be as close (in an averaged sense) to the most regular possible mesh, *i.e.*, a completely uniform one. Remarkably, this minimization problem has a unique solution with a very elegant expression for the transformation.

Theorem 3.3. There *exists* a *unique* optimal mapping $\mathbf{F}(\boldsymbol{\xi}, t)$ satisfying the equidistribution equation. This map has the same regularity as M. Furthermore, $\mathbf{F}(\boldsymbol{\xi}, t)$ is the unique mapping from this class which can be written as the gradient (with respect to $\boldsymbol{\xi}$) of a *convex* (mesh) potential $P(\boldsymbol{\xi}, t)$, so that

$$\mathbf{F}(\boldsymbol{\xi}, t) = \boldsymbol{\nabla}_{\boldsymbol{\xi}} P(\boldsymbol{\xi}, t), \quad \Delta_{\boldsymbol{\xi}} P(\boldsymbol{\xi}, t) > 0. \tag{3.40}$$

Proof. See Brenier (1991) or Caffarelli (1992, 1996) for an abstract proof and Delzanno *et al.* (2008) for a proof in the context of adaptive mesh generation. □

The following is then immediate.

Lemma 3.4. The map $\mathbf{F}$ is *irrotational* so that $\boldsymbol{\nabla}_{\boldsymbol{\xi}} \times \mathbf{F} = \mathbf{0}$, and the Jacobian of $\mathbf{F}$ is *symmetric*.

Significantly, the transformation above is an example of a *Legendre transformation* (Sewell 2002). Such transformations include translations and linear maps by positive definite symmetric matrices. We now show how to calculate such a transformation.

3.3.2. Properties of optimally transported meshes

It is immediate that if $\mathbf{x} = \boldsymbol{\nabla}_{\boldsymbol{\xi}} P$ then

$$\frac{\partial \mathbf{x}}{\partial \boldsymbol{\xi}} = H(P),$$

where $H(P)$ is the *Hessian* of P. Additionally, if the measure $M \in W^2(\Omega_P)$ is strictly positive on its supports (assumed to be convex), then the potential $P \in W^2_{\mathrm{loc}}(\Omega_C)$, and satisfies, in the classical sense, the Monge–Ampère equation

$$M(\boldsymbol{\nabla}_{\boldsymbol{\xi}} P, t) H(P) = \theta(t). \tag{3.41}$$

https://doi.org/10.1017/S0962492906400015 Published online by Cambridge University Press

Here $H(P)$ denotes the determinant of the Hessian matrix of P. This is a famous equation in differential geometry. Solving it defines the map $\mathbf{F}$ *uniquely*. In order to solve it we must specify boundary conditions for the solution. In general applications of mesh generation we consider bounded domains mapping to bounded domains. We can then prescribe a boundary condition where equation (3.41) is supplemented with the condition that the boundary must map to the boundary. Suppose that the points on the boundary of Ω_C satisfy the implicit equation $G_C(\boldsymbol{\xi}) = 0$ and those on the boundary of Ω_P satisfy the implicit equation $G_P(\mathbf{x}) = 0$, we then have the following (nonlinear) Neumann boundary condition for (3.41):

$$G_P(\boldsymbol{\nabla}_{\boldsymbol{\xi}} P, t) = 0 \quad \text{if} \quad G_C(\boldsymbol{\xi}, t) = 0. \tag{3.42}$$

The existence, uniqueness and regularity of the solutions of (3.41) and (3.42) has been well studied (Brenier 1991, Caffarelli 1992, Caffarelli 1996). From the point of view of grid generation this puts us into the nice situation of being able to infer properties of the mesh from those of a function P with known regularity. We have the following very important result.

Theorem 3.5. If both Ω_C and Ω_P are *smooth*, *convex* domains then (3.41) and (3.42) have a unique solution (up to an additive constant), which is as regular as the monitor function M. This in turn leads to a unique regular mesh.

Proof. This follows immediately from the results of Brenier (1991) and Caffarelli (1992, 1996). □

If Ω_C or Ω_P are not smooth then there is a possible loss of mesh regularity. In the case of solutions which are logical rectangles, this is not severe and applies only at the corners, where it can be shown (Cullen 1989) that $P \in C^3$ and $F \in C^2$. This is sufficient regularity for most applications.

An immediate consequence of this result is that the solution of the Monge–Ampère equation defines a map not only from Ω_C to Ω_P, but also between the boundaries of the respective domains. This is a desirable property from the perspective of mesh generation as we do not have to consider separate equations for the mesh on the boundary. This is in contrast to the variational methods described in Section 3.2.1, which require separate equations to describe the mesh on the boundaries. As an example, we can consider meshes on logical cubes, taking

$$\Omega_C = [0,1]^d = \Omega_P. \tag{3.43}$$

The boundary conditions above then reduce to

$$P_\xi = 0, 1 \quad \text{if} \quad \xi = 0, 1, \quad P_\eta = 0, 1 \quad \text{if} \quad \eta = 0, 1. \tag{3.44}$$

The boundary condition (3.44) applied in two dimensions implies the orthogonality of the grid lines at the boundaries of the square. To see this,

https://doi.org/10.1017/S0962492906400015 Published online by Cambridge University Press

consider the bottom boundary of the square in the physical domain, for which $Y = 0$. A grid line Γ which intersects this side is given by

$$\Gamma = \{(x, y) : 0 \leq \eta \leq 1, \quad \xi \quad \text{fixed}\}.$$

The tangent to this line in the physical domain is given by $\boldsymbol{\tau} = (x_\eta, y_\eta)^T$, and, trivially, the tangent to the bottom boundary of the square by the vector $\mathbf{t} = (1, 0)^T$. However, on the bottom boundary, the function P satisfies the identity $P_\eta(\xi, 0) = 0$ and by definition $x = P_\xi$. It follows immediately that when $\eta = 0$,

$$x_\eta(\xi, 0) = P_{\eta\xi}(\xi, 0) = 0,$$

so that on the lower boundary $\boldsymbol{\tau} \cdot \mathbf{t} = 0$. Thus the mesh is orthogonal to the lower boundary. Similar results apply to the other sides as well. The condition of mesh orthogonality at the boundary of the square is often desirable in certain circumstances (Thompson *et al.* 1985). However, it may cause problems when resolving features, such as fronts, which intersect boundaries at an angle. In such cases it may be useful to refine the mesh close to the boundary, either by introducing a finer computational mesh there, or by locally increasing the value of the monitor function M at mesh points adjacent to the boundary.

Mesh symmetries. Some very desirable properties of the mesh follow immediately from the properties of the Monge–Ampère equation. It is trivial to see that the equation is invariant under translations in (ξ, η). It is also easy to see that (in a similar manner to the Laplacian operator) the Monge–Ampère equation is also invariant under any *orthogonal* map such as a rotation or a reflection. This is because the Monge–Ampère equation is the determinant of the Hessian, which transforms covariantly under such maps. This simple observation implies that (away from boundaries) the meshes generated by solving the Monge–Ampère equation should have no difficulty aligning themselves to structures, such as shocks, which may occur anywhere in a domain and at any orientation. It is immediate that the Monge–Ampère equation is also invariant under *scaling transformations* of the form $\xi \to \lambda\xi$, $\eta \to \mu\eta$, $P \to \nu P$, provided that M is chosen carefully.

Mesh skewness. The regularity of the mesh generated by this approach gives a useful feature in seeing control in the variation of the element size across the domain. In general the meshes generated by the Monge–Ampère equation have good regularity properties and are effective in interpolating functions (Delzanno *et al.* 2008). It is possible to make some estimates for the resulting skewness of the mesh in terms of the properties of the function P. Consider a two-dimensional problem for which the map from Ω_C to Ω_P has

https://doi.org/10.1017/S0962492906400015 Published online by Cambridge University Press

the Jacobian J. A measure for the skewness s of the mesh in Ω_P is given by

$$s = \frac{\lambda_1}{\lambda_2} + \frac{\lambda_2}{\lambda_1} = \frac{(\lambda_1 + \lambda_2)^2}{\lambda_1 \lambda_2} - 2 = \frac{\mathrm{trace}(J)}{\det(J)} - 2 = \frac{\Delta(P)^2}{H(P)} - 2, \qquad (3.45)$$

where λ_1 and λ_2 are the (real and positive) eigenvalues of J. The skewness can be estimated in certain cases. One example of this arises in the scale-invariant meshes for the local singularities blow-up problems studied in Section 5, in which a sequence of meshes are calculated which, close to the singularity, take the form $P(\xi, t) = \Lambda(t)\hat{P}(\xi)$ for an appropriate scaling function $\Lambda(t)$. It is immediate that

$$\frac{\Delta(P)^2}{H(P)} - 2 = \frac{\Delta(\hat{P})^2}{H(\hat{P})} - 2,$$

so that the skewness of the rescaled mesh is the same as the original. Hence, if an initially uniform mesh is used then the mesh close to the singularity will retain local uniformity.

3.3.3. Solution of the Monge–Ampère equation

The equation (3.41) can be solved either directly (Delzanno *et al.* 2008) or by a relaxation method.

The direct method. The Monge–Ampère equation (Evans 1999, Gutiérrez 2001) belongs to the class of fully nonlinear second-order equations and has two sources of nonlinearity. Firstly, the Hessian $H(P)$ is nonlinear in the second derivatives (except in the one-dimensional case). Secondly, the monitor function in general depends nonlinearly on the first derivatives of P (either directly or through the solution of the original PDE). For any suitably smooth positive monitor function the equation has a unique solution, which is a convex function. Linearization of the equation shows that it is elliptic in the space of convex functions. The Monge–Ampère equation arises from prescribing the product of the eigenvalues (the determinant) of the Jacobian matrix of a gradient mapping. If we prescribe the sum of the eigenvalues (the trace) then we obtain a standard Poisson equation. For the Poisson equation, multigrid methods can find the solution of a discretization on a grid with $\mathcal{O}(N)$ unknowns using $\mathcal{O}(N)$ operations. Methods for solving the Monge–Ampère equation aim to obtain the same computational complexity.

Oliker and Prussner (1988) propose a specially designed discretization and iterative method which explicitly preserve the convexity of the iterates. Benamou and Brenier (2000) transform the Monge–Ampère equation into a time-dependent fluid mechanics problem, which is solved using an iterative method based on an augmented Lagrangian approach. Dean and Glowinski (2003, 2004) propose finite element discretizations based on an

https://doi.org/10.1017/S0962492906400015 Published online by Cambridge University Press

augmented Lagrangian approach and a least-squares formulation respectively. Feng and Neilan (2009) consider the nonlinear second-order equation as the limiting equation of a singularly perturbed fourth-order quasilinear equation. Chartrand, Vixie, Wohlberg and Bollt (2007) show that the Monge–Ampère equation can be reformulated as an unconstrained optimization problem, which can be solved by a gradient descent method. A special property of the mappings generated by the Monge–Ampère equation is that they are irrotational, *i.e.*, the curl is zero. Haker and Tannenbaum (2003) propose a gradient descent method that uses a Poisson solve in each step to 'remove the curl'. The nonlinear multigrid method developed in Fulton (1989) for the semigeostrophic equation should be easily adapted to our problem. A Newton–Krylov-multigrid method is proposed in Delzanno *et al.* (2008). The above methods all try to solve the fully nonlinear Monge–Ampère equation directly. It was a remarkable achievement of Kantorovich to show that the problem can be relaxed to a linear one by considering not a transport map $\boldsymbol{\xi} \to \mathbf{x} = \mathbf{F}(\boldsymbol{\xi})$, but a transport plan $G(\boldsymbol{\xi}, \mathbf{x})$ indicating the amount of material to be transported from ξ to x (Rachev and Rüschendorf 1998, Evans 1999). Robust methods exist for solving the corresponding linear programming problem, but to the best of our knowledge these methods typically require $\mathcal{O}(N^2)$ operations (Kaijser 1998, Balinski 1986), which is unacceptable except for small problems.

The parabolic Monge–Ampère (PMA) *method.* An alternative approach motivated by the discussion of the MMPDEs given earlier, is to introduce a parabolic regularization to (3.41) so that the gradient of solutions of this evolve toward the gradient of the solutions of (3.41) over a (relatively) short time scale. This method also couples naturally to the solution of a time-dependent PDE. Accordingly we consider using *relaxation* to generate an approximate solution of (3.41), which evolves together with the solution of the underlying PDE. Accordingly we consider a time-evolving function $Q(\boldsymbol{\xi}, t)$ with associated mesh $\mathbf{x}(\boldsymbol{\xi}, t) = \boldsymbol{\nabla}_{\boldsymbol{\xi}} Q(\boldsymbol{\xi}, t)$, with the property that this mesh should be close to that determined by the solution of the Monge–Ampère equation. To do this we consider a relaxed form of (3.41) taking the form of a parabolic Monge–Ampère equation (PMA) of the form

$$\epsilon(I - \gamma\Delta_{\boldsymbol{\xi}})Q_t = \big(H(Q)M(\boldsymbol{\nabla}_{\boldsymbol{\xi}} Q)\big)^{1/n}. \tag{3.46}$$

To find a moving mesh, we start with an initially uniform mesh for which

$$Q(\boldsymbol{\xi}, 0) = \frac{1}{2}|\boldsymbol{\xi}|^2.$$

The function Q then evolves according to (3.46). In (3.46) the scaling power $1/n$ is necessary for global existence of the solution. This is because if Q is scaled by a factor $L(t)$ then the Hessian term $H(Q)$ scales as $L(t)^n$.

https://doi.org/10.1017/S0962492906400015 Published online by Cambridge University Press

If M is constant, then equation (3.46) without the power law scaling admits a variables-separable solution for which $L_t = CL^n$. If $n > 1$ then this equation has solutions which blow up in a finite time. The rescaling prevents this possibility. The operator on the left of this system is a smoothing operator, similar to the operator used in (2.14), (3.9), which reduces the stiffness of this system when it is discretized. Observe that the term $\theta(t)$ has not been included in (3.46). Indeed this term arises naturally as a constant of integration. The PMA equation (3.46) has many properties in common with the moving mesh equation (3.9). In particular, if M is independent of time then the solution of (3.41) corresponds to a stable solution of (3.46). Indeed, we have the following results.

Lemma 3.6.

(a) Suppose that $M_t = 0$ and the Monge–Ampère equation (3.41) admits a (steady) convex solution $P(\boldsymbol{\xi})$ with associated map $\mathbf{x}(\boldsymbol{\xi})$ for which $H(P) > 0$, so that P satisfies the equation

$$M(\boldsymbol{\nabla} P)H(P) = \theta.$$

Then:

(i) the PMA equation (3.46) admits a time-dependent solution

$$Q(\boldsymbol{\xi}, t) = \frac{\theta^{1/n} t}{\epsilon} + P(\boldsymbol{\xi}) \tag{3.47}$$

for which $\boldsymbol{\nabla}_{\boldsymbol{\xi}} Q = \boldsymbol{\nabla}_{\boldsymbol{\xi}} P = \mathbf{x}(\boldsymbol{\xi})$;

(ii) the resulting mesh is locally stable.

(b) If M is slowly varying, then the solution of (3.46) remains ϵ-close to a solution of (3.41) for all time.

Proof. This is given in Budd and Williams (2009) and is very similar to the corresponding proof given for the stability of (3.9) □

It is also possible to show (Budd and Williams 2009) that, throughout the evolution of the mesh, if $H(Q)$ and ΔQ are initially positive then they stay positive for all time. This application of the maximum principle guarantees that the map generating the mesh is locally invertible for all time, and hence no mesh tangling can occur. This is a very useful feature of such r-adaptive methods, and we will see numerical examples of this in the following calculations.

3.3.4. Discretizing the parabolic Monge–Ampère equation (3.46)

To discretize (3.46) in space we can impose a uniform grid of mesh size $\Delta\xi$ on the computational space and assume that Q and Q_t take point values

https://doi.org/10.1017/S0962492906400015 Published online by Cambridge University Press

$Q_{i,j}(t)$, $i, j = 0 \dots N$, *etc.*, on this grid. The Hessian operator $H(Q)$ can be discretized with central differencing using a nine-point stencil interior to the domain Ω_C to evaluate all second derivatives in $H(Q)$. For the boundary points, the central differences are replaced by Taylor series expansions, using the respective conditions $Q_\xi = 0$ or $Q_\xi = 1$, and so on. The gradient $\boldsymbol{\nabla} Q$ is calculated similarly, so that the right-hand side of (3.46) can be determined. To determine the values of Q_t at the mesh points we then invert the operator $(I - \gamma \Delta_{\boldsymbol{\xi}})$. As the system is posed on a uniform (rectangular) mesh in the computational domain, this inversion can be done very rapidly by using a fast spectral solver based upon the discrete cosine transform (invoking the Neumann boundary conditions for Q_t). Knowing Q_t we may then determine $\mathbf{x}_t$ by taking the gradient.

3.3.5. Examples of meshes generated using the PMA method

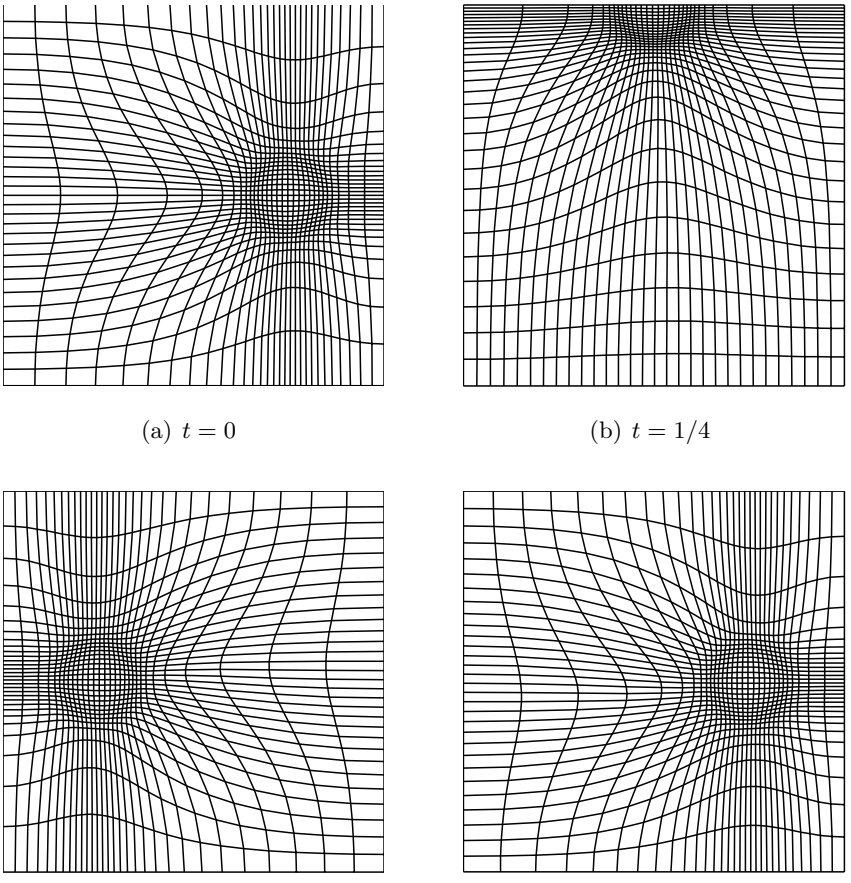
To give some flavour of the behaviour of moving mesh methods, we now consider some meshes generated using the PMA method for a known monitor function $M(x, y, t)$, choosing examples which can be compared with other methods presented both in the literature and in other sections of this article. In all of these following calculations we take $\epsilon = 0.01$, and the ODEs obtained by the discretization described above are solved in MATLAB using the routine `ode45`. All runs took under 5 minutes on a standard desktop computer.

Example 1. We first take a case motivated by Cao *et al.* (2002) (see also Section 4) with a monitor function localized over a moving circle of the form

$$M_1(x, y, t) = 1 + 5 \exp(-50|(x - 1/2 - 1/4 \cos(2\pi t))^2 + (y - 1/2 - \sin(2\pi t)/2)^2 - 0.01|).$$

This can be a severe test of a moving mesh method, and the meshes calculated from this using the (velocity-based) geometric conservation law method (Cao *et al.* 2002) have a high degree of skewness. To compute a corresponding moving mesh using the parabolic Monge–Ampère method (and also the solutions in all of the examples in this subsection) we use a uniform computational mesh to solve (3.46) with $N = 30$ mesh points in each direction and mapping the unit square to the unit square. We see from this calculation that the resulting mesh closely follows the moving circle with no evidence of skewness or irregularity. Note the orthogonality and regularity of the mesh at the boundary of the domain. Notice further that in Figure 3.7 the solution partially exits the domain with no ill consequence, and that the grid at $t = 10$ is virtually indistinguishable from that at $t = 0$. It is clear from these figures that the mesh generated has excellent regularity. Observe the high degree of mesh uniformity close to the solution maximum.

https://doi.org/10.1017/S0962492906400015 Published online by Cambridge University Press



(a) $t = 0$ (b) $t = 1/4$

(c) $t = 1/2$ (d) $t = 10$

Figure 3.7. *Example 1.* Snapshots at $t = 0$ (a), $t = 1/4$ (b), $t = 1/2$ (c), $t = 10$ (d). As the solution is advected, the grid follows the maxima of the solution and does not ever fall behind or become distorted.

https://doi.org/10.1017/S0962492906400015 Published online by Cambridge University Press

Example 2. In an example taken directly from Cao *et al.* (2002), we consider a monitor function localized on a sine wave of the form

$$M_2(x, y, t) = 1 + 5\exp(-50|(y - 1/2 - 1/4\sin(2\pi x)\sin(2\pi t)|),$$

and proceed to use exactly the same method as described in Example 1. See Figure 3.8.

In this example we again see that the PMA method has generated a very regular and periodic (in time) mesh.

Example 3. In this example we consider a monitor function localized on the support of two travelling linear fronts moving toward each other and show the resulting mesh in Figure 3.9. For this we take

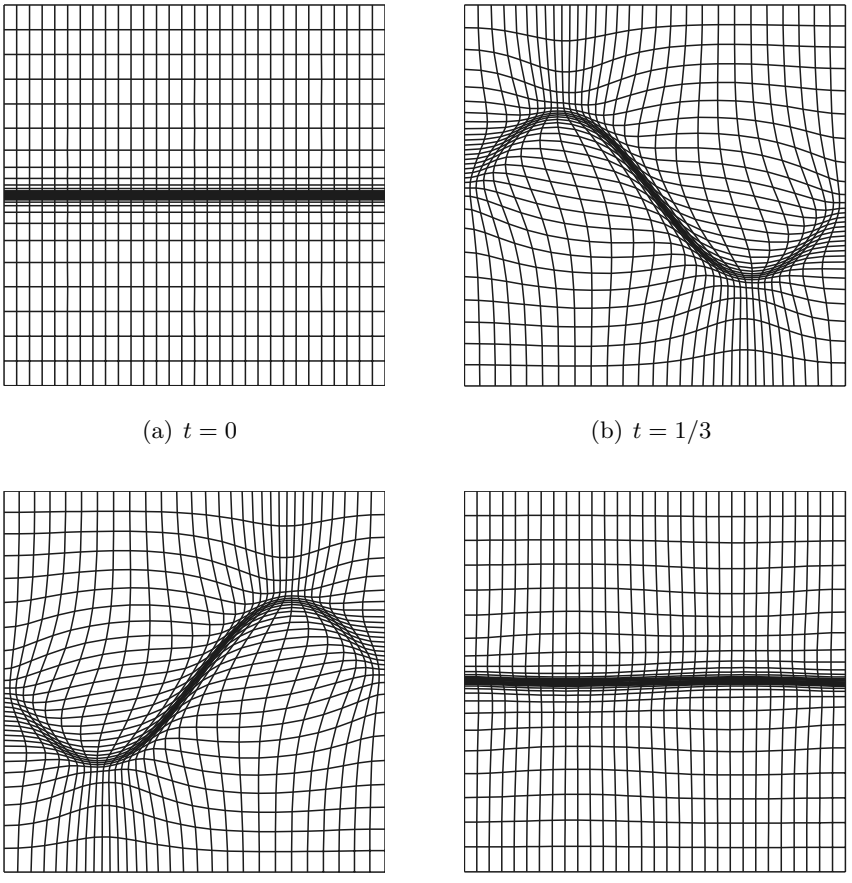
$$\begin{aligned} &x_0 = t, && y_0 = 0.2 + t/2, && u_0 = \gamma\,\mathrm{sech}(\lambda(x - x_0 + y - y_0)),\\ &x_1 = 1 - t, && y_1 = 0.8 - t/2, && u_1 = \gamma\,\mathrm{sech}(\lambda(x - x_1 + y - y_1)),\\ &M_3(x, y, t) = 1 + u_0 + u_1, \end{aligned}$$

with $\gamma = 5$ and $\lambda = 100$. We note that the fronts pass through each other without generating spurious oscillations in the mesh. Note also that the solution points do not follow the front (moving in and out of the region of high mesh density), but that the *density* of the solution points does. Observe that the mesh automatically aligns itself along the front. A close-up of the mesh close to the front is given in Figure 3.11 (see p. 187). This shows very good resolution of the local structure close to the front and a smooth transition from a uniform mesh to one refined at the front. If γ is large, then close to the front we see a mesh compression proportional to γ orthogonal to the front, with a local skewness of $s = \gamma$. The PMA method in this case thus generates a smooth mesh, for which the degree of skewness can be controlled via the choice of γ. More details of this calculation are given in Walsh *et al.* (2009). We can also see the effects of mesh orthogonality close to the boundaries of the domain.

Example 4. In this example we look at a monitor function localized on the support of two fronts meeting at an angle: see Figure 3.10. The behaviour of the mesh close to the front is similar to that in the last example. Significantly, there is no mesh tangling as the two fronts intersect. In Figure 3.12 we show a close-up of the intersection region, showing the high degree of mesh regularity. For this we take

$$\begin{aligned} &x_0 = t, && y_0 = 0.2 + t/2, && u_0 = \gamma\,\mathrm{sech}(\lambda(x - x_0 + y - y_0)),\\ &x_1 = 1 - t, && y_1 = 0.8 - t, && u_1 = \gamma\,\mathrm{sech}(\lambda(x - x_1 + (y - y_1)/2)),\\ &M_4(x, y, t) = 1 + u_0 + u_1. \end{aligned}$$

https://doi.org/10.1017/S0962492906400015 Published online by Cambridge University Press

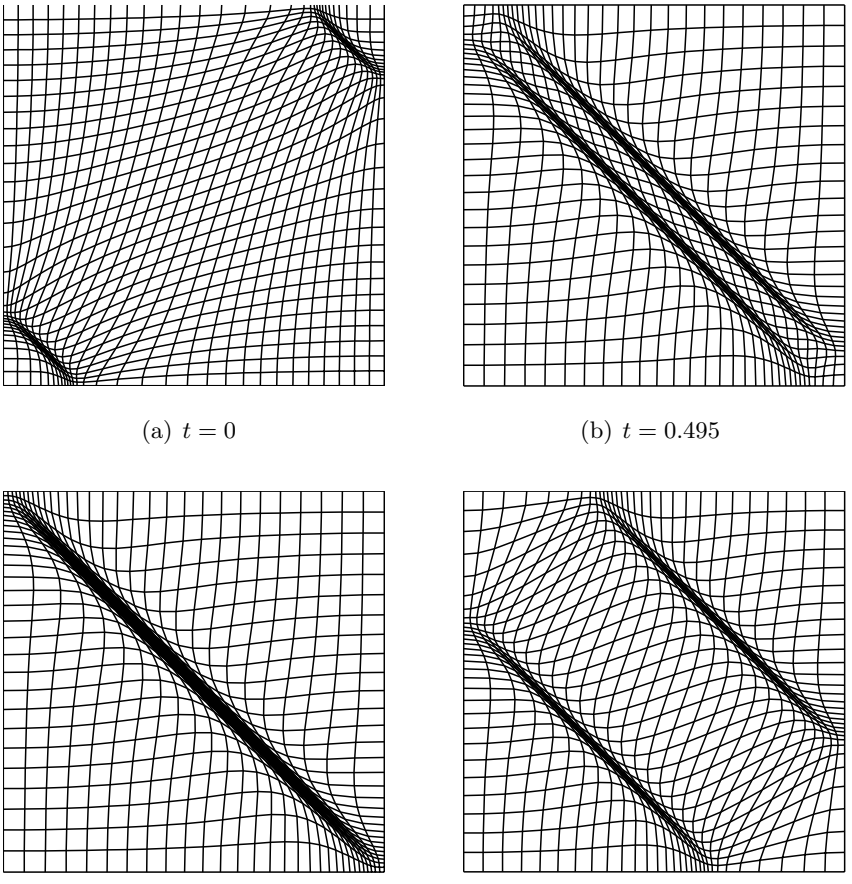


(a) $t = 0$ (b) $t = 1/3$

(c) $t = 2/3$ (d) $t = 1$

Figure 3.8. *Example 2.* Snapshots at $t = 0$ (a), $t = 1/3$ (b), $t = 2/3$ (c), $t = 1$ (d). In this figure we see both the smoothness and the periodic (in time) form of the mesh.

https://doi.org/10.1017/S0962492906400015 Published online by Cambridge University Press

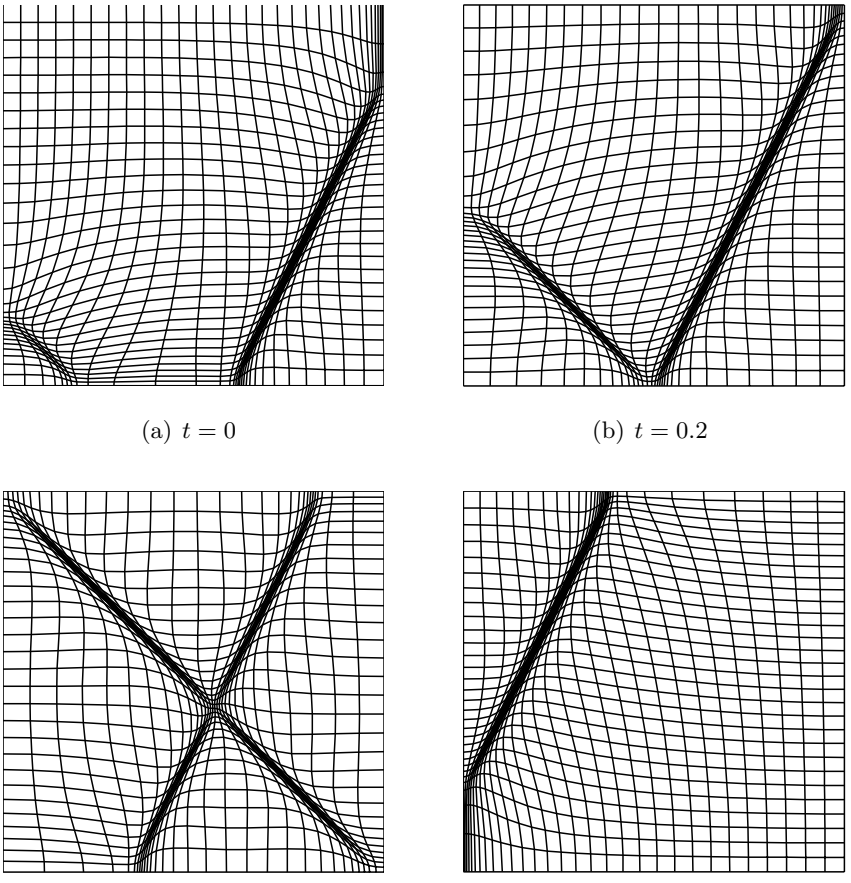


(a) $t = 0$ (b) $t = 0.495$

(c) $t = 0.525$ (d) $t = 0.75$

Figure 3.9. *Example 3.* Snapshots at $t = 0$ (a), $t = 0.495$ (b), $t = 0.525$ (c), $t = 0.75$ (d). Here we have simulated two fronts passing through each other in parallel, and see no difficulties with the resulting mesh. Note the way that the mesh automatically aligns itself parallel to the front.

https://doi.org/10.1017/S0962492906400015 Published online by Cambridge University Press



(a) $t = 0$ (b) $t = 0.2$

(c) $t = 0.525$ (d) $t = 1.4$

Figure 3.10. *Example 4.* Snapshots at $t = 0$ (a), $t = 0.2$ (b), $t = 0.525$ (c), $t = 1.4$ (d). Here we have simulated two linear travelling fronts passing through each other at an angle and see no difficulties in generating and moving the mesh.

https://doi.org/10.1017/S0962492906400015 Published online by Cambridge University Press

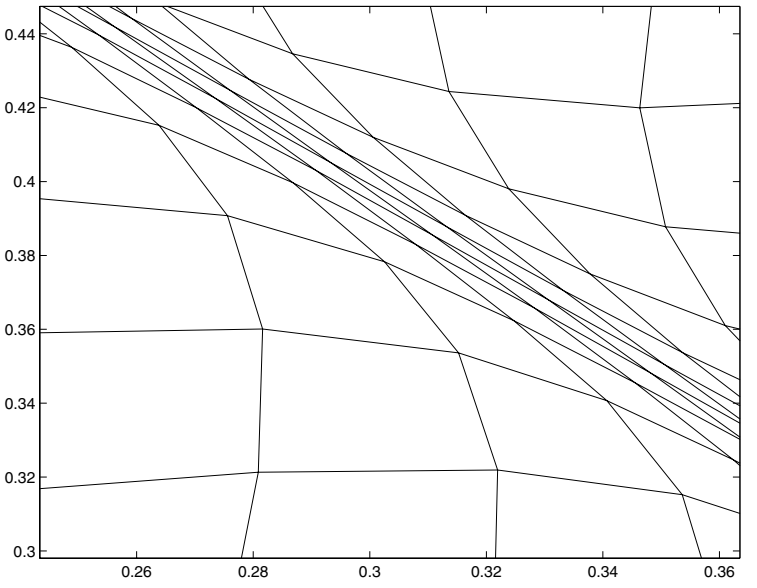


Figure 3.11. *Example 3.* A close-up of the mesh close to the front, showing the transition from a uniform mesh to one compressed by a factor γ orthogonal to the front.

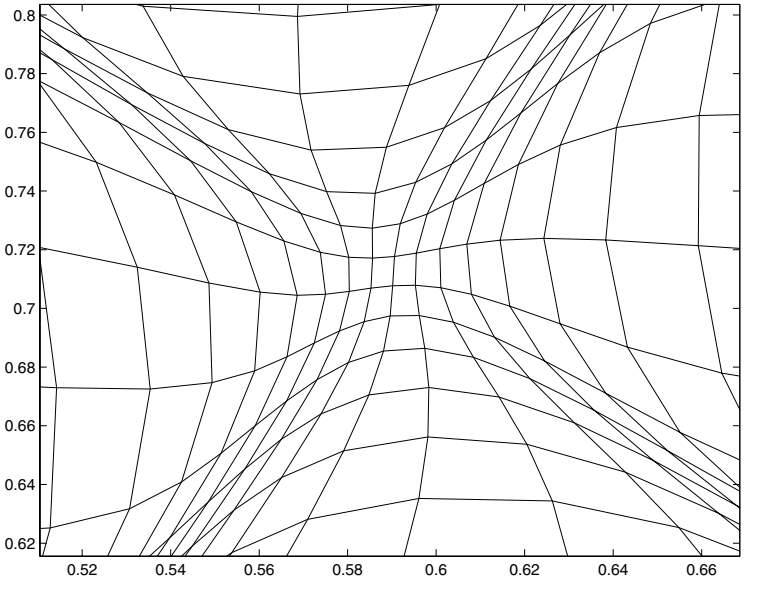


Figure 3.12. *Example 4.* A close-up of the region where the two fronts intersect.

https://doi.org/10.1017/S0962492906400015 Published online by Cambridge University Press

Further examples in which we couple the PMA algorithm to generate moving meshes for certain partial differential equations are presented in Section 5.

3.4. Adaptive discretization of PDEs in higher spatial dimensions

We now extend the discussion earlier, in Sections 3.1.1–3.1.4, in which we looked at coupling an MMPDE to a one-dimensional PDE, to consider the harder problem of coupling a moving mesh method (derived either from a variational approach or from a Monge–Ampère-based approach) to a partial differential equation in several spatial dimensions, which we assume has the form

$$\mathbf{u}_t = \mathbf{f}(t, \mathbf{x}, \mathbf{u}, \boldsymbol{\nabla}\mathbf{u}, \Delta\mathbf{u}). \tag{3.48}$$

Obviously, in this case the errors in using a non-uniform mesh are more pronounced, and the additional convective terms introduced by the moving mesh are potentially destabilizing. A moving mesh method becomes an adaptive method when it is coupled to a discretization of a partial differential equation. There is no unique way to perform this coupling, and it depends upon whether the PDE is discretized in the *computational domain* (typically with a finite difference method) or in the *physical domain* (typically with a finite element or a finite volume method). The nature of the coupling also depends upon whether or not the adaptive method is going to be coupled to existing software (such as a standard CFD method). The former usually involves some form of interpolation of the solution to map it onto a mesh suitable for the existing solver to use. The coupling of the mesh to the underlying PDE should also preserve important structures of the PDE; in particular, any conservation laws or solution symmetries should ideally be preserved in the coupled system. This can be done in various ways: see Tang (2005), Huang (2007) for reviews of these. The *quasi-Lagrangian* approaches (which avoid interpolation) allow directly for mesh movement, and express the PDE in Lagrangian variables, generalizing the expression (3.16):

$$\dot{\mathbf{u}} = f(t, \mathbf{x}, \mathbf{u}, \boldsymbol{\nabla}_{\mathbf{x}}\mathbf{u}, \Delta_x u) + \boldsymbol{\nabla}_{\mathbf{x}}\mathbf{u} \cdot \dot{\mathbf{x}}, \tag{3.49}$$

where $\dot{\mathbf{u}}$, $\dot{\mathbf{x}}$ denote derivatives with respect to time, with the computational variable $\boldsymbol{\xi}$ fixed. The MMPDEs and (3.49) can then both be discretized on the *computational mesh* and solved *simultaneously*. As described earlier, this procedure is generally the method of choice when used in calculations in one spatial dimension (Huang and Russell 1996). However, it is much harder to use in higher dimensions as the coupled system can be very stiff and the equations are very nonlinear. This method has the advantages that there is no need to interpolate a solution from one mesh to the next as the mesh evolves, and also that the mesh can inherit useful dynamical

https://doi.org/10.1017/S0962492906400015 Published online by Cambridge University Press

properties of the solution such as scaling structures (Budd *et al.* 1996, Budd and Williams 2006, Baines *et al.* 2006). Alternatively, the moving mesh equations and (3.49) can be solved *alternately* (Huang 2007, Huang and Russell 1999, Ceniceros and Hou 2001). This reduces the stiffness problems but can lead to a lag in the mesh movement.

Alternatively, a *rezoning* method can be used (Tang 2005). In such methods, the MMPDEs are solved to advance the mesh by one time step. The current solution $\mathbf{u}$ is then interpolated onto this new mesh in the physical domain, and the original PDE (3.48) solved on the new mesh in this domain (often using a finite element or finite volume method). The advantage of this method is that standard software can be used to solve the PDE, but at the expense of an interpolation step. We now describe these methods in more detail.

3.4.1. Simultaneous solution in the computational domain

We first briefly detail the implementation of the *simultaneous solution method* solving the MMPDEs and (3.49) by using finite differences in the *computational* domain. To do this we associate each mesh point in the fixed computational mesh with a solution point $U_{i,j}(t)$. To discretize (3.49) we transform the derivatives in the physical domain to ones in the computational domain. For example, in two dimensions, if we have general transformation F with Jacobian J then the derivatives of u can be expressed in terms of the computational variables in the following manner:

$$
\begin{aligned}
u_x &= \frac{1}{J}\big(y_\eta u_\xi - y_\xi u_\eta\big), \qquad (3.50)\\
u_y &= \frac{1}{J}\big(-x_\eta u_\xi + x_\xi u_\eta\big),\\
u_{xx} &= \frac{1}{J}\big(y_\eta\big(J^{-1}y_\eta u_\xi\big)_\xi - y_\eta\big(J^{-1}y_\xi u_\eta\big)_\xi - y_\xi\big(J^{-1}y_\eta u_\xi\big)_\eta + y_\xi\big(J^{-1}y_\xi u_\eta\big)_\eta\big),\\
u_{yy} &= \frac{1}{J}\Big(x_\eta\big(J^{-1}x_\eta u_\xi\big)_\xi - x_\eta\big(J^{-1}x_\xi u_\eta\big)_\xi - x_\xi\big(J^{-1}x_\eta u_\xi\big)_\eta + x_\xi\big(J^{-1}x_\xi u_\eta\big)_\eta\Big).
\end{aligned}
$$

As the computational domain has a uniform mesh, and the Jacobian J may be determined directly from the mesh mapping F, it follows that (3.50) can be discretized to high accuracy in space using a standard finite difference or finite element discretization. The solution u is then determined by solving (3.46) and (3.49) together using an appropriate ODE solver such as SDIRK or a predictor–corrector method. Examples of the use of this method are given in Section 5.

3.4.2. Alternating solution in the computational domain

The alternating solution method is often used in higher-dimensional calculations to alternatively solve the system and to move the mesh. This method

https://doi.org/10.1017/S0962492906400015 Published online by Cambridge University Press

avoids the highly nonlinear coupling of the mesh and the physical solution and preserves many structures such as ellipticity and sparsity in each of the mesh and physical PDEs. This can lead to significant efficiency gains, but at the disadvantage of a possible lag in the movement of the mesh and possible mesh instabilities.

Suppose that the physical solution $\mathbf{u}^n$, the mesh $\mathbf{x}^n$, and a solution time step Δt^n are known at a time t^n. The alternating solution procedure is typically implemented as follows.

(1) The monitor function $M^n(\mathbf{x}) = M(t^n, \mathbf{u}^n, \mathbf{x}^n)$ is calculated using $\mathbf{u}^n$ and $\mathbf{x}^n$.

(2) The MMPDE is discretized in space and then integrated over the time $[t^n, t^n + \Delta t^n]$ to give a new mesh $\mathbf{x}^{n+1}$ at the time $t^n + \Delta t_n]$. The underlying solution u^n is not changed during this calculation. This calculation can be done by using the (fixed) monitor function M^n, or by updating it during the integration by using linear interpolation (Huang 2007).

(3) The physical PDE (3.49) is then discretized in (computational) space and integrated using an SDIRK or similar method. In this calculation, the convective terms involving $\mathbf{x}_t$ use the approximation

$$\dot{\mathbf{x}} = \frac{\mathbf{x}^{n+1} - \mathbf{x}^n}{\Delta t^n}.$$

The mesh used in the discretization is calculated by using linear interpolation so that

$$\mathbf{x}(t) = \mathbf{x}^n + (t - t^n)\dot{\mathbf{x}}.$$

(4) It may be necessary to use the new solution $\mathbf{u}^{n+1}$ to update the monitor function M^n and to iterate from step (2) above in order to gain better control of the grid. In this case repeat these steps until the new mesh does not change.

(5) This procedure is then repeated from step (1) above.

Ceniceros and Hou (2001) use this method together with the MMPDE (3.34) (without updating the monitor function between time steps) to solve problems involving vortex singularities in the Boussinesq equations.

3.4.3. Rezoning in the physical domain

There are various problems associated with solving the Lagrangian form of the PDE (3.49) in the computational domain. A significant one of these is that certain properties of the original PDE may be lost when it is put into the Lagrangian form and coupled to a moving mesh equation. Two examples of this occurring are the loss of a conservation form of the equation

https://doi.org/10.1017/S0962492906400015 Published online by Cambridge University Press

(for example when adaptive methods are used to solve the Euler equations) or the loss of a Hamiltonian structure when solving problems such as the KdV or the NLS equations. These problems can be avoided by completely decoupling the solution of the PDE and the moving mesh equations over each time step, so that when solving the PDE the mesh is regarded as being static. The PDE can then be solved over that time step using a method (for example the finite volume method for problems with a conservation law) that preserves the significant features of the solution. The rezoning method can be briefly described as follows.

(1) At time step t^n let the solution be $\mathbf{u}^n$ and the mesh $\mathbf{x}^n$. Calculate the corresponding monitor function M^n.

(2) Using this monitor function, solve the moving mesh PDE over the time interval $[t^n, t^n + \Delta t^n]$ to give a new mesh $\mathbf{x}^{n+1}$.

(3) *Interpolate* the solution $\mathbf{u}^n$ onto the *new mesh* $\mathbf{x}^{n+1}$, to give an interpolated solution $\hat{\mathbf{u}}^n$.

(4) If necessary, repeat steps (2) and (3), updating M until the new mesh does not change.

(5) Starting from $\hat{\mathbf{u}}^n$ solve the original PDE (3.48). Typically, in the *physical domain* using high-resolution standard software such as the finite volume method) over the time interval $[t^n, t^n + \Delta t^n]$, doing all the calculations on the new mesh $\mathbf{x}^{n+1}$.

(6) Repeat this from step (1).

This method is of course closely related to the quasi-Lagrangian approach. To see this in a one-dimensional example, suppose that the mesh velocity is $\dot{x}$ and the underlying solution is u with $U_i^n \approx u(X_i^n, t^n)$; then in step (3) we have

$$\hat{U}_i^n \approx u(X_i^{n+1}, t^n) = u(X_i^n + \delta t_n \dot{x}) \approx U_i^n + \Delta t_n u_x \dot{x}.$$

Thus, if we use a simple forward Euler method to approximate the solution of (3.48) we obtain

$$U_i^{n+1} = \hat{U}_i^n + \Delta t_n f_i = U_i^n + \Delta t_n u_x \dot{x} + \Delta t_n f_i = U_i^n + \delta t_n \big(f_i + u_x \dot{x}\big),$$

which is of course the result of applying the forward Euler method to the Lagrangian form of the PDE given by (3.49).

The key to the success of this approach is the interpolation step (3), and an interpolation scheme that preserves some quantities of the solution is often necessary. We summarize some rezoning methods based on this approach for solving conservation laws in one and two dimensions, using the finite volume method, which are described in Tang (2005) and Tang and Tang (2003).

https://doi.org/10.1017/S0962492906400015 Published online by Cambridge University Press

A one-dimensional calculation. Suppose that the ith new grid point at time t^{n+1} is X_i^{n+1}. In a finite volume method the key quantities are the *cell averages* given by

$$U_{j+1/2} = \frac{1}{X_{j+1} - X_j} \int_{X_j}^{X_{j+1}} u \, \mathrm{d}x, \quad X_{j+1/2} = \frac{1}{2}(X_j + X_{j+1}).$$

If these are known on the mesh x^n then they can be interpolated onto the new mesh x^{n+1}. Suppose that the new mesh points satisfy $X_{j+1/2}^{n+1} \in [X_{k-1/2}^n, X_{k+1/2}^n]$; then, naively, this can be done via the formula

$$\hat{U}_{j+1/2}^n = U_{k+1/2}^n + \frac{U_{k+1/2}^n - U_{k-1/2}^n}{X_{k+1/2}^n - X_{k-1/2}^n}(X_{j+1/2}^{n+1} - X_{k+1/2}^{n+1}).$$

Unfortunately, this simple linear interpolation *does not conserve discrete solution mass*, in the sense that

$$\sum \hat{U}_{j+1/2}^n (X_{j+1}^{n+1} - X_j^{n+1}) \neq \sum U_{j+1/2}^n (X_{j+1}^n - X_j^n),$$

and consequently leads to unsatisfactory results (Tang and Tang 2003) when used to solve hyperbolic conservation laws. An improved method in Tang and Tang (2003) mimics in part the discussion above for the relation between the quasi-Lagrangian method and the rezoning method. Suppose that $x^{n+1} = x^n + \delta t \, \dot{x}$; then it follows from an application of the Reynolds transport theorem that, to leading order,

$$\begin{aligned}(X_{j+1}^{n+1} - X_j^{n+1})\hat{U}_{j+1/2}^n &\approx \int_{X_j^{n+1}}^{X_{j+1}^{n+1}} \hat{u}^n \, \mathrm{d}x \\ &\approx (X_{j+1}^n - X_j^n)U_{j+1/2}^n + \Delta t((\dot{x}U^n)_{j+1} - (\dot{x}U^n)_j).\end{aligned}$$

This prompts the use of the conservative (to leading order) interpolation formula given by

$$(X_{j+1}^{n+1} - X_j^{n+1})\hat{U}_{j+1/2}^n = (X_{j+1}^n - X_j^n)u_{j+1/2}^n + \Delta t((\dot{x}U^n)_{j+1} - (\dot{x}U^n)_j), \tag{3.51}$$

which automatically conserves discrete mass. Tang and Tang (2003) use this method with success to solve conservation laws of the form

$$u_t + f(u)_x = 0$$

with the PDE being integrated using a MUSCL method (LeVeque 1990) and using the MMPDE (3.9) to advance the mesh.

Two-dimensional calculations. In two dimensions, Tang and Tang (2003) use the moving mesh method described in Ceniceros and Hou (2001) to advance the mesh (X, Y) from time t^n to time t^{n+1} using the MMPDE (3.34).

https://doi.org/10.1017/S0962492906400015 Published online by Cambridge University Press

In this calculation we suppose that

$$(x^{n+1}, y^{n+1}) = (x^n, y^n) + \Delta t(\dot{x}, \dot{y}).$$

Cell averages at time t^n over a (time-evolving mesh cell) of area $A^n_{j+1/2,k+1/2}$ are now given by $U^n_{j+1/2,k+1/2}$, *etc.*, and the normal mesh speed relative to the surfaces of the mesh cell is given by

$$v = \dot{x}n_x + \dot{y}n_y, \quad \text{where the unit normal is given by } (n_x, n_y).$$

The conservative interpolation scheme proposed is

$$\begin{aligned} A^{n+1}_{j+1/2,k+1/2}\hat{U}^n_{j+1/2,k+1/2} = A^n_{j+1/2,k+1/2}U^n_{j+1/2,k+1/2} \\ + \Delta t\big(\big[(vU^n)_{j+1,k+1/2} + (vU^n)_{j,k+1/2}\big] \\ + \big[(vU^n)_{j+1/2,k+1} + (vU^n)_{j+1/2,k}\big]\big). \end{aligned} \tag{3.52}$$

This scheme preserves discrete mass to leading order. Again a MUSCL method can be used to advance the solution of the PDE. This method is then used to solve the double-Mach reflection problem and various other problems with contact discontinuities arising in the solution of the Euler equations.

4. Velocity-based moving mesh methods

In this section we will look in some more detail at *velocity-based methods* for moving meshes. These are also called *Lagrangian methods*, and they rely on calculating the *mesh point velocities* and from this the mesh point locations. In some ways these methods are very natural, since in (say) fluid mechanics calculations, natural solution features are often convected with the flow, and it is natural to evolve the mesh points to follow the flow itself. (Note the huge popularity of the semi-Lagrangian and the characteristic Galerkin methods.) However, velocity-based methods can easily have severe implementation problems, and overcoming them remains a challenging issue. These include significant mesh tangling, with associated skewness, and also a tendency to create meshes which lag behind the solution. Indeed, it is very possible for such meshes to have unstable movement, to move well away from equidistributed solutions and to lead to permanently distorted skewed and even frozen meshes, even after the significant solution structures have long gone. Some examples of this type of behaviour will be presented in our discussion of the GCL method. For these reasons the overall performance of these methods is, in general, not as good as that of the position-based methods described in the last section, and hence we will spend less time discussing them. We now describe three velocity-based methods: the moving finite element method (MFE), the geometric conservation law method (GCL), and the deformation map method.

https://doi.org/10.1017/S0962492906400015 Published online by Cambridge University Press

4.1. Moving mesh finite element methods

The moving finite element method was originally developed by Miller and Miller (1981) and Miller (1981), and represents a very important class of velocity-based moving mesh methods, with much underlying theory and many applications. See, for example, Adjerid and Flaherty (1986), Baines *et al.* (2005), Beckett *et al.* (2001*a*), Cao, Huang and Russell (1999*a*), Carlson and Miller (1998*a*, 1998*b*), Di *et al.* (2005), Lang *et al.* (2003), Li *et al.* (2002) and Wathen and Baines (1985). A very complete survey of these and related methods is given in Baines (1994) and we will only describe them briefly here. The MFE method determines a mesh velocity $\dot{\mathbf{x}} = \mathbf{v}$ through a variational principle coupled to the solution of a PDE by using a finite element method. Specifically, we consider the time-dependent PDE

$$\frac{\partial u}{\partial t} = \mathcal{L}u, \tag{4.1}$$

with $\mathcal{L}$ a spatial differential operator. The continuous version of the MFE determines the *solution and the mesh together* by minimizing the residual given by

$$\min_{v, \frac{Du}{Dt}} I\left[\mathbf{v}, \frac{Du}{Dt}\right] \equiv \int_{\Omega_P} \left(\frac{Du}{Dt} - \boldsymbol{\nabla} u \cdot \mathbf{v} - \mathcal{L}u\right)^2 W \, \mathrm{d}\mathbf{x}. \tag{4.2}$$

Here the function W is a weight function for which

$$W = 1$$

in the usual version of MFE described in Miller and Miller (1981) and Miller (1981); alternatively, we can take

$$W = \frac{1}{1 + |\boldsymbol{\nabla} u|^2},$$

for the weighted form of MFE described in Carlson and Miller (1998*a*, 1998*b*). Observe that MFE is naturally trying to advect the mesh along with the solution flow. Of course, in practice this equation is discretized using a Galerkin method.

This method is elegant, and when tuned correctly works well (Baines 1994). However, it does have significant disadvantages. One of these is that the functional derivative of I with respect to $\mathbf{v}$ can become singular, and regularization is needed in practice.

4.2. Geometric conservation law (GCL) *methods*

The geometric conservation law (GCL) methods are based upon a direct differentiation of the equidistribution equation with respect to time, to derive an equation for the mesh velocity. In its simplest form the method assumes that the monitor function M is normalized so that the integral of M over

https://doi.org/10.1017/S0962492906400015 Published online by Cambridge University Press

Ω_P is constant (typically unity). If A is an arbitrary measurable set in Ω_C it follows that

$$I = \int_A \mathrm{d}\boldsymbol{\xi} = \int_B M \,\mathrm{d}\mathbf{x},$$

where $B = F(A)$. Now, even if A is fixed, then, as the mesh is moving the set B will typically change with time, with the points on the boundary of B moving with velocity $\mathbf{v}$. An application of the Reynolds transport theorem implies that

$$\frac{\mathrm{d}}{\mathrm{d}t}\int_B M \,\mathrm{d}\mathbf{x} = \int_B M_t \,\mathrm{d}\mathbf{x} + \int_{\partial B} M\mathbf{v}\cdot \,\mathrm{d}S = \int_B (M_t + \boldsymbol{\nabla}\cdot(M\mathbf{v}))\,\mathrm{d}\mathbf{x}.$$

However, as A is fixed, it follows that $\mathrm{d}I/\mathrm{d}t = 0$. Furthermore, the set A is arbitrary. It follows that M and hence $\mathbf{v}$ must satisfy the (geometric) conservation law

$$M_t + \boldsymbol{\nabla}\cdot(M\mathbf{v}) = 0. \tag{4.3}$$

If M is known, then (4.3) gives an equation for the (mesh) velocity $\mathbf{v}$. This equation must be augmented with the boundary condition

$$\mathbf{v}\cdot\mathbf{n} \quad \text{on} \quad \partial\Omega_P. \tag{4.4}$$

The equations (4.3) and (4.4) have a unique solution in one dimension but many solutions in higher dimensions. To determine $\mathbf{v}$ uniquely, additional conditions must be imposed. In the derivation of the optimal transport methods we saw the use of an additional condition on the curl of the solution in the computational space. In the various forms of the geometric conservation law (GCL) methods the curl of the velocity is imposed in the *physical space*. In particular, for a suitable weight function w and a background velocity field $\mathbf{u}$, the condition

$$\boldsymbol{\nabla}\times w(\mathbf{v}-\mathbf{u}) \tag{4.5}$$

is imposed, so that for an appropriate potential function ϕ we have

$$\mathbf{v} = \mathbf{u} + \frac{1}{w}\boldsymbol{\nabla}\phi.$$

Here ϕ is unknown, and we presume that $\mathbf{u}$ is specified in advance. Substituting into the conservation law, it then follows that ϕ satisfies the *elliptic partial differential equation*

$$\boldsymbol{\nabla}\cdot\left(\frac{M}{w}\boldsymbol{\nabla}\phi\right) = -M_t - \boldsymbol{\nabla}\cdot(M\mathbf{u}), \tag{4.6}$$

with the boundary condition on $\partial\Omega_P$ given by

$$\frac{\partial\phi}{\partial n} = -w\mathbf{u}\cdot\mathbf{n}.$$

This equation is a *scalar linear equation* for ϕ when posed (and solved) in

https://doi.org/10.1017/S0962492906400015 Published online by Cambridge University Press

the computational space. Unlike the MFE methods, this partial differential equation is well-defined for all time. In a similar manner to the optimal mesh methods, we need only solve a scalar equation; however, unlike the optimal mesh methods this equation is linear in the physical coordinates. Observe, further, that unlike certain of the MMPDE-based and variational-based methods described in Section 3, this system automatically deals with the mesh location on the boundaries. Having determined ϕ from this equation, the mesh velocity $\mathbf{v}$ can be determined directly, and the mesh then found from integrating the equation $\mathbf{x}_t = \mathbf{v}$ with respect to time using, for example, an SDIRK method. This time integration to give $\mathbf{x}$ has the disadvantage of possibly introducing mesh tangling, and of mesh points moving out of the domain during the course of the integration, if an appropriately coarse discretization is used. This method is described in Cao *et al.* (2002)

An alternative formulation, also described in Cao *et al.* (2002), considers a variational formulation, where it is shown that the solution of (4.3) is also the minimizer of the functional

$$I[\mathbf{v}] = \frac{1}{2}\int_{\Omega_P}\left(|\boldsymbol{\nabla}\cdot(M\mathbf{v}) + M_t|^2 + \left(\frac{M}{w}\right)^2 |\boldsymbol{\nabla}\times w(\mathbf{v}-u)|^2\right)\mathrm{d}\mathbf{x}. \quad (4.7)$$

This equation can be discretized using a finite element method with basis functions defined over the mesh in the physical space, and $\mathbf{v}$ found using a simple Galerkin method. The mesh points can then also be found from $\mathbf{v}$ through a Galerkin calculation. Details of these calculations are given in Baines *et al.* (2005, 2006), where the GCL method is coupled to an ALE (arbitrary Lagrangian–Eulerian) method for discretizing the underlying PDE.

In the usual implementation of the GCL method the weight function

$$w = 1$$

is taken. This gives an irrotational mesh (in the physical coordinates) when the background velocity $\mathbf{u} = 0$. In many implementations of GCL, $\mathbf{u} = 0$. However, for certain applications, such as in computational fluid dynamics, the background velocity can be taken to be the flow velocity.

The appeal of the GCL methods is that to find ϕ (and hence $\mathbf{v}$) we need only solve a scalar linear elliptic partial differential equation. This seems to have the advantage over the optimal transport methods, which require the solution of a nonlinear equation. However, like other velocity-based methods it has the potential disadvantages of having problems with mesh tangling and mesh skewness as the mesh points follow the moving features in a monitor function. Furthermore, we require the solution of the mesh equations in the physical domain rather than the computational domain. This loses some of the speed advantages gained (by, for example, the use of spectral methods) when solving the mesh equations on a very uniform mesh in the computational domain.

https://doi.org/10.1017/S0962492906400015 Published online by Cambridge University Press

We now consider two examples taken from Cao *et al.* (2002) of the application of the GCL method, which allow direct comparison with the optimal-transport-based methods described in Section 3.

Example 1. This first example looks at the mesh generated by a monitor function which concentrates points around a moving disc. This is considered to be a difficult test problem for a moving mesh method. We have

$$M_1(x,y,t) = \frac{d(x,y,t)}{\int_{\Omega_P} d(\tilde{x},\tilde{y},t)\,\mathrm{d}\tilde{x}\,\mathrm{d}\tilde{y}},$$

where

$$d(x,y,t) = 1 + 5\exp\left(-50\left|\left(x - \frac{1}{2} - \frac{1}{4}\cos(2\pi t)\right)^2 + \left(y - \frac{1}{2} - \frac{1}{4}\sin(2\pi t)\right)^2 - 0.01\right|\right).$$

Results are shown in Figure 4.1.

If we compare the calculated mesh to that of the identical Example 1 in the application of the PMA method in Section 3 (see p. 181), we see that the GCL method has not performed as well in this case. In particular, we see some significant effects of mesh distortion, and of mesh points lagging behind, with the Lagrangian-based method leading to mesh skewness and eventually to tangling and singular behaviour. This is in contrast to the much more regular mesh generated by the position-based PMA method.

Example 2. In this second example we consider a monitor function which concentrates mesh points around an oscillating front:

$$M_1(x,y,t) = \frac{d(x,y,t)}{\int_{\Omega_P} d(\tilde{x},\tilde{y},t)\,\mathrm{d}\tilde{x}\,\mathrm{d}\tilde{y}},$$

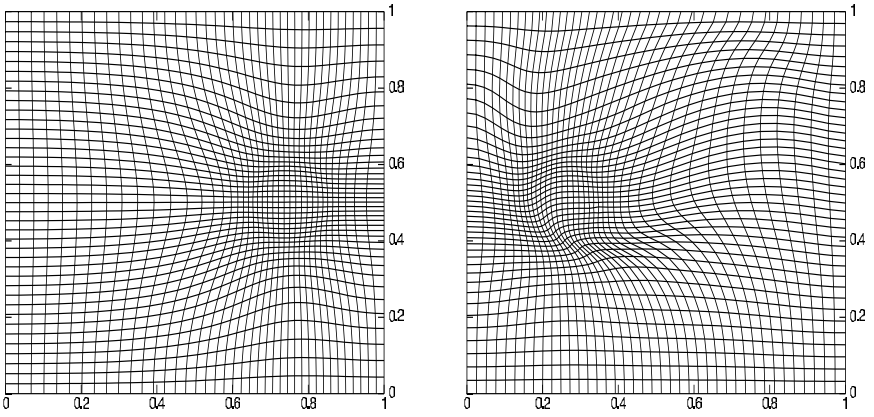
where

$$d(x,y,t) = 1 + 5\exp\left(-50\left|y - \frac{1}{2} - \frac{1}{4}\sin(2\pi x)\sin(2\pi t)\right|\right).$$

The results of using the GCL method in this case are shown in Figure 4.2.

We can compare this mesh to that generated in Example 2 of the application of the PMA method (see p. 183). We can see that the GCL method has successfully followed the moving sine wave, but unlike the mesh generated by the PMA method, there is a small degree of instability, manifested by some oscillations of the mesh visible when $t = 1$ which are not present in the mesh when $t = 0$.

https://doi.org/10.1017/S0962492906400015 Published online by Cambridge University Press

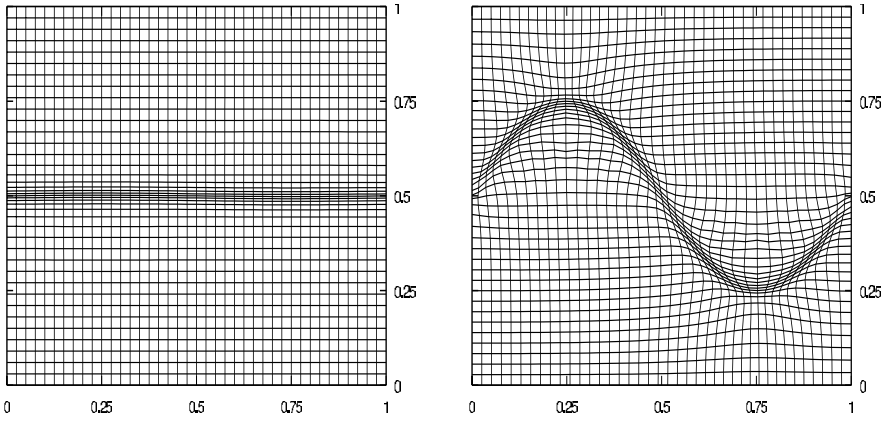


(a) $t = 0$ (b) $t = 0.5$

(c) $t = 0.75$ (d) $t = 1$

Figure 4.1. *Example 1.* Moving meshes at time $t = 0$ (a), $t = 0.5$ (b), $t = 0.75$ (c), $t = 1$ (d).

https://doi.org/10.1017/S0962492906400015 Published online by Cambridge University Press



(a) $t = 0$ (b) $t = 0.25$

(c) $t = 0.75$ (d) $t = 1$

Figure 4.2. *Example 2.* Moving meshes generated by the GCL method at times $t = 0$ (a), $t = 0.25$ (b), $t = 0.75$ (c), $t = 0$ (d).

https://doi.org/10.1017/S0962492906400015 Published online by Cambridge University Press

4.3. The deformation map method

Deformation map methods take a strongly differential geometric approach to moving mesh generation. Liao and his co-workers (Liao and Anderson 1992, Semper and Liao 1995, Liao and Xue 2006) have proposed a moving mesh method based on *deformation maps*. Such maps were introduced by Moser (1965) and Dacorogna and Moser (1990) in their study of volume elements of a compact Riemannian manifold, to prove the existence of a C^1 diffeomorphism with specified Jacobian. In this method, the mapping $\mathbf{x} = F(\boldsymbol{\xi}, t) : \Omega_C \to \Omega_P$ is determined from the system of equations

$$\begin{aligned} \mathbf{x}_t &= \frac{1}{M(\mathbf{x},t)} \boldsymbol{\nabla} \phi(\mathbf{x},t) \quad \text{in} \quad \Omega_P, \\ \Delta \phi &= -\frac{\partial M}{\partial t} \qquad\qquad\quad \text{in} \quad \Omega_P, \\ \frac{\partial \phi}{\partial n} &= 0 \qquad\qquad\qquad\quad \text{on} \quad \partial\Omega_P. \end{aligned} \tag{4.8}$$

It is easy to see that (4.8) corresponds to the system (4.6), the GCL method formulation which involves the potential function ϕ in the case where $\mathbf{u} = 0$ and $w = M$.

Dacorogna and Moser also use the alternative formulation in Bochev, Liao and Pena (1996), given by

$$\begin{aligned} \mathbf{x}_t &= \frac{\boldsymbol{\nu}(\mathbf{x},t)}{M(\mathbf{x},t)} \quad \text{in} \quad \Omega_P, \\ \boldsymbol{\nabla} \cdot \boldsymbol{\nu} &= -\frac{\partial M}{\partial t} \quad \text{in} \quad \Omega_P, \\ \boldsymbol{\nabla} \times \boldsymbol{\nu} &= 0 \qquad\quad \text{on} \quad \partial\Omega_P. \end{aligned} \tag{4.9}$$

Note that letting $\boldsymbol{\nu} = M\mathbf{v}$, this becomes the div-curl system (4.3) and (4.5) with $\mathbf{u} = 0$ and $w = M$.

The equation for $\mathbf{x}_t$ in both cases is nonlinear, and for simplicity explicit time integration schemes are used by Liao and his co-workers. For (4.8), the solution of the potential equation for ϕ is straightforward. However, an implicit integration of (4.8) requires interpolation of the potential function ϕ for values at points other than grid nodes, and the flux-free boundary condition cannot generally be preserved. For (4.9), the div-curl system is solved using a least-squares approach.

4.4. Some other velocity-based methods

The natural idea of moving mesh points, so that the velocity of the points reflects the underlying dynamics of the solution, has led to many other velocity-based methods besides those described above. In the velocity-based methods of Anderson and Rai (1983), the mesh is moved according to

https://doi.org/10.1017/S0962492906400015 Published online by Cambridge University Press

attractive and repulsive pseudo-forces between nodes, motivated by a spring model in mechanics. Petzold (1987) obtains an equation for mesh velocity by minimizing the time variation of both the unknown variable and the spatial coordinate in computational coordinates and adding a diffusion-like term to the mesh equation. The method of Hyman and Larrouturou (1986, 1989) also simulates attraction and repulsion pseudo-forces.

In contrast, Dorodnitsyn (1991, 1993*a*, 1993*b*) and his co-workers (Dorodnitsyn and Kozlov 1997, Kozlov 2000) have derived a series of velocity-based methods in which the underlying symmetries of the PDE to be solved are used to guide the movement of the grid points. Such methods have the potential to preserve all of the symmetric invariants of the underlying PDE in the discretized system, and indeed precisely these invariants are used in the calculation of the mesh points. They are closely related to the (position-based) scale-invariant methods described in the next section. Such methods can also lead to conservation laws derived from a discrete version of Noether's theorem. They have been applied in Dorodnitsyn and Kozlov (1997) to solve a variety of nonlinear diffusion equations, and in Budd and Dorodnitsyn (2001) to integrate the nonlinear Schrödinger equation. The main disadvantage of these methods is that they tend to be highly nonlinear, and the equations for the mesh points hard to solve. More details of the implementation and application of these methods are given in Budd and Piggott (2005).

5. Applications of moving mesh methods

In this final section we look at some applications of moving mesh methods to a variety of problems related to the solution of partial differential equations. As described in Section 1, there are a vast number of problems for which moving mesh methods have been used with great success, and we cannot hope to summarize all of them in this section. For example, one of the most important applications arises in fluid mechanics, and reviews of these, comparing many different methods and problems, are given in Baines (1994), Eisman (1985), Tang (2005), Tang and Tang (2003) and Yanenko *et al.* (1976).

Instead, we look in this section at some specific problems and classes of problems which aim to highlight some of the special advantages and disadvantages of the moving mesh method for solving partial differential equations. In particular we look at problems where moving meshes can exploit natural solution scaling structures (including self-similarity); blow-up problems in which solution singularities arise in finite time; and problems such as Burgers' equation, where moving meshes are used to capture the motion of moving fronts, and two physical problems, one in combustion and the other in meteorology. Two primary goals are to describe analytical techniques for

https://doi.org/10.1017/S0962492906400015 Published online by Cambridge University Press

solving nonlinear PDEs which can often be naturally modified for moving mesh algorithms, in such a way that the discrete solutions share common properties with the (unknown) analytical solutions; and to show that the sharing of the common structures leads to efficient adaptive methods.

5.1. Symmetry, self-similar solutions and scale invariance

Many naturally occurring physical systems have an invariance under symmetries including *translations*, *rotations* and *changes of scale*, and this is reflected in the partial differential equations that describe them. The solutions of these equations may then either be themselves invariant under (combinations of) these symmetries, the *self-similar solutions*, or they can be transformed into other solutions through the application of symmetry operators. Conservation laws can be linked through Noether's theorem (Olver 1986, Dorodnitsyn 1993*b*) to many of the continuous symmetries.

An example of such a system is Burgers' equation,

$$\mathbf{u}_t + \mathbf{u} \cdot \boldsymbol{\nabla} u = \nu \Delta \mathbf{u},$$

which is invariant under *rotations* in space and *translations* in both space and time. It admits travelling-wave solutions which are self-similar solutions coupling spatial and temporal translation, with the wave speed giving the coupling. The waves can be at any orientation, and the action of a rotation is to map one wave to another. In other systems a rescaling of space, time and of the solution leaves the partial differential equations governing the system invariant. Such changes of scale were first observed by Kepler in his studies of the solar system and summarized in his famous *third law*, in which he observed that if a planetary orbit existed with a solution (in polar coordinates) given by $(r(t), \theta(t))$ then there was also a solution of the form $\big((\lambda^3 r(\lambda^2 t)), \mathcal{O}(\lambda^2 t)\big)$ for any positive value of λ. Such scaling invariance also arises in the equations of fluid and gas dynamics, nonlinear optics and many biological systems. An excellent summary of scale-invariant systems with such properties is given in the book by Barenblatt (1996).

We can then ask the question of whether a numerical method can be constructed which is also invariant under symmetries. More generally, an adaptive method can be designed to exploit the symmetries in the problem. In a sense, the answer to this question is obvious as we can always perform an *a priori* scaling of the problem and then use a method in the scaled coordinates. However, this assumes more knowledge of the physical system than we may easily have available to us. Indeed, for some systems there are a number of different possible changes of scale, and it is not *a priori* obvious which one correctly describes the system evolution.

We now show how several of the moving mesh strategies described earlier, particularly those based on moving mesh partial differential equations, can be very effectively applied to such problems with symmetry. Such methods

https://doi.org/10.1017/S0962492906400015 Published online by Cambridge University Press

have several important properties. If carefully designed they can admit discrete self-similar solution, they can have (local truncation) errors which are invariant under changes in the scale of the problem, they can have discrete conservation laws, and they can cope with symmetric singular structures. Such problems have been studied by a number of authors: Budd *et al.* (1996), Baines *et al.* (2006), Budd and Piggott (2005), Ceniceros and Hou (2001), Dorodnitsyn (1991, 1993*b*) and Kozlov (2000).

The underlying problem that we will consider is the partial differential equation

$$u_t = f(u, \boldsymbol{\nabla} u, \Delta u, \ldots). \tag{5.1}$$

Observe that this equation is invariant under translations in space and time and also rotations in space. We also assume it to be invariant under the action of the scaling symmetry (or symmetries)

$$t \to \lambda, \quad \mathbf{x} \to \lambda^{\alpha}\mathbf{x}, \quad u \to \lambda^{\beta} u. \tag{5.2}$$

The objective is now to derive an adaptive method which reflects the underlying symmetries. This can be achieved if, away from any finite boundaries, the equations describing the mesh (regardless of whether these are position- or velocity-based) are *invariant under the action of the same symmetry operations as the underlying PDE*, so that translations in space and time rotations and scalings of the form (5.1) leave the mesh equations invariant. This is in many ways a very natural question to ask of an r-adaptive method, for which the mesh may be regarded as a dynamic object, amenable to the action of symmetries involving space and time. It is much harder to see how h- and p-type methods can be considered in this manner.

As an example of such a problem (see also Baines *et al.* (2006) for the use of an adaptive ALE method in higher dimensions, and Dorodnitsyn (1993*a*) and Dorodnitsyn and Kozlov (1997) for a more abstract treatment), we consider the one-dimensional *porous medium equation* given by

$$u_t = (u^m)_{xx}, \tag{5.3}$$

where we consider this equation posed on the whole real line, with mild decay conditions on the solution u at ∞. This partial differential equation is invariant under two different, and independent, changes of scale, one of space and the other of the solution. These are given by

$$t \to \lambda t, \quad x \to \lambda^{1/2} x$$

and

$$t \to \mu t, \quad u \to \mu^{1/(m-1)} u.$$

Any (linear) combination of these two changes of scale will also leave the equation (5.3) invariant.

https://doi.org/10.1017/S0962492906400015 Published online by Cambridge University Press

Whilst the PDE may be invariant under the action of a symmetry group, not all of the solutions have this property, although any one solution can be mapped into another by the action of the symmetry operator. Those solutions which are themselves invariant under the action of the symmetry operator are termed the *self-similar solutions*. A self-similar solution satisfies the functional equation

$$u(\lambda t, \lambda^{\alpha}\mathbf{x}) = \lambda^{\beta} u(t, \mathbf{x}). \tag{5.4}$$

Such a solution can be described in terms of a new set of coordinates, typically of the form

$$u(t, \mathbf{x}) = t^{\beta} v(\mathbf{z}), \quad \mathbf{z} = \mathbf{x}/t^{\beta}. \tag{5.5}$$

In the case of the porous medium equation, the self-similar solution with *constant mass* takes the form

$$u(t, x) = t^{-1/3} v(x/t^{1/3}).$$

The function $v(\mathbf{z})$ generally satisfies an ordinary differential equation, which is much simpler than the original PDE. The solutions of this ODE which correspond to solutions of the PDE are generally those with certain decay or boundedness conditions as $|\mathbf{z}| \to \infty$. This allows the construction of exact solutions to PDEs in many cases. In the example of the porous medium equation we have the famous Barenblatt–Pattle solution (Barenblatt 1996), given by

$$u(x, t) = t^{-1/3}(a - x^2/t^{2/3})_+,$$

where a is a constant. Significantly such solutions are *globally attracting* (in the sense of L_1-convergence. An extensive description of such problems is given in Barenblatt (1996) and Olver (1986).

More generally, solutions of PDEs with symmetries may also take the form

$$u(t, \mathbf{x}) = U(t) v(\mathbf{z}), \quad \text{where} \quad \mathbf{z} = \mathbf{x}/L(t). \tag{5.6}$$

Here $U(t)$ and $L(t)$ are appropriate solution and length scales. In the case of self-similar solutions these are pure powers of t (or a translation of t) but they can take more general forms. For example, in the case of the blow-up equation,

$$u_t = u_{xx} + u^3,$$

with $u \to \infty$ as $t \to T$, we have

$$U(t) = (T - t)^{-1/2} \quad \text{and} \quad L(t) = (T - t)^{1/2} |\log(T - t)|.$$

Such solutions are called *approximately self-similar solutions* (Samarskii, Galaktionov, Kurdyumov and Mikhailov 1973). Examples of this type of

https://doi.org/10.1017/S0962492906400015 Published online by Cambridge University Press

behaviour also arise in the nonlinear Schrödinger equation in dimension two, and in the chemotaxis equations of mathematical biology.

The self-similar (and approximately self-similar) solutions of PDEs can play an important role in the description of the solution (beyond the fact that they lead to exact solutions). This is because they often describe very well the *intermediate asymptotics* of the solution, which is the behaviour of the solution after the transient effects of any initial conditions and before boundary terms become important. They are also often effective in describing certain singular types of behaviour such as the peaks in the blow-up and related problems, and also the interfaces in various problems in gas dynamics (Barenblatt 1996). It is therefore useful to have numerical methods which can accurately reproduce self-similar behaviour when it arises in applications. One method that has been used is to make an *a priori* choice of (self-similar) variables, so that the PDE can be reduced to an ODE and to then solve this ODE numerically. This method, however, has a number of disadvantages. Firstly, it cannot deal with general initial and boundary conditions satisfied by the PDE. Secondly, there may often be several symmetry groups acting on a partial differential equation and it may often not be at all clear which (if any) leads to a self-similar solution. Indeed, there are many problems (for example the heat equation posed on a finite interval with an initially highly localized solution) which may have one form of self-similar behaviour for part of the evolution and another over longer times (for example when the solution of the heat equation interacts with the boundary). Problems of this form (called type II self-similar solutions in Barenblatt (1996)) are extremely hard to analyse in advance of any PDE calculation.

An alternative approach, which makes considerable use of the r-adaptive methods, is to use a numerical method which *admits the same scaling invariances as the original PDE away from any boundaries*. Such methods are called *scale-invariant* (Budd and Piggott 2005, Baines *et al.* 2006) as they perform identically under the scaling transformations.

The key to the design and implementation of such methods lies in the use of the moving mesh partial differential equations to describe the location of the mesh points. By an appropriate choice of monitor function it is often possible to construct such MMPDEs to be invariant under the action of the scaling transformations. The advantages of such methods are as follows.

- They usually have *discrete self-similar solutions* which inherit many of the properties of the underlying self-similar solutions.
- If designed carefully they may work for several types of scaling symmetry and thus can be used in the case of type II self-similarity when the exact scaling group is not known in advance.

https://doi.org/10.1017/S0962492906400015 Published online by Cambridge University Press

- They can be applied to problems with arbitrary initial and boundary conditions
- They can have relative truncation errors which are *independent of the scale of the solution* (Budd, Leimkuhler and Piggott 2001, Baines *et al.* 2006)

We give a partial proof of these results presently. A further, but less general, advantage of such methods is that they also often preserve the asymptotic properties of the (approximately) self-similar solutions. This is seen both in the global convergence towards the self-similar solutions of the porous medium equation, and the local convergence towards the singular profile described by the approximately self-similar solution of the blow-up equation.

We start this calculation by looking at a moving mesh method in one dimension for which the moving mesh PDE is given by MMPDE1 and for which the monitor function is a function of u and u_x, so that

$$(M(u,u_x)x_\xi)_\xi = 0.$$

If this is to be invariant under the action of the scaling symmetry $t \to \lambda t, x \to \lambda^\beta x, u \to \lambda^\gamma u$, we require that

$$(M(\lambda^\gamma u, \lambda^{\gamma-\beta}u_x)\lambda^\beta x_\xi)_\xi = 0.$$

This is satisfied (for all β) provided that the monitor function satisfies the functional equation

$$M(\lambda^\gamma u, \lambda^{\gamma-\beta}u_x) = \lambda^\theta M(u,u_x), \tag{5.7}$$

where θ is arbitrary. Many monitor functions do not satisfy this functional equation, for example the simple arclength monitor $M = \sqrt{1+u_x^2}$ (although it approximately satisfies it when $|u_x|$ is large). However, it is certainly possible to find functions that do, and a simple example is given by

$$M(u,u_x) = u^\delta$$

for some choice of δ. Observe that this monitor function is invariant under a very arbitrary set of scaling symmetries and using it poses no explicit *a priori* scaling on the solution. It is thus very useful when considering self-similar solutions of type II.

As an example we consider the porous medium equation in the form

$$u_t = (uu_x)_x \quad |u| \to 0 \quad \text{as} \quad |x| \to \infty. \tag{5.8}$$

It is easy to see that the first integral of this solution is constant, and we may scale the solution so that, for all t, we have

$$\int_{-\infty}^{\infty} u \, \mathrm{d}x = 1.$$

https://doi.org/10.1017/S0962492906400015 Published online by Cambridge University Press

It is then natural to choose $M = u$ so that the monitor function has unit integral over the physical domain. It follows immediately that

$$Mx_\xi = 1. \tag{5.9}$$

Furthermore, from the geometric conservation law given by

$$M_t + (M\dot{x})_x = 0,$$

we have

$$u_t + (u\dot{x})_x = 0.$$

Substituting for u_t and integrating gives

$$u(u_x + \dot{x}) = 0,$$

so that the Lagrangian equation for the mesh points is given by

$$\dot{x} = -u_x. \tag{5.10}$$

This equation is used in Dorodnitsyn (1993*a*) and Dorodnitsyn and Kozlov (1997) as the equation of motion of all of the mesh points. Note that this is also the equation for the movement of the leading edge of the front of those solutions of the porous medium equation which have compact support. The same monitor function is used in Baines *et al.* (2006) to compute solutions of the porous medium equation using the scale-invariant ALE method.

In the usual manner, either of the equations (5.9) and (5.10) can be discretized and solved simultaneously with the porous medium equation (5.8) (see Budd, Collins, Huang and Russell (1999*b*) for more details), so that the discrete solution and mesh points are given by

$$U_i \approx u(X_i, t), \quad X_i = x(i\Delta\xi).$$

A similar procedure can also be used with a variational formulation in higher dimensions (Baines *et al.* 2006)

It is *immediate* (see Budd *et al.* (1999*b*)) that any such discretization admits a *discrete self-similar solution* of the form

$$U_i = t^{-1/3}V_i, \quad X_i = t^{1/3}Z_i. \tag{5.11}$$

It can also be shown (Budd and Piggott 2005) that such self-similar solutions are not only locally stable, but are also *global attractors*, so that they correctly organize the qualitative long-term dynamics of the solution and even obey a discrete maximum principle.

5.1.1. Construction of scale-invariant MMPDEs

The porous medium equation has relatively benign dynamics, which allows us to use a relatively simple moving mesh equation to evolve the mesh. In the case of systems with more extreme forms of dynamics, such as that

https://doi.org/10.1017/S0962492906400015 Published online by Cambridge University Press

arising in shocks or localized singularities, it is usually necessary to use a more sophisticated moving mesh equation to avoid mesh instabilities.

In one dimension two possible equations for the mesh are the moving mesh PDEs MMPDE5 and MMPDE6, given by

$$\epsilon x_t = (M x_\xi)_\xi, \quad -\epsilon x_{\xi\xi t} = (M x_\xi)_\xi. \tag{5.12}$$

Suppose that these are used to solve a system which has intrinsic solution, length and time scales given respectively by U, L and T and a derived scale Λ for the monitor function M. As the computational variable ξ is *independent of scale*, the left-hand side of each of these two MMPDEs scales as L/T and the right-hand side as ΛL. These two balance (so that the mesh evolves at the same rate as the underlying solution) provided that

$$\frac{1}{T} = \Lambda. \tag{5.13}$$

Observe that this condition is independent of the spatial length scale L. The implication of this is that if the monitor function $M(u, x)$ depends upon u and x, then this satisfies (5.13) provided that

$$M(Uu, Lx) = \frac{1}{T} M(u, x). \tag{5.14}$$

This is a more severe condition than the condition (5.14) for MMPDE1, but is necessary to ensure that the mesh calculation does not destabilize the calculation of the solution of the PDE. It has the useful property that it often gives a precise characterization of the necessary form of the monitor function appropriate to one scaling transformation. A disadvantage of this approach is, however, that it may not always (or indeed generally) be possible to capture *all* possible scaling transformations in *a single monitor function* satisfying (5.14). Thus some *a priori* knowledge of the expected solution behaviour might be necessary in this case.

As an example we will consider the radially symmetric solutions of the cubic nonlinear Schrödinger equation. This equation has the form

$$\mathrm{i}u_t + u_{rr} + \frac{n-1}{r} u_r + u|u|^2 = 0, \tag{5.15}$$

where $r = |x|$ and n is the spatial dimension. If $n \geq 2$ this can have solutions which develop singularities (in amplitude and phase) in a finite time. The equation (5.15) is invariant under the action of the scaling group

$$t \to \lambda t, \quad r \to \lambda^{1/2} r \quad u \to \lambda^{-1/2} u,$$

as well as the unitary multiplicative group

$$t \to t, \quad r \to r, \quad u \to \mathrm{e}^{\mathrm{i}\phi} u, \quad \phi \in R.$$

This system develops singularities in a finite time T with a natural time

https://doi.org/10.1017/S0962492906400015 Published online by Cambridge University Press

scale of $(T-t)$, a length scale of $L=(T-t)^{1/2}$, and a solution scale of $U=(T-t)^{-1/2}$. For the moving mesh PDE based on a simple monitor function of the form $M(u)$ to be invariant under the action of the unitary multiplicative group, we require that

$$M(u)=M(|u|).$$

The condition (5.14) then implies that

$$M((T-t)^{-1/2}u)=\frac{1}{(T-t)}M(u).$$

Both conditions are satisfied if

$$M(u)=|u|^2. \tag{5.16}$$

Calculations using a regularized form of this monitor function are described in Section 5.2.2.

Scale-invariant moving mesh methods for a general class of scale-invariant PDEs can also be constructed in higher dimensions, say $\mathbf{x}\in\mathbb{R}^n$. We consider two cases, firstly the method of Ceniceros and Hou (2001), and then the optimal transport method. The first of these describes a two-dimensional moving mesh generated by the PDE system

$$x_t=\boldsymbol{\nabla}_{\boldsymbol{\xi}}.(M\boldsymbol{\nabla}_{\boldsymbol{\xi}}x),\quad y_t=\boldsymbol{\nabla}_{\boldsymbol{\xi}}.(M\boldsymbol{\nabla}_{\boldsymbol{\xi}}y).$$

This system scales in an identical manner to both MMPDE5 and MMPDE6, and consequently is scale-invariant provided that the monitor function M satisfies the condition (5.14). In the case of optimal transport in an n-dimensional system, the PMA equation gives a mesh from $\boldsymbol{\nabla}_{\boldsymbol{\xi}}Q$, where Q satisfies the PDE

$$(I-\gamma\Delta)Q_t=(M(u)H(Q))^{1/n}. \tag{5.17}$$

Now, if the underlying problem has the natural scaling symmetry $\mathbf{x}\to\lambda\mathbf{x}$, then this is equivalent to the scaling symmetry $Q\to LQ$. It is immediate that

$$H(LQ)=L^nH(Q).$$

It then follows immediately that (5.17) is invariant under the action of the scaling symmetries provided that the monitor function satisfies the functional equation

$$M(Uu,L\mathbf{x})^{1/n}=\frac{1}{T}M(u,\mathbf{x}). \tag{5.18}$$

We note that, in two dimensions, the scaling structure of the function Q also implies that the mesh skewness s, as defined in Section 3 by the relation

$$s=\frac{\Delta(Q)^2}{H(Q)}-2,$$

https://doi.org/10.1017/S0962492906400015 Published online by Cambridge University Press

is *invariant under the scale change* $Q \to LQ$. This implies that, if the mesh is generated by a scale-invariant PMA-type method, then any mesh regularity is *preserved under scaling.*

5.1.2. Discrete self-similar and approximately self-similar solutions

As mentioned above, a significant benefit of using a scale-invariant adaptive scheme is that it admits discrete self-similar solutions. One reason for this is the almost trivial, yet very important, observation that:

The actions of discretization and of rescaling commute,

where here a discretization can be any of a finite difference, collocation, finite element or a finite volume method. (This means that a discretization of a rescaled solution will be identical to a rescaling of a discrete solution.) More formally, if the PDE is invariant under the action of the scaling group

$$t \to \lambda t, \quad \mathbf{x} \to \lambda^{\beta}\mathbf{x}, u \to \lambda^{\alpha} u,$$

then a *continuous* self-similar solution takes the form

$$u(\mathbf{x}, t) = t^{\alpha} v(\mathbf{y}) \quad \mathbf{y} = \mathbf{x}/t^{\beta}. \tag{5.19}$$

In terms of the computational variables, this becomes

$$u(\mathbf{x}(\boldsymbol{\xi}, t)) = t^{\alpha} v(\boldsymbol{\xi}), \quad \mathbf{x}(\boldsymbol{\xi}, t) = t^{\beta}\mathbf{y}(\boldsymbol{\xi}),$$

for appropriate functions v and y. This leads immediately to a *discrete self-similar solution* of the form

$$U_i(t) = t^{\alpha} V_i, \quad X_i(t) = t^{\beta} Y_i, \tag{5.20}$$

For convenience we now study this discrete self-similar solution in the context of a prototypical example, a one-dimensional system governed by a semilinear second-order PDE of the form

$$u_t = u_{xx} + f(u), \quad \text{or in Lagrangian form} \quad u_t = u_{xx} + f(u) + \dot{x} u_x.$$

This PDE is invariant under the action of the scaling group

$$t \to \lambda t, \quad x \to \lambda^{1/2} x, \quad u \to \lambda^{\alpha} u$$

(so that $\beta = 1/2$), provided that the function $f(u)$ satisfies the functional equation

$$f(\lambda^{\alpha} u) = \lambda^{\alpha - 1} f(u).$$

Substituting the expression for the self-similar solution (5.19), and setting $\beta = 1/2$, we see that the function $v(y)$ must satisfy the *ordinary differential equation*

$$\alpha v - \frac{y}{2} v_y = v_{yy} + f(v), \quad \text{so that} \quad \alpha v = v_{yy} + f(v) + \frac{y}{2} v_y. \tag{5.21}$$

https://doi.org/10.1017/S0962492906400015 Published online by Cambridge University Press

Now consider a simple centred finite difference discretization of the Lagrangian form of the underlying PDE, which takes the form

$$\dot{U}_i = \frac{\frac{U_{i+1}-U_i}{X_{i+1}-X_i} - \frac{U_i-U_{i-1}}{X_i-X_{i-1}}}{\frac{1}{2}(X_{i+1}-X_{i-1})} + f(U_i) + \dot{X}_i \frac{U_{i+1}-U_{i-1}}{(X_{i+1}-X_{i-1})}.$$

We can substitute (5.20) directly into this expression to give

$$\alpha V_i = \frac{\frac{V_{i+1}-V_i}{Y_{i+1}-Y_i} - \frac{V_i-V_{i-1}}{Y_i-Y_{i-1}}}{\frac{1}{2}(Y_{i+1}-Y_{i-1})} + f(V_i) + \frac{Y_i}{2}\frac{V_{i+1}-V_{i-1}}{(Y_{i+1}-Y_{i-1})}. \tag{5.22}$$

It is immediately obvious that (5.22) is a consistent discretization of the ordinary differential equation (5.21) so that the function $v(y)$ will be approximated by V_i at the (time-independent computational) mesh point Y_i. Note further that the discretization error in approximating v by V_i is *independent of the solution scale*. In the case of systems such as the blow-up problems of Section 5.2, this implies that the asymptotic form of the singularity at the peak will be approximated with uniform accuracy for peaks with very small spatial scales (and correspondingly large solution scales). We note, however, that other errors do arise at points where the (rapidly) moving mesh following the evolving peak matches a nearly stationary mesh in the regions closer to the boundary of the domain.

To determine the location of the points Y_i in terms of the computational variables, we must apply the MMPDE used to evolve the mesh. Again, to give an example we consider MMPDE5. Substituting (5.20) into a standard discretization of MMPDE5 gives the following discrete equation for Y_i:

$$\frac{1}{2}Y_i = \frac{1}{2\Delta\xi^2}\big(M_{i+1/2}(Y_{i+1}-Y_i) - M_{i-1/2}(Y_i-Y_{i-1})\big). \tag{5.23}$$

Crucially, we note that the functional equation (5.14) satisfied by the monitor function M allows this rescaling to be made. Similar discrete equations arise for other choices of MMPDE, provided that M satisfies (5.14).

We note that exactly the same rescalings are possible in higher-dimensional problems using moving meshes generated by any other methods described in this subsection, and for any other form of discretization (provided that the processes of discretization and rescaling commute).

It is also possible to construct approximate discrete self-similar solutions in cases where the underlying solution is better described by approximate self-similar variables. Details of the calculations in this case are given in Budd and Williams (2006).

As an example of this we return to the porous medium equation in one dimension. For this problem, for all constants $C > 0$ there is a self-similar solution $u_s(x,t)$ of the form

$$u_s(x,t) = (t+C)^{-1/3}v(y), \quad x = (t+C)^{1/3}y,$$

https://doi.org/10.1017/S0962492906400015 Published online by Cambridge University Press

where the function $v(y)$ is given by the Barenblatt–Pattle profile (Barenblatt 1996). It is also well known that any positive initial data lead to a solution $u(x,t)$, which converges towards to a self-similar solution in the sense that

$$t^{1/3}u(t^{1/3}y,t) \to v(y).$$

Similarly, it is shown in Budd *et al.* (1999*b*) that if the monitor function is chosen to give a scale-invariant scheme (for example $M = u$), then this scheme admits a set of *discrete self-similar solutions* on a moving mesh which take the form

$$U_i(t) = (t+C)^{-1/3}V_i, \quad X_i(t) = (t+C)^{1/3}Y_i.$$

Note that the product

$$W_i \equiv U_iX_i = V_iY_i$$

is invariant in time. In Figure 5.1 we show the results of a computation presented in the computational domain, using a scale-invariant moving mesh method with $M = u$ and a centred finite difference discretization. In this calculation the initial data at $t = 0$ were taken to be an irregular function, and results are plotted at times $t = 0$ and $t = 10$. We also show (dashed) two discrete self-similar solutions with values of C chosen so that they initially lie above and below the solution. Note that the solution calculated is sandwiched between these two functions. We also present the corresponding mesh $X_i(t)$ and the scaled mesh $Y_i(t) = X_i(t)/t^{1/3}$. It is clear from these figures that the computed solution converges towards the discrete self-similar solutions (in correspondence with the continuous theory) and that the moving mesh tends towards the one for which Y_i is constant in time so that $X_i(t)$ scales asymptotically as $t^{1/3}$. Similar figures for solutions of the porous medium equation computed using a scale-invariant ALE method in two dimensions are given in Baines *et al.* (2006).

5.2. Blow-up and related problems

5.2.1. Parabolic blow-up

As mentioned in Section 5.1, a significant success in the application of moving mesh methods occurs in the study of parabolic partial differential equations (and also of systems of PDEs) which have solutions that blow up, so that the solution, or some derivative of it, becomes infinite in a finite time T. We now consider such problems in a little more detail. Blow-up in the solution often represents an important change in the properties of the model that the equation represents (such as the ignition of a heated gas mixture), and it is important that it is reproduced accurately in a numerical computation. A survey of many different types of blow-up problem is presented in Samarskii *et al.* (1973). Blow-up typically occurs on increasingly small time and length scales, and hence it is usually essential to use both

https://doi.org/10.1017/S0962492906400015 Published online by Cambridge University Press

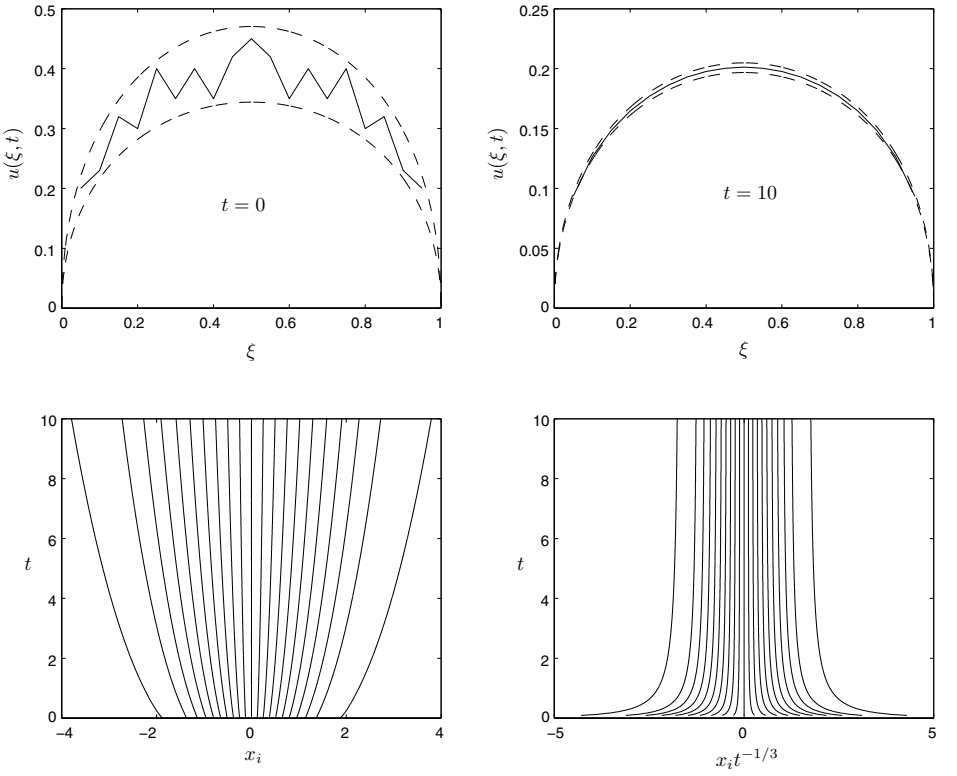


Figure 5.1. Convergence of the solution in the computational domain to the discrete self-similar solution. Note the invariance of the solution profile in this domain. We also show the evolution of the mesh and note that this scales as $t^{1/3}$.

temporarily and spatially adaptive methods for any such computation. A survey of methods and underlying numerical theory for blow-up-type problems is given in Budd *et al.* (1996), with more recent references in Budd and Williams (2006), Ceniceros and Hou (2001) and Huang, Ma and Russell (2008). Mesh refinement (h-adaptive) methods have been used in some numerical studies of blow-up, including the dynamic rescaling methods, such as those described in Berger and Kohn (1988), but moving mesh methods have proved to be more effective in both one and two dimensions. This is due, in part, to the strong scaling symmetry properties of the solution close to blow-up (where the effects of boundary and initial conditions become progressively less important), and the way that this can be exploited by using the scale-invariant methods described in Section 5.1.

https://doi.org/10.1017/S0962492906400015 Published online by Cambridge University Press

A prototype example of a blow-up system is the parabolic partial differential equation

$$u_t = \Delta u + u^p, x \in \Omega, \quad p > 1, \quad u|_{\partial\Omega} = 0. \tag{5.24}$$

This has the property of *single-point blow-up* in that for certain types of sufficiently large initial data, there is a point $\mathbf{x}^*$ and a finite time T so that

$$u(x^*, t) \to \infty \quad \text{as} \quad t \to T.$$

Close to the point $\mathbf{x}^*$ the solution develops a narrow peak which evolves in an approximately self-similar manner. It is not uncommon to consider solutions which change by ten orders of magnitude, with a reduction in the solution length scale by a similar amount. It is essential to use an adaptive method to capture such behaviour accurately.

Example 1. The first example that we consider is given by

$$\begin{aligned} u_t &= \Delta u + u^3, & \mathbf{x} = (x, y) \in \Omega = (0, 1)^2, \\ u(\mathbf{x}, t) &= 0, & \mathbf{x} \in \partial\Omega, \\ u(\mathbf{x}, 0) &= 5 \exp(-25(x - 0.45)^2 - 25(y - 0.35)^2). \end{aligned} \tag{5.25}$$

This problem has the natural scaling symmetry

$$t \to \lambda t, \quad \mathbf{x} \to \lambda^{1/2}\mathbf{x}, \quad u \to \lambda^{-1/2}u,$$

it has a natural time scale of $(T-t)$, and it is shown in Samarskii *et al.* (1973) that the natural space and solution scales are given by the approximately self-similar variables

$$L = (T - t)^{1/2} |\log(T - t)|^{1/2} \quad U = (T - t)^{-1/2}.$$

To compute a solution, we augment this problem with the PMA equation (5.17) to determine the moving mesh with a monitor function of the form $M \equiv M(u)$. To obtain scale invariance for this system we require that M must satisfy the function equation (5.18) so that

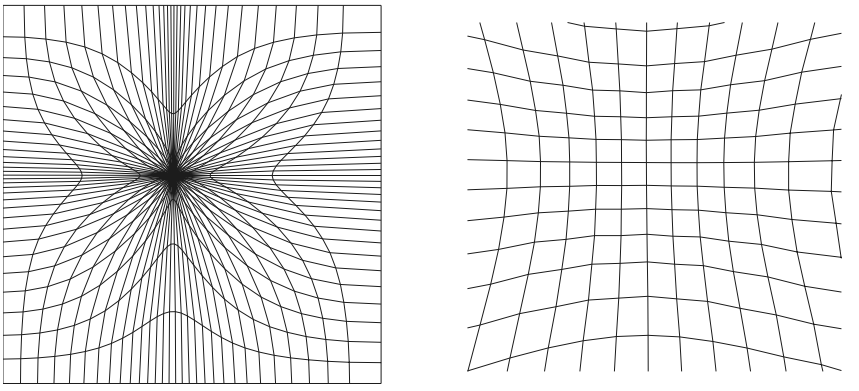
$$M((T - t)^{-1/2}u)^{1/2} = \frac{1}{(T - t)} M(u).$$

A simple solution of this is $M(u) = u^4$. In practice this monitor function can lead to instabilities due to placing too many points in the singular region and not sufficiently closer to the boundary of the domain, and to overcome this we apply a McKenzie regularization to give

$$M(u) = u(\mathbf{x}, t)^4 + \int_{\Omega_P} u(\mathbf{x}', t)^4 \, \mathrm{d}\mathbf{x}'.$$

This choice of monitor leads to a mesh which automatically inherits the correct dynamic length scale of the underlying solution in the singular regions

https://doi.org/10.1017/S0962492906400015 Published online by Cambridge University Press



(a) (b)

Figure 5.2. *Example 1.* Final grid for the blow-up example. (a) Entire grid. (b) Detail near the blow-up point. Note that the grid is quite regular in the vicinity of the singularity, with no evidence of any skewness or tangling.

where u is large. We can then find a solution of the blow-up problem in the computational domain Ω_C, using a finite difference method with a uniform $N = 30 \times 30$ mesh in the computational domain to discretize both the PMA equation and the Lagrangian form of the underlying PDE. The resulting system of ODEs was then solved *simultaneously* using a BDF method. In this calculation, as the blow-up time was approached an adaptive time step was used by applying the Sundman transformation, as described in Budd *et al.* (2001). For this we take

$$\Delta t = \frac{1}{(\max u)^2}.$$

In Figure 5.2 we show the final grid both over the whole domain and close to the peak near the centre, as well as the initial and final solutions. The integration was performed until $|u|_\infty = 10^{15}$, for which the peak has an approximate length scale of 10^{-15}.

Over the course of the evolution we see a mesh compression (and a solution amplification) by a factor of 10^{12} in the physical domain. Note that this has been achieved with a very modest number of mesh points. The final mesh shows a similar gradation of mesh elements from size $\mathcal{O}(10^{-2})$ to size $\mathcal{O}(10^{-14})$. However, if we study the mesh close to the solution peak, as illustrated in Figure 5.2, we see that this shows a strong degree of local regularity, with no evidence of long thin elements or skewness in the region where the solution gradients are very large. This is exactly as predicted by

https://doi.org/10.1017/S0962492906400015 Published online by Cambridge University Press

the previous theory. (Away from the solution peak the mesh is less smooth; however, in this region the solution gradients are much smaller than in the peak, and the local truncation errors are thus lower.)

Example 2. In order to consider these results in the context of some of the error analysis presented in Sections 2 and 3, it is instructive to look at a second one-dimensional example, in which we consider the blow-up problem

$$u_t = u_{xx} + u^3, \quad u_x(0) = u(1) = 0.$$

It is known (Samarskii *et al.* 1973) that this equation has solutions which blow up at the origin, and in the peak the asymptotic blow-up profile of this solution takes the form

$$u(x,t) = \frac{1}{\sqrt{T-t}} \frac{1}{\sqrt{1 + ax^2/L^2}}, \tag{5.26}$$

where a is a constant (depending weakly on the initial conditions) which we may take equal to unity, and $L(t)$ is the natural length scale given by

$$L(t) = \sqrt{(T-t)|\log(T-t)|}.$$

As this is now a problem in one dimension, we initially take $M = u^2$ so that, in the peak,

$$M = \frac{1}{(T-t)} \frac{1}{1 + x^2/L^2}.$$

The integral of M is overwhelmingly dominated by the contribution in the peak, so that

$$\theta = \int_0^1 M \, \mathrm{d}x = \frac{L}{(T-t)} \tan^{-1}(1/L) \approx \frac{\pi L}{2(T-t)}.$$

We can then take a regularized monitor function of the form

$$\bar{M} = M + \theta, \quad \text{with} \quad \int_0^1 \bar{M} = 2\theta,$$

to ensure that we have a 50:50 mesh. In the peak, $\bar{M} \approx M$ and an equidistributed mesh satisfies the equation $Mx_\xi = 2\theta$ so that

$$x_\xi = \pi L(1 + x^2/L^2).$$

It follows immediately that in the peak we have

$$x(\xi,t) = L(t) \tan(\pi\xi). \tag{5.27}$$

Observe that, if $\xi < 1/2$, then $x = \mathcal{O}(L)$, and that this mesh matches naturally to one for which $x = \mathcal{O}(1)$ as $\xi \to 1/2$, so that we have (as required) half of the mesh points in the peak and half outside the peak.

https://doi.org/10.1017/S0962492906400015 Published online by Cambridge University Press

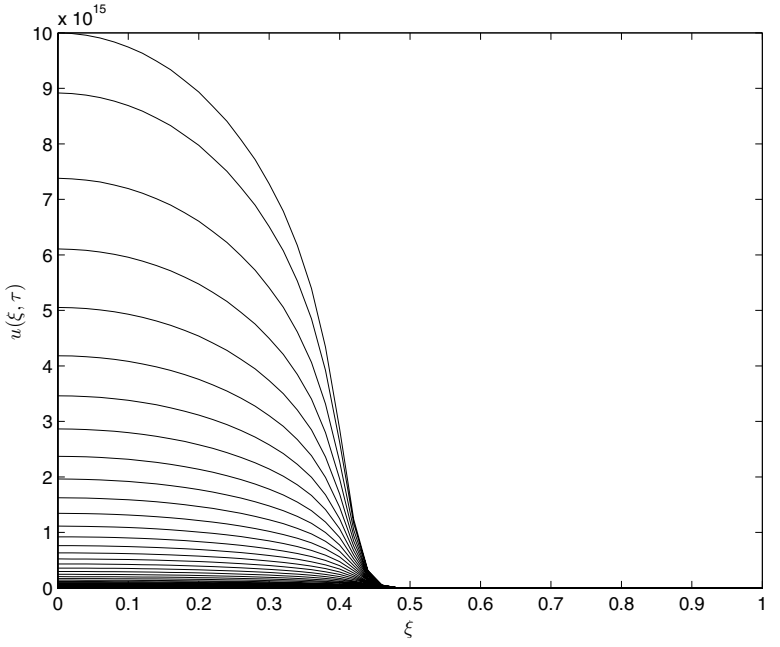


Figure 5.3. *Example 2.* Solution profile for the blow-up problem computed in the computational space up to a peak value of 10^{15}.

In Figure 5.3 we show the solution computed in the computational plane using a simple centred discretization of the PDE using a uniform mesh with $N = 30$ points in the computational space. Observe that the peak in the region $\xi < 1/2$ has a regular form with no evidence of instability.

In Figure 5.4 we present the mesh evolving in time and also a plot of $\tau \equiv \log(T - t)$ as a function of $\log(x)$. Observe that the mesh in the first of these figures has concentrated in the peak, but that there is still good resolution of the solution away from the peak. In the second figure we see that all of the grid cells move at the same rate close to the origin, demonstrating the self-similar form there.

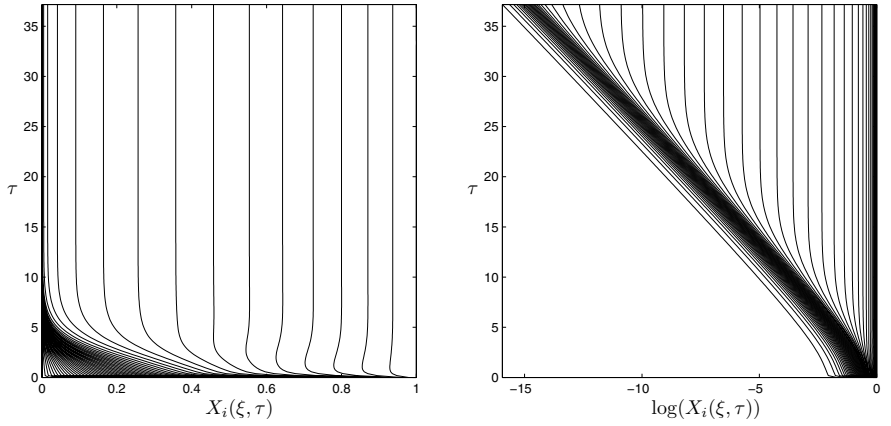
The expression (5.27) allows a direct evaluation of the leading-order terms in the truncation error Tr. Recall from (2.49) that the leading term in the truncation error in the discretization of u_{xx} is given by

$$\mathrm{Tr} = \Delta\xi^2 \left(\frac{1}{3} x_{\xi\xi} u_{xxx} + \frac{1}{12} x_\xi^2 u_{xxxx} \right).$$

From (5.27) we have

$$x = L\tan(\pi\xi), \quad x_\xi = \pi L \sec^2(\pi\xi), \quad x_{\xi\xi} = 2\pi^2 L \tan(\pi\xi)\sec^2(\pi\xi).$$

https://doi.org/10.1017/S0962492906400015 Published online by Cambridge University Press



(a) (b)

Figure 5.4. *Example 2.* Blow-up mesh. (a) Grid in the natural coordinates. (b) Plotting $\tau = |\log(T-t)|$ as a function of $\log(X_i)$ at equally spaced values of ξ, showing the contraction rate and approximately self-similar behaviour close to the origin.

A straightforward calculation based on the scaling structures of u shows that, in the peak region,

$$u = \mathcal{O}\left(\frac{1}{\sqrt{T-t}}\right), \qquad u_{xx} = \mathcal{O}\left(\frac{1}{L^2\sqrt{T-t}}\right),$$
$$u_{xxx} = \mathcal{O}\left(\frac{1}{L^3\sqrt{T-t}}\right), \quad u_{xxxx} = \mathcal{O}\left(\frac{1}{L^4\sqrt{T-t}}\right).$$

If $\xi < 1/2$ we can also see that x and its derivatives are all of $\mathcal{O}(L)$. As a consequence, substituting into the expression for T, we have that in this region

$$\mathrm{Tr} = \mathcal{O}\left(\frac{\Delta\xi^2}{L^2\sqrt{T-t}}\right), \quad \text{so that} \quad \frac{\mathrm{Tr}}{u_{xx}} = \mathcal{O}\left(\Delta\xi^2\right).$$

We can see from this expression that the *relative truncation error* $\mathrm{Tr}\,/u_{xx}$ in discretizing u_{xx} depends only on $\Delta\xi$ and not on the intrinsic solution scale. This analysis starts to break down as $\xi \to 1/2$, and the terms $x_{\xi\xi}$, *etc.*, become large as the mesh adapted to the peak evolves into a uniform mesh close to the boundary. However, the results shown above do not indicate instability in the mesh in this limit.

https://doi.org/10.1017/S0962492906400015 Published online by Cambridge University Press

5.2.2. Focusing solutions of the nonlinear Schrödinger equation
The nonlinear Schrödinger equation described in Section 5.1.1,

$$\mathrm{i}u_t + \Delta u + u|u|^2 = 0, \quad \mathbf{x} \in \mathbb{R}^n, \tag{5.28}$$

is a model for the modulational instability of water waves and plasma waves, and is important in studies of nonlinear optics where the refractive index of a material depends on the intensity of a laser beam. In all dimensions it has the conserved quantities

$$\int |u|^2 \,\mathrm{d}\mathbf{x} \quad \text{and} \quad \int \left(|\boldsymbol{\nabla} u|^2 - \frac{1}{2}|u|^4 \right) \mathrm{d}\mathbf{x},$$

corresponding to mass and energy respectively. In one dimension (5.28) is integrable and can give rise to soliton-type solutions. More generally, it is an example of a Hamiltonian PDE. Many numerical (usually non-adaptive) methods have been derived to take advantage of this integrability (Budd and Piggott 2005, McLachlan 1994). If posed in n dimensions, where $n \geq 2$, then the PDE (5.28) is no longer integrable and it may admit singular (focusing) solutions for certain initial data. A review of these is given by Sulem and Sulem (1999), who also describe some numerical computations using a moving mesh method based on Winslow's algorithm. Numerically this is a very difficult problem, as high resolution in time and space is required to capture the strong self-focusing of the solution, to deal with the highly oscillatory nature of the solution 'tail', and to compute over a large domain to avoid boundary effects (Budd *et al.* 1999*a*, Ceniceros 2002). In such singular solutions both the maximum value of the solution modulus, and its phase, blow up in a finite time T. The precise form of this blow-up and the initial conditions that lead to blow-up are the subject of much investigation (see the review in Sulem and Sulem (1999)), and much remains unresolved. Two significant open questions are: (1) What is the exact nature of the blow-up profile in two dimensions (where it is known to be approximately self-similar but the precise form is still unclear), and (2) Do there exist radially symmetric self-similar solutions in three dimensions? In the latter case these are conjectured to take the form

$$u(r,t) = \frac{1}{\sqrt{(T-t)}} \mathrm{e}^{\mathrm{i}a \log(T-t)} Q(y), \quad r = \sqrt{T-t}\, y, \quad r = |\mathbf{x}|,$$

where a is an unknown constant. The existence of such a solution can be addressed by a scale-invariant method applied to the (one-dimensional) class of radially symmetric solutions. In this we take the monitor function

$$M = |u(r,t)|^2,$$

derived in Section 5.1.1, and use a collocation-based discretization with $N = 81$ points. In such a calculation we would expect to observe a discrete

https://doi.org/10.1017/S0962492906400015 Published online by Cambridge University Press

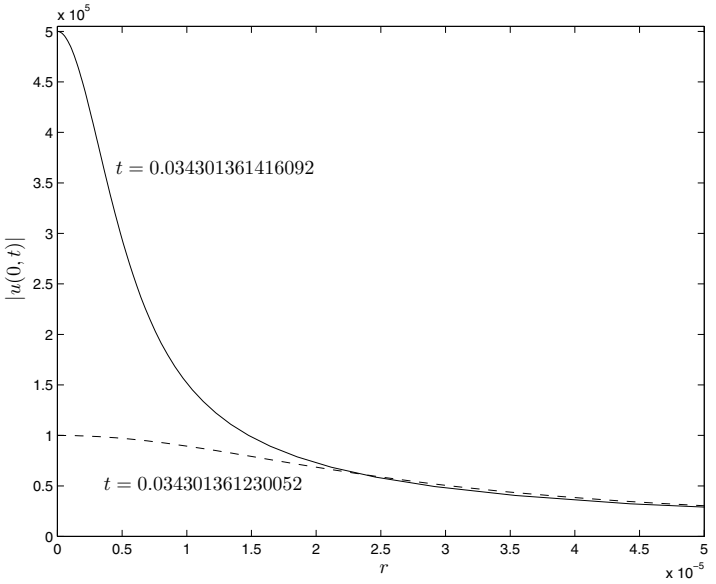


Figure 5.5. The solution when $|u(0,t)| = 100000$ and 500000. Note the narrow width of the peak.

self-similar solution for which the mesh points X_i should take the form $X_i = \sqrt{T-t}Y_i$, so that

$$|u(0,t)|X_i = Q(0)Y_i$$

is constant in time. In Figure 5.5 we plot two solutions starting from initial data $u(r,0) = 6\sqrt{2}\exp(-r^2)$, which have a computed blow-up time of $T = 0.0343013614215$. Observe the excellent resolution of the peak even when the peak amplitude is around 10^5 and the peak width is around 10^{-5}. In Figure 5.6 we show the computed values of $W_i \equiv |u(0,t)|X_i$ as functions of $\tau = \log(T-t)$ for a range in which $|u|$ varies from 100 to 500000. These are clearly tending towards constants, indicating that both the solution and the mesh are evolving in a self-similar manner.

It is interesting to note that the scale-invariant methods are easy to use and give rather better results in this case than symplectic methods described in McLachlan (1994), despite the Hamiltonian structure of the problem. This is because the adaptive methods give much better resolution of the peak.

In contrast, further computations of focusing solutions of the nonlinear Schrödinger equation are given by Ceniceros (2002). In this case the following highly dispersive problem was studied:

$$\mathrm{i}\epsilon u_t + \frac{1}{2}\epsilon^2 u_{xx} + u|u|^2 = 0, \quad u(x,0) \equiv u_0 = A_0(x)\mathrm{e}^{\mathrm{i}S_0(x)/\epsilon}, \tag{5.29}$$

https://doi.org/10.1017/S0962492906400015 Published online by Cambridge University Press

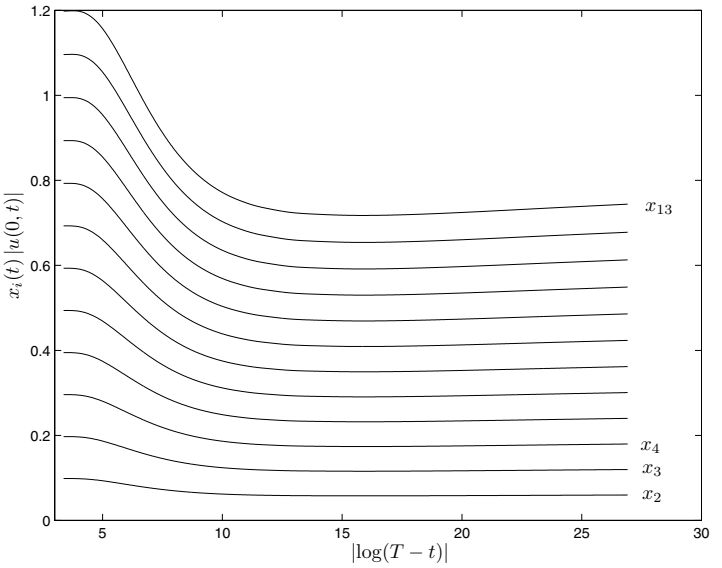


Figure 5.6. The evolution of the mesh as the blow-up time T is approached. Observe that the product $X_i|u(0,t)|$ converges to a constant, indicating that both solution and mesh are evolving in a self-similar manner.

with $\epsilon \ll 1$. In this calculation a moving mesh method with smoothing was used, as described in Section 3. This took the form

$$(1 - \gamma\partial^2_{\xi\xi})\dot{x} = (Mx_\xi)_\xi), \tag{5.30}$$

with $\gamma = \max(M)$. In Ceniceros (2002) the Lagrangian form of the PDE (5.29) was discretized in the computational domain and solved alternatively with the MMPDE (5.30) using the methods described in Section 3. In particular, a semi-implicit BDF method was used for the time integration of both the moving mesh equation and the underlying PDE. A monitor function of the form

$$M = \sqrt{1 + \beta^2|u_\xi|^2 + \alpha^2|u|^4}$$

was employed, with

$$\beta = (2L)^2 \frac{\|u_{0,x}\|_\infty}{\|u_0\|}$$

and L a measure of the size of the computational domain. In this calculation, particular care had to be taken with the spatial discretization of the mesh movement terms of the form $\dot{x}u_x$, arising in the Lagrangian form of (5.29) as the dispersive nature of (5.29) meant that there was no natural damping to the high-frequency terms in the errors associated with a central difference

https://doi.org/10.1017/S0962492906400015 Published online by Cambridge University Press

discretization This is in contrast to the highly dissipative nature of the discretization of (5.30), which took the form

$$\frac{X_j^{n+1}-X_j^n}{\Delta t}=\gamma\frac{X_{j+1}^{n+1}-2X_j^{n+1}+X_{j-1}^{n+1}}{\Delta\xi^2}-\gamma\frac{X_{j+1}^{n}-2X_j^{n}+X_{j-1}^{n}}{\Delta\xi^2}$$
$$+\frac{1}{\Delta\xi^2}\left[M_{j+1/2}^n(X_{j+1}^n-X_j^n)-M_{j-1/2}^n(X_j^n-X_{j-1}^n)\right].$$

To avoid some of the resulting instabilities reported in Li *et al.* (1998) and discussed in Section 5.3 in the context of the solution of Burgers' equation, a high-order (fourth-order central difference) expression was used to discretize the Lagrangian advective term $\dot{x}u_x$. The resulting semi-implicit BDF discretization then took the form

$$\frac{1}{2\Delta t}[3U_j^{n+1}-4U_j^n+U_j^{n-1}]=$$
$$\mathrm{i}\frac{\epsilon\sigma_j^{n+1}}{2\Delta\xi^2}\left[\sigma_{j+1/2}^{n+1}(U_j^{n+1}-U_j^{n+1})-\sigma_{j-1/2}^{n+1}(U_j^{n+1}-U_{j-1}^{n+1}\right]$$
$$+2\left[\frac{\mathrm{i}}{\epsilon}|U_j^n|^2U_j^n+\dot{X}_j^n\frac{U_{j-2}^n-8U_{j-1}^n+8U_{j+1}^n-U_{j+2}^n}{X_{j-2}^n-8X_{j-1}^n+8X_{j+1}^n-X_{j+2}^n}\right]$$
$$-\left[\frac{\mathrm{i}}{\epsilon}|U_j^{n-1}|^2U_j^{n-1}+\dot{X}_j^{n-1}\frac{U_{j-2}^{n-1}-8U_{j-1}^{n-1}+8U_{j+1}^{n-1}-U_{j+2}^{n-1}}{X_{j-2}^{n-1}-8X_{j-1}^{n-1}+8X_{j+1}^{n-1}-X_{j+2}^{n-1}}\right],$$

with $\sigma=1/x_\xi$. The resulting moving mesh method was then found to be highly effective in computing the focusing solutions.

Remark. It bears mentioning that finding self-similar or approximately self-similar structures for analytical solutions to PDEs can be extremely demanding, and moving mesh methods with built-in scale invariance can often be used to gain insight into the form of such structures. A case in point is the paper by Budd, Galaktionov and Williams (2004), which analysed an unexpected form of blow-up for a fourth-order PDE, entirely motivated by the results of numerical calculations with a moving mesh method.

5.3. Some problems with moving fronts

A classical problem leading to the formation of sharp fronts is Burgers' equation given (in two dimensions) by

$$u_t+\frac{1}{2}(u^2)_x+\frac{1}{2}(u^2)_y=\nu\Delta u,\quad \nu\ll 1. \tag{5.31}$$

This equation has been used as a benchmark for a number of different moving mesh algorithms (Huang and Russell 1997*a*, Mackenzie and Mekwi 2007*a*, Zhang and Tang 2002, Tang and Xu 2007, Li *et al.* 1998).

https://doi.org/10.1017/S0962492906400015 Published online by Cambridge University Press

Example 1. As a first calculation we consider a problem with the initial and boundary values chosen over the unit square, so that (5.31) has the exact solution given by

$$u(x,y,t) = \left(1 + \mathrm{e}^{(x+y-t)/2\nu}\right)^{-1}. \tag{5.32}$$

This solution has a sharp moving front. For the purposes of this example we consider coupling this system to the PMA algorithm described in Section 3, to generate a moving mesh which can both compute an approximation to this solution and follow the front as it evolves over the time interval $t \in [1/4, 2]$. To do this we discretize (5.31) in the Lagrangian form

$$u_t = \nu\Delta u - \left(\frac{1}{2}(u^2)_x + \frac{1}{2}(u^2)_y\right) + \dot{x}u_x + \dot{y}u_y, \quad \nu \ll 1. \tag{5.33}$$

with all discretizations made in the computational variables. The conservation form of the equation above is used for this calculation so that, for example, the advective term u_x^2 is rescaled as

$$u_x^2 = \frac{1}{J}\left[y_\eta u_\xi^2 - y_\xi u_\eta^2\right],$$

which is then discretized using a central difference scheme. For this calculation we also take similar discretizations for the other advective terms. The equation posed in the computational variables is then coupled to the discretized form of PMA equation (5.17) with the values of the approximation $U_{i,j}$ to $u(X_i, Y_j)$ and of Q given on the mesh vertices. In these computations we take an $N \times N$ computational mesh (typically $N = 40$), a viscosity of $\nu = 0.005$, and use the arclength monitor function

$$M = \sqrt{1 + \alpha\left(u_x^2 + u_y^2\right)},$$

with $\alpha = 1$. A number of different strategies could be used to evolve this coupled system forward in time, but in practice a simple scheme which solved the PMA equation and (5.33) *simultaneously* using a simple forward Euler method is effective with a time step Δt, as given in Zhang and Tang (2002), determined by the CFL condition. In the PMA equation we used $\epsilon = 1, \gamma = 0.335$ to find the initial mesh (before evolving the solution PDE) when $t = 1/4$, and then $\epsilon = 0.01, \gamma = \sqrt{\max(M)}$ to follow the front up to $t = 2$. More details are given in Walsh *et al.* (2009). We note that solving the PMA equation coupled to (5.33), using an alternating solution strategy coupled with an up-winding discretization, has also been shown to be effective (Sulman 2008). In Figure 5.7 we present the results of a series of computations using this method, when $N = 40$, showing both the solution for (5.31) and the corresponding mesh. In this figure we see excellent resolution of the solution at the front.

https://doi.org/10.1017/S0962492906400015 Published online by Cambridge University Press

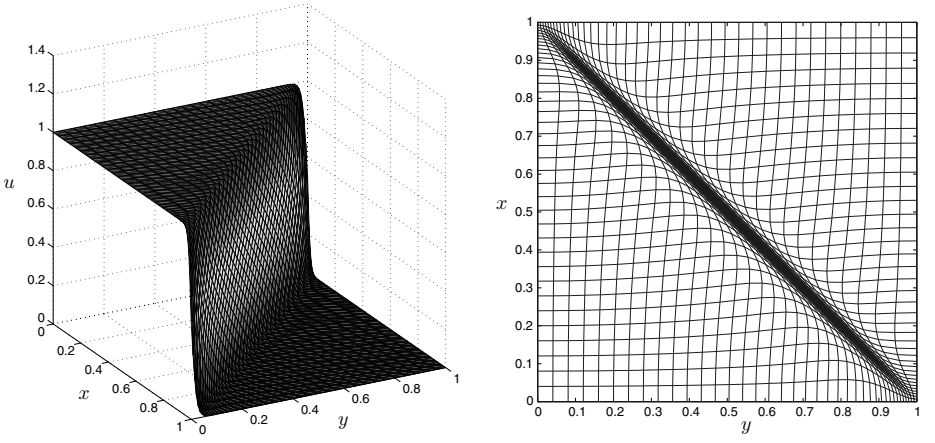


Figure 5.7. *Example 1.* The solution of Burgers' equation and the corresponding mesh at the time $t = 1$.

Table 5.1.

N	L_2-error on a uniform mesh	L_2-error on the moving mesh
20	6e-2	8e-3
40	2e-2	2e-3
80	6e-3	1e-3

A quantitative measure of the error in the computed solution at $t = 1$ can be given by determining the L_2-norm of the difference between it and the exact solution. We consider this error both for a uniform and a moving mesh for various values of N: see Table 5.1.

Sulman (2008) obtained a similar table by using a PMA method in which the convective terms are calculated by using an upwind method and the PMA system, and solved the underlying PDE alternately. It is also interesting to compare this calculation with the results presented in Zhang and Tang (2002). In this paper a harmonic mapping method of the form described in Section 4 was used to generate the mesh, and this was then coupled to a finite volume discretization of (5.31.) We see from Table 5.1 that a useful reduction in the error for calculating the solution to (5.31) resulted from the PMA method. This reduction is similar to that observed in Zhang and Tang (2002) for the harmonic map method.

https://doi.org/10.1017/S0962492906400015 Published online by Cambridge University Press

Example 2. In closely related calculations we can compare with a similar moving mesh calculation of the solution of Burgers' equation, over the interval $x \in [0, 1]$, when $\nu = 1e - 4$ and with initial data $u_0 = \sin(2\pi x) + (1/2)\sin(\pi x)$. In this case we compute the mesh using a one-dimensional form of PMA with the arclength monitor function and $N = 30$ mesh points, central differencing in the computational domain for all spatial derivatives, and solve the resulting ODEs using the MATLAB routine ode15s. We start with an initially uniform mesh, and evolve the mesh and solution together using PMA with $\epsilon = 1$. In this calculation, and with this choice of ϵ, the mesh evolves from being uniform to one which is equidistributed, over a time $t \approx 0.05$. In this time period the underlying solution remains fairly smooth. At the time $t \approx 0.2$ the solution develops a sharp front, which is well approximated, and then followed, by the evolving mesh. The solution is presented in the physical domain at a series of different times in Figure 5.8, and the resulting mesh trajectories are presented in Figure 5.9. Observe the manner in which the mesh points resolve the front with no oscillations in this case (due in part to the regularity of the initial data).

It is interesting to compare this calculation with a very similar calculation made by Li and Petzold (1997), who looked at the solution of Burgers' equation when $\nu = 1e - 4$ with the less regular initial data given by

$$u(x, 0) \equiv u_0 = 0.2, \quad x \leq 0.1, \quad u_0 = 8x - 0.6, \quad 0.1 \leq x \leq 0.2$$
$$u_0 = 1, \quad 0.2 \leq x \leq 0.5, \quad u_0 = -10x + 6, \quad 0.5 \leq x \leq 0.6,$$
$$u_0 = 0, \quad 0.6 \leq x \leq 1.$$

This is a more severe test of the moving mesh method than the previous example, as the initial data are much less smooth. This calculation employed an arclength-based monitor function together with a regularized differential algebraic formulation of the moving mesh equations, very similar to using MMPDE6, and based on a method proposed in Adjerid and Flaherty (1986), with the mesh-smoothing algorithm proposed by Dorfi and Drury (1987), described in Section 2. Li and Petzold (1997) considered three different discretizations: a central difference discretization, an ENO (Roe) method, and a piecewise hyberbolic method (PHM) due to Marquina (1994). It was found that in this case the central difference method tended to lead to spurious oscillations due (as commented on in the example of the nonlinear Schrödinger equation) to the destabilizing effect of the anti-diffusive terms arising in the discretization of the advective terms describing the mesh motion. Li and Petzold (1997) showed that these oscillations were reduced with the ENO scheme and eliminated using the PHM method.

The related paper by Li *et al.* (1998) also considered applying the same moving mesh method to a number of other reaction–diffusion problems,

https://doi.org/10.1017/S0962492906400015 Published online by Cambridge University Press

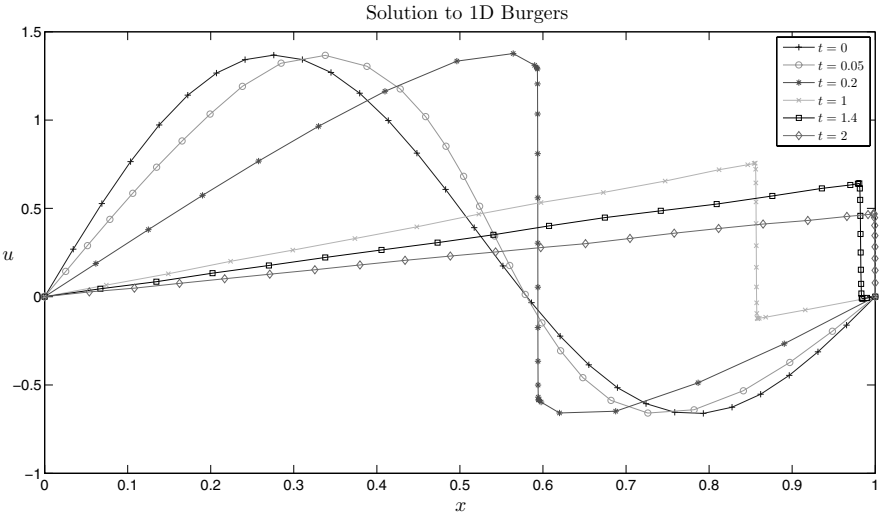


Figure 5.8. The computed solution of Burgers' equation in one dimension at times $t = 0, 0.05, 0.2, 1, 1.4, 2$.

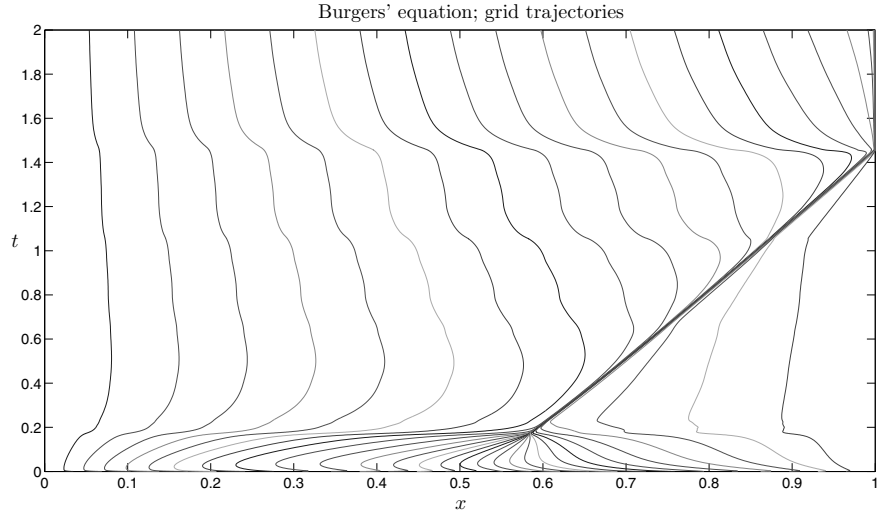


Figure 5.9. The motion of the mesh points when solving Burgers' equation in one dimension.

https://doi.org/10.1017/S0962492906400015 Published online by Cambridge University Press

including the Fisher equation,

$$u_t = \beta u_{xx} + \alpha u(1-u). \tag{5.34}$$

This equation has an exact solution with a moving front given by

$$u = (1 + \exp(\sqrt{\alpha/6}x - 5\alpha t/6))^{-2}.$$

Whilst it was found that the wave front was well resolved, the moving mesh method appeared to give worse results than for the fixed grid, with the front moving at the wrong speed (too fast). Li *et al.* (1998) proposed that this error was largely due to the effects of discretizing the additional convective terms due to the moving mesh, as discussed in Section 3, which can lead both to a high truncation error and instabilities in the solution. A possible solution is to use higher-order methods or a curvature-dependent monitor function; *e.g.*, see Qiu and Sloan (1998). However, there is an interesting alternative reason for the error. In problems such as (5.34), the speed of motion of the front is not so much determined by the shape of the front itself but by the nature of the exponential terms in the tails of the solution and how they interact with the boundaries. Similar behaviour arises in the Cahn–Hilliard equation, and also in similar systems such as the Gray–Scott equation in chemistry. Somewhat paradoxically, the solution needs to be well resolved in the boundary regions where it appears to be behaving smoothly, in order for the front speed to be accurately resolved. Thus a uniform mesh may well perform better than a moving mesh in these cases, as it will probably be placing more mesh points close to the boundary.

5.4. Problems involving a change of phase and/or combustion

A very rich set of examples of the use of moving mesh methods is given by Stefan-type problems, involving phase changes or combustion, and examples of these can be found in Beckett *et al.* (2001*a*), Mackenzie and Mekwi (2007*a*), Mackenzie and Robertson (2002), Miller, Gleyzer and Imhoff (1998), Huang and Zhan (2004), Zegeling (2005), Tan (2007) and Tan *et al.* (2007).

As an example we consider the combustion problem described in Cao *et al.* (1999*a*) and Moore and Flaherty (1992). The mathematical model is a system of coupled nonlinear reaction–diffusion equations,

$$\frac{\partial u}{\partial t} - \boldsymbol{\nabla}^2 u = -\frac{R}{\alpha\delta} u\, \mathrm{e}^{\delta(1-1/T)},$$
$$\frac{\partial T}{\partial t} - \frac{1}{Le}\boldsymbol{\nabla}^2 T = \frac{R}{\delta Le} u\, \mathrm{e}^{\delta(1-1/T)},$$

where u and T represent the dimensionless concentration and temperature of a chemical which is undertaking a one-step reaction. We consider the J-shape solution domain shown in Figure 5.10. The initial and boundary

https://doi.org/10.1017/S0962492906400015 Published online by Cambridge University Press

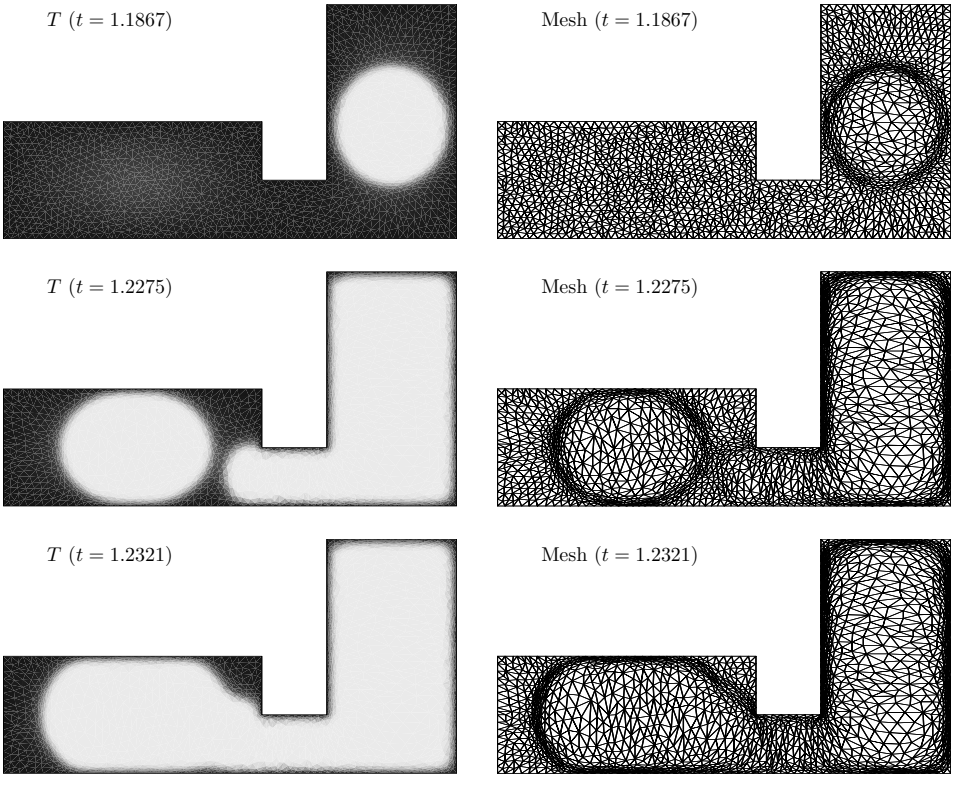


Figure 5.10. The contour plot of the temperature T (where white represents 2.2 and black represents 1) and the moving meshes are shown at various times.

conditions are

$$u|_{t=0} = T|_{t=0} = 1, \quad \text{in } \Omega,$$
$$u|_{\partial\Omega} = T|_{\partial\Omega} = 1, \quad \text{for } t > 0$$

and the physical parameters are set to be $Le = 0.9, \alpha = 1, \delta = 20$, and $R = 5$. A resulting calculation obtained with an MMPDE finite element method as described in Section 3 (with details in Cao *et al.* (1999*a*)) is shown in Figure 5.10.

5.5. Convection-driven problems in meteorology

A system of interest to meteorologists is the *Eady problem*, which describes the evolution of (localized) extra-tropical (mid-latitude) cyclones. The Eady problem is a two-dimensional reduction of the Euler equations describing the (incompressible) air velocity (u, w) and pressure P in the (x, z)-plane, where $x \in [-L, L]$ is a horizontal coordinate along lines of constant latitude,

https://doi.org/10.1017/S0962492906400015 Published online by Cambridge University Press

and $z \in [0, H]$ represents height. (A shallow atmosphere model is used with $H \ll L$, together with an f-plane approximation which uses a locally flat approximation to the Earth's curvature.) This model also includes both the potential temperature θ (relative to a reference temperature θ_0) and Coriolis effects. It is described in detail in Cullen (2006) and takes the form

$$\begin{aligned} \frac{Du}{Dt} - fv + P_x &= 0, \\ \frac{Dv}{Dt} + fu - \frac{Cg}{\theta_0}(z - H/2) &= 0, \\ \frac{D\theta}{Dt} - Cv &= 0, \\ \frac{Dw}{Dt} + P_z - \frac{g\theta}{\theta_0} &= 0, \\ u_x + w_z &= 0. \end{aligned}$$

Here D is the advective (total) derivative, f is the Coriolis parameter (assumed constant), g is the gravitational constant and $C = -\theta_y$ is assumed constant. All variables are periodic in x, with w and P_x vanishing at $z = 0$ and $z = H$. From certain initially smooth data (as described by Nakamura (1994)), it is possible (Cullen 2006) for the solutions of the Eady problem to develop severe fronts in a small number of days, and some sort of adaptive mesh is needed to resolve the fine structure of the solution close to the fronts. In Figure 5.11 we present the solution to the Eady problem close to the formation of a severe tropical storm, obtained by using a pressure-correction method on a semi-staggered grid, looking at the contours in the horizontal and vertical coordinates (x, z) of the longitudinal wind speed v and potential temperature θ.

We consider two different monitor functions coupled to PMA to find adaptive meshes for this problem. In the first case we take the arclength monitor function

$$M_1 = \sqrt{1 + |\boldsymbol{\nabla} v|^2}.$$

In the second case we take the monitor function M_2 to be an estimate of the *potential vorticity* q of the solution, so that M_2 is taken to be the maximum eigenvalue of the matrix

$$Q = \begin{pmatrix} v_x + f & v_z \\ \theta_x & \theta_z \end{pmatrix},$$

for which $q = \det(Q)$. The resulting meshes are shown in Figure 5.12. In both cases we see well-structured and regular meshes with good resolution at the boundaries and of the front, and with no evidence of mesh tangling. However, use of the potential vorticity monitor function M_2 leads to a mesh which more precisely follows the physical solution. Further details are given in Walsh *et al.* (2009).

https://doi.org/10.1017/S0962492906400015 Published online by Cambridge University Press

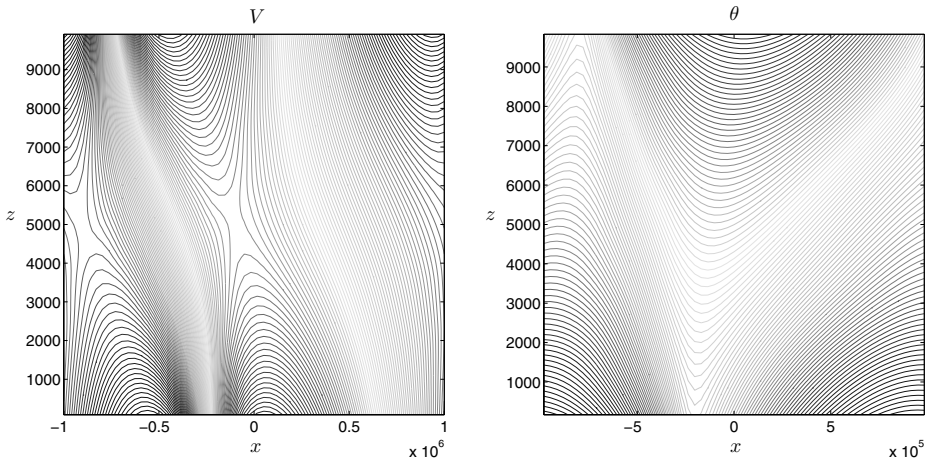


Figure 5.11. The (x, z) contours of the longitudinal velocity and potential temperature of the Eady problem close to the formation of a tropical storm.

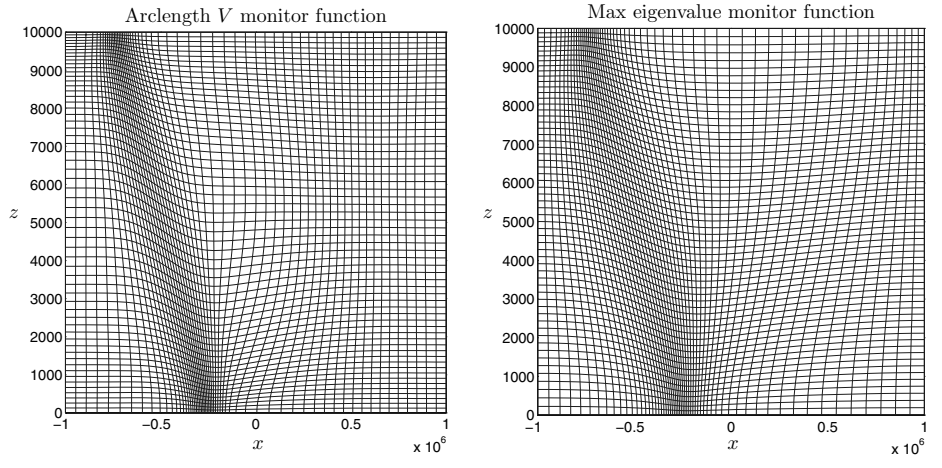


Figure 5.12. Two meshes adapted to the solution of the Eady problem presented above. In the first figure we use the arclength monitor function M_1 and in the second the potential vorticity monitor function M_2.

https://doi.org/10.1017/S0962492906400015 Published online by Cambridge University Press

Acknowledgements

It is a pleasure to thank Emily Walsh for Figures 5.7, 5.8, 5.9, 5.11 and 5.12 and J. F. Williams for Figures 3.7, 3.8, 3.9, 3.11, 5.2 and 5.4. Both also helped by reading this text and through many useful discussions. This work was supported in part by the EPSRC Critical Mass Grant GR/586525/01.

REFERENCES

S. Adjerid and J. E. Flaherty (1986), 'A moving finite element method with error estimation and refinement for one-dimensional time dependent partial differential equations', *SIAM J. Numer. Anal.* **23**, 778–795.

M. Ainsworth and J. T. Oden (2000), *A Posteriori Error Estimation in Finite Element Analysis*, Pure and Applied Mathematics, Wiley-Interscience.

V. F. Almeida (1999), 'Domain deformation mapping: Application to variational mesh generation', *SIAM J. Sci Comput.* **20**, 1252–1275.

D. A. Anderson and M. M. Rai (1983), The use of solution adaptive grids in solving partial differential equations, in *Numerical Grid Generation* (J. H. Thompson, ed.), pp. 317–338.

V. B. Andreev and N. B. Kopteva (1998), 'On the convergence, uniform with respect to a small parameter, of monotone three-point difference approximations', *Diff. Urav.* **34**, 921–929.

U. Ascher, J. Christiansen and R. D. Russell (1981), 'Collocation software for boundary value ODEs', *ACM Trans. Math. Software* **7**, 209–222.

I. Babuška and W. C. Rheinboldt (1979), 'Analysis of optimal finite element meshes in $\mathbb{R}^1$', *Math. Comput.* **33**, 435–463.

M. J. Baines (1994), *Moving Finite Elements*, Clarendon Press, Oxford.

M. J. Baines and S. L. Wakelin (1991), Equidistribution and the Legendre transformation. Numerical Analysis report 4/91, University of Reading.

M. J. Baines, M. E. Hubbard, and P. K. Jimack (2005), 'A moving mesh finite strategy for the adaptive solution of time-dependent partial differential equations with moving boundaries', *Appl. Numer. Math.* **54**, 450–469.

M. J. Baines, M. E. Hubbard, P. K. Jimack, and A. C. Jones (2006), 'Scale-invariant moving finite elements for nonlinear partial differential equations in two dimensions', *Appl. Numer. Math.* **56**, 230–252.

M. L. Balinski (1986), 'A competitive (dual) simplex method for the assignment problem', *Math. Program.* **34**, 125–141.

R. E. Bank and R. K. Smith (1997), 'Mesh smoothing using *a posteriori* error estimates', *SIAM J. Numer. Anal.* **34**, 979–997.

G. I. Barenblatt (1996), *Scaling, Self-Similarity, and Intermediate Asymptotics: Dimensional Analysis and Intermediate Asymptotics*, Cambridge Texts in Applied Mathematics, Cambridge University Press.

G. Beckett and J. A. Mackenzie (2000), 'Convergence analysis of finite-difference approximations on equidistributed grids to a singularly perturbed boundary value problem', *Appl. Numer. Math.* **35**, 87–109.

G. Beckett and J. A. Mackenzie (2001*a*), 'On a uniformly accurate finite difference approximation of a singularly perturbed reaction–diffusion problem using grid equidistribution', *J. Comput. Appl. Math.* **131**, 381–405.

https://doi.org/10.1017/S0962492906400015 Published online by Cambridge University Press

G. Beckett and J. A. Mackenzie (2001*b*), 'Uniformly convergent high order finite element solutions of a singularly perturbed reaction–diffusion equation using mesh equidistribution', *Appl. Numer. Math.* **39**, 31–45.

G. Beckett, J. A. Mackenzie and M. L. Robertson (2001*a*), 'A moving mesh finite element method for the solution of two-dimensional Stefan problems', *J. Comput. Phys.* **186**, 500–518.

G. Beckett, J. A. Mackenzie, A. Ramage and D. M. Sloan (2001*b*), 'On the numerical solution of one-dimensional PDEs using adaptive methods based on equidistribution', *J. Comput. Phys.* **167**, 372–392.

J. D. Benamou and Y. Brenier (2000), 'A computational fluid mechanics solution to the Monge–Kantorovich mass transfer problem', *Numer. Math.* **84**, 375–393.

M. Berger and R. Kohn (1988), 'A rescaling algorithm for the numerical calculation of blowing-up solutions', *Comm. Pure. Appl. Math.* **41**, 841–863.

M. Berzins (1998), 'A solution-based triangular and tetrahedral mesh quality indicator', *SIAM J. Sci. Comput.* **19**, 2051–2060.

J. G. Blom and J. G. Verwer (1989), On the use of the arclength and curvature monitor in a moving grid method which is based on the method of lines. Technical Report NM-N8902, CWI, Amsterdam.

P. Bochev, G. Liao and G. d. Pena (1996), 'Analysis and computation of adaptive moving grids by deformation', *Numer. Methods PDEs* **12**, 489–506.

C. de Boor (1973), *Good Approximations by Splines with Variable Knots II*, Vol. 363 of *Lecture Notes in Mathematics*, Springer, Berlin.

J. U. Brackbill (1993), 'An adaptive grid with directional control', *J. Comput. Phys.* **108**, 38–50.

J. U. Brackbill and J. S. Saltzman (1982), 'Adaptive zoning for singular problems in two dimensions', *J. Comput. Phys.* **46**, 342–368.

L. Branets and G. F. Carey (2003), A local cell quality metric and variational grid smoothing algorithm, in *Proc. 12th International Meshing Roundtable*, Sandia National Laboratories, Albuquerque, NM.

Y. Brenier (1991), 'Polar factorization and monotone rearrangement of vector-valued functions', *Comm. Pure Appl. Math.* **44**, 375–417.

C. J. Budd and V. A. Dorodnitsyn (2001), 'Symmetry adapted moving mesh schemes for the nonlinear Schrödinger equation', *J. Phys. A* **34**, 103887–10400.

C. J. Budd and M. D. Piggott (2005), Geometric integration and its applications, in *Handbook of Numerical Analysis* (F. Cucker, ed.), pp. 35–139.

C. J. Budd and J. F. Williams (2006), 'Parabolic Monge–Ampère methods for blow-up problems in several spatial dimensions', *J. Phys. A* **39**, 5425–5444.

C. J. Budd and J. F. Williams (2009), Mesh generation using the parabolic Monge–Ampère method. Submitted.

C. J. Budd, W. Z. Huang, and R. D. Russell (1996), 'Moving mesh methods for problems with blow-up', *SIAM J. Sci. Comput.* **17**, 305–327.

C. J. Budd, S.-N. Chen and R. D. R. Russell (1999*a*), 'New self-similar solutions of the nonlinear Schrödinger equation, with moving mesh computations', *J. Comput. Phys.* **152**, 756–789.

https://doi.org/10.1017/S0962492906400015 Published online by Cambridge University Press

C. J. Budd, G. J. Collins, W.-Z. Huang and R. D. Russell (1999*b*), 'Self-similar discrete solutions of the porous medium equation', *Philos. Trans. Roy. Soc. London A* **357**, 1047–1078.

C. J. Budd, B. Leimkuhler, and M. D. Piggott (2001), 'Scaling invariance and adaptivity', *Appl. Numer. Math.* **39**, 261–288.

C. J. Budd, V. A. Galaktionov and J. F. Williams (2004), 'Self-similar blow-up in higher-order semilinear parabolic equations', *SIAM J. Appl. Math.* **64**, 1775–1809.

C. J. Budd, R. Carretero-Gonzalez, and R. D. Russell (2005), 'Precise computations of chemotactic collapse using moving mesh methods', *J. Comput. Phys.* **202**, 462–487.

C. J. Budd, M. D. Piggott, and J. F. Williams (2009), Adaptive numerical methods and the geostrophic coordinate transformation. Submitted to *Monthly Weather Review*.

L. A. Caffarelli (1992), 'The regularity of mappings with a convex potential', *J. Amer. Math. Soc.* **5**, 99–104.

L. A. Caffarelli (1996), 'Boundary regularity of maps with convex potentials', *Ann. of Math.* **3**, 453–496.

X. Cai, D. Fleitas, B. Jiang and G. Liao (2004), 'Adaptive grid generation based on the least squares finite element method', *Comput. Math. Appl.* **48**, 1077–1085.

D. A. Calhoun, C. Helzel and R. J. LeVeque (2008), 'Logically rectangular grids and finite volume methods for PDEs in circular and spherical domains', *SIAM Review* **50**, 723–752.

W. Cao (2005), 'On the error of linear interpolation and the orientation, aspect ratio and internal angles of a triangle', *SIAM J. Numer. Anal.* **43**, 19–40.

W. Cao (2007*a*), 'An interpolation error estimate on anisotropic meshes in $\mathbb{R}^n$ and optimal metrics for mesh refinement', *SIAM J. Numer. Anal.* **45**, 2368–2391

W. Cao (2007*b*), 'Anisotropic measures of third order derivatives and the quadratic interpolation error on triangular elements', *SIAM J. Sci. Comput.* **29**, 756–781.

W. Cao (2008), 'An interpolation error estimate in $\mathbb{R}^2$ based on the anisotropic measures of higher order derivatives', *Math. Comput.* **77**, 265–286.

W. Cao, W. Huang, and R. D. Russell (1999*a*), 'An r-adaptive finite element method based upon moving mesh PDEs', *J. Comput. Phys.* **149**, 221–244.

W. Cao, W. Huang, and R. D. Russell (1999*b*), 'A study of monitor functions for two-dimensional adaptive mesh generation', *SIAM J. Sci. Comput.* **20**, 1978–1994.

W. Cao, W. Huang, and R. D. Russell (2002), 'A moving mesh method based on the geometric conservation law', *SIAM J. Sci. Comput.* **24**, 118–142.

W. Cao, W. Huang, and R. D. Russell (2003), 'Approaches for generating moving adaptive meshes: Location versus velocity', *Appl. Numer. Math.* **47**, 121–138.

M. Capiński and E. Kopp (2004), *Measure, Integral and Probability*, Springer Undergraduate Mathematics Series, Springer.

G. Carey (1997), *Computational Grids: Generation, Adaptation and Solution Strategies*, Taylor and Francis.

N. Carlson and K. Miller (1998*a*), 'Design and application of a gradient-weighted moving finite element code I: In 1-D', *SIAM J. Sci. Comput.* **19**, 728–765.

https://doi.org/10.1017/S0962492906400015 Published online by Cambridge University Press

N. Carlson and K. Miller (1998*b*), 'Design and application of a gradient-weighted moving finite element code II: In 2-D', *SIAM J. Sci. Comput.* **19**, 766–798.

H. D. Ceniceros (2002), 'A semi-implicit moving mesh method for the focusing nonlinear Schrödinger equation', *Comm. Pure Appl. Anal.* **4**, 1–14.

H. D. Ceniceros and T. Y. Hou (2001), 'An efficient dynamically adaptive mesh for potentially singular solutions', *J. Comput. Phys.* **172**, 609–639.

L. Chacón and G. Lapenta (2006), 'A fully implicit, nonlinear adaptive grid strategy', *J. Comput. Phys.* **212**, 703–717.

R. Chartrand, K. R. Vixie, B. Wohlberg and E. M. Bollt (2007), A gradient descent solution to the Monge–Kantorovich problem. math.lanl.gov/Research/Publications/Docs/chartrand-2007-gradient.pdf.

K. Chen (1994), 'Error equidistribution and mesh adaptation', *SIAM J. Sci. Comput.* **15**, 798–818.

L. Chen, P. Sun and J. Xu (2007), 'Optimal anisotropic meshes for minimizing interpolation errors in the L^p-norm', *Math. Comput.* **76**, 179–204.

S. Chynoweth and M. J. Baines (1989), Legendre transform solutions to semigeostrophic frontogenesis, in *Finite Element Analysis in Fluids* (T. J. Chung and G. R. Kerr, eds), pp. 697–703.

S. Chynoweth and M. J. Sewell (1989), 'Dual variables in semigeostrophic theory', *Proc. R. Soc. London A* **424**, 155–186.

M. J. P. Cullen (1989), 'Implicit finite difference methods for modelling discontinuous atmospheric flows', *J. Comput. Phys.* **81**, 319–348.

M. J. P. Cullen (2006), *A Mathematical Theory of Large-Scale Atmosphere/Ocean Flow*, Imperial College Press.

M. J. P. Cullen and R. J. Purser (1984), 'An extended Lagrangian theory of semigeostrophic frontogenesis', *J. Atmos. Sci.* **41**, 1477–1497.

M. J. P. Cullen, J. Norbury, and R. J. Purser (1991), 'Generalised Lagrangian solutions for atmospheric and oceanic flows', *SIAM J. Appl. Math.* **51**, 20–31.

B. Dacorogna and J. Moser (1990), 'On a partial differential equation involving the Jacobian determinant', *Ann. Inst. Henri Poincaré Analyse non linéaire* **7**, 1–26.

E. Dean and R. Glowinski (2003), 'Numerical solution of the two-dimensional elliptic Monge–Ampère equation with Dirichlet boundary conditions: An augmented Lagrangian approach', *Comptes rendus Mathématique* **336**, 779–784.

E. Dean and R. Glowinski (2004), 'Numerical solution of the two-dimensional elliptic Monge–Ampère equation with Dirichlet boundary conditions: A least-squares approach', *Comptes rendus Mathématique* **339**, 887–892.

G. Delzanno, L. Chacón, J. Finn, Y. Chung and G. Lapenta (2008), 'An optimal robust equidistribution method for two-dimensional grid adaptation based on Monge–Kantorovich optimization', *J. Comput. Phys.* **227**, 9841–9864.

Y. Di, R. Li, T. Tang and P. Zhang (2005), 'Moving mesh finite element methods for the incompressible Navier–Stokes equations', *SIAM J. Sci. Comput.* **26**, 1036–1056.

E. A. Dorfi and L. O'C. Drury (1987), 'Simple adaptive grids for 1-D initial value problems', *J. Comput. Phys.* **69**, 175–195.

https://doi.org/10.1017/S0962492906400015 Published online by Cambridge University Press

V. A. Dorodnitsyn (1991), 'Transformation groups in mesh spaces', *J. Sov. Math.* **55**, 1490–1517.

V. A. Dorodnitsyn (1993*a*), Finite-difference models exactly inheriting symmetry of original differential equations, in *Modern Group Analysis: Advanced Analytical and Computational Methods in Mathematical Physics* (N. Ibragimov *et al.*, eds), Kluwer, Dordrecht, pp. 191–201.

V. A. Dorodnitsyn (1993*b*), 'Finite difference analog of the Noether theorem', *Dokl. Akad. Nauk* **328**, 678–690.

V. A. Dorodnitsyn and R. Kozlov (1997), The whole set of symmetry preserving discrete versions of a heat transfer equation with a source. Preprint 4/1997, NTNU, Trondheim.

A. S. Dvinsky (1991), 'Adaptive grid generation from harmonic maps on Riemannian manifolds', *J. Comput. Phys.* **95**, 450–476.

P. R. Eisman (1985), 'Grid generation for fluid mechanics computation', *Ann. Rev. Fluid Mech.* **17**, 487–522.

P. R. Eisman (1987), 'Adaptive grid generation', *Comput. Meth. Appl. Mech. Engrg* **64**, 321–376.

L. C. Evans (1999), Partial differential equations and Monge–Kantorovich mass transfer, in *Current Developments in Mathematics, 1997* (Cambridge, MA), International Press, Boston, MA, pp. 65–126.

X. Feng and M. Neilan (2009), 'Vanishing moment method and moment solutions for fully nonlinear second order partial differential equations', *J. Sci. Comput.*, to appear.

W. M. Feng, P. Yu, S. Y. Hu, Z. K. Liu, Q. Du and L. Q. Chen (2006), 'Spectral implementation of an adaptive moving mesh method for phase-field equations', *J. Comput. Phys.* **220**, 498–510.

S. Fulton (1989), 'Multigrid solution of the semigeostrophic invertibility relation', *Monthly Weather Review* **117**, 2059–2066.

W. Gangbo and R. J. McCann (1996), 'The geometry of optimal transport', *Acta Math.* **177**, 113–161.

C. E. Gutiérrez (2001), *The Monge–Ampère Equation*, Vol. 44 of *Progress in Nonlinear Differential Equations and their Applications*, Birkhäuser, Boston, MA.

S. Haker and A. Tannenbaum (2003), On the Monge–Kantorovich problem and image warping, in *Mathematical Methods in Computer Vision*, Vol. 133 of *IMA Vol. Math. Appl.*, Springer, New York, pp. 65–85.

D. F. Hawken, J. J. Gottlieb and J. S. Hansen (1991), 'Review of some adaptive node-movement techniques in finite element and finite difference solutions of PDEs', *J. Comput. Phys.* **95**, 254–302.

Y. He and W. Huang (2009), *A posteriori* error analysis for finite element solution of elliptic differential equations using equidistributing meshes. Submitted.

W. Huang (2001*a*), 'Practical aspects of formulation and solution of moving mesh partial differential equations', *J. Comput. Phys.* **171**, 753–775.

W. Huang (2001*b*), 'Variational mesh adaption: Isotropy and equidistribution', *J. Comput. Phys.* **174**, 903–924.

W. Huang (2005*a*), 'Measuring mesh qualities and application to variational mesh adaption', *SIAM J. Sci. Comput.* **26**, 1643–1666.

https://doi.org/10.1017/S0962492906400015 Published online by Cambridge University Press

W. Huang (2005*b*), 'Metric tensors for anisotropic mesh generation', *J. Comput. Phys.* **204**, 663–665.

W. Huang (2005*c*), 'Convergence analysis of finite element solution of one-dimensional singularly perturbed differential equations on equidistributing meshes', *Internat. J. Numer. Anal. Model.* **2**, 57–74.

W. Huang (2007), Anisotropic mesh adaption and movement, in *Adaptive Computations: Theory and Algorithms* (T. Tang and J. Xu, eds), Science Press, Beijing, pp. 68–158.

W. Huang and B. Leimkuhler (1997), 'The adaptive Verlet method', *SIAM J. Sci. Comput.* **18**, 239–256.

W. Huang and X. P. Li (2009), 'An anisotropic mesh adaptation method for the finite element solution of variational problems', *Finite Elements in Analysis and Design*, to appear.

W. Huang and R. D. Russell (1996), 'A moving collocation method for solving time dependent partial differential equations', *Appl. Numer. Math.* **20**, 101–116.

W. Huang and R. D. Russell (1997*a*), 'Analysis of moving mesh partial differential equations with spatial smoothing', *SIAM J. Numer. Anal.* **34**, 1106–1126.

W. Huang and R. D. Russell (1997*b*), 'A high dimensional moving mesh strategy', *Appl. Numer. Math.* **26**, 63–76.

W. Huang and R. D. Russell (1999), 'A moving mesh strategy based on a gradient flow equation for two-dimensional problems', *SIAM J. Sci. Comput.* **20**, 998–1015.

W. Huang and R. D. Russell (2001) 'Adaptive mesh movement: The MMPDE approach and its applications', *J. Comput. Appl. Math.* **128**, 383–398.

W. Huang and D. Sloan (1994), 'A simple adaptive grid method in two dimensions', *SIAM J. Sci. Comput.* **15**, 776–797.

W. Huang and W. Sun (2003), 'Variational mesh adaption II: Error estimates and monitor functions', *J. Comput. Phys.* **184**, 619–648.

W. Huang and X. Zhan (2004), Adaptive moving mesh modeling for two dimensional groundwater flow and transport, in *Recent Advances in Adaptive Computation*, Vol. 383 of *Contemporary Mathematics*, AMS, pp. 283–296.

W. Huang, Y. Ren, and R. D. Russell (1994), 'Moving mesh partial differential equations (MMPDEs) based on the equidistribution principle', *SIAM J. Numer. Anal.* **31**, 709–730.

W. Huang, L. Zheng and X. Zhan (2002), 'Adaptive moving mesh methods for simulating one-dimensional groundwater problems with sharp moving fronts', *Internat. J. Numer. Meth. Engng* **54**, 1579–1603.

W. Huang, J. Ma and R. D. Russell (2008), 'A study of moving mesh PDE methods for numerical simulation of blowup in reaction diffusion equations', *J. Comput. Phys.* **227**, 6532–6552.

W. Huang, L. Kamenski and J. Lang (2009), Anisotropic mesh adaptation based upon *a posteriori* error estimates. Submitted.

J. M. Hyman and B. Larrouturou (1986), Dynamic rezone methods for partial differential equations in one space dimension. Technical Report LA-UR-86-1678, Los Alamos National laboratory, Los Alamos, NM.

J. M. Hyman and B. Larrouturou (1989), 'Dynamic rezone methods for partial

https://doi.org/10.1017/S0962492906400015 Published online by Cambridge University Press

differential equations in one space dimension', *Appl. Numer. Math.* **5**, 435–450.
O.-P. Jacquotte (1988), 'A mechanical model for a new grid generation method in computational fluid dynamics', *Comput. Methods Appl. Mech. Engrg* **66**, 323–338.
O.-P. Jacquotte and G. Coussement(1992), 'Structured mesh adaption: Space accuracy and interpolation methods', *Comput. Methods Appl. Mech. Engrg* **101**, 397–432.
C. Johnson (1987), *Numerical Solution of Partial Differential Equations by the Finite Element Method*, Cambridge University Press.
T. Kaijser (1998), 'Computing the Kantorovich distance for images', *J. Math. Imaging Vision* **9**, 173–191.
J. Kautsky and N. K. Nichols (1980), 'Equidistributing meshes with constraints', *SIAM J. Sci. Statist. Comput.* **1**, 499–511.
J. Kautsky and N. K. Nichols (1982), 'Smooth regrading of discretized data', *SIAM J. Sci. Statist. Comput.* **3**, 145–159.
P. M. Knupp (1995), 'Mesh generation using vector fields', *J. Comput. Phys.* **119**, 142–148.
P. M. Knupp (1996), 'Jacobian-weighted elliptic grid generation', *SIAM J. Sci. Comput.* **17**, 1475–1490.
P. M. Knupp (2001), 'Algebraic mesh quality metrics', *SIAM J. Sci. Comput.* **23**, 193–218.
P. Knupp and N. Robidoux (2000), 'A framework for variational grid generation: Conditioning the Jacobian matrix with matrix norms', *SIAM J. Sci. Comput.* **21**, 2029–2047.
P. Knupp and S. Steinberg (1994), *Fundamentals of Grid Generation*, CRC Press, Boca Raton.
P. M. Knupp, L. Margolin and M. Shashkov (2002), 'Reference Jacobian optimization-based rezoning strategies for arbitrary Lagrangian Eulerian methods', *J. Comput. Phys.* **176**, 93–128.
N. Kopteva (2007), Convergence theory of moving grid methods, in *Adaptive Computations: Theory and Algorithms* (T. Tang and J. Xu, eds), Science Press, Beijing, pp. 159–210.
N. Kopteva and M. Stynes (2001), 'A robust adaptive method for a quasilinear one-dimensional convection–diffusion problem', *SIAM J. Numer. Anal.* **39**, 1446–1467.
R. Kozlov (2000), Symmetry applications to difference and differential-difference equations. PhD Thesis, Institut for matematiske fag, NTNU, Trondheim.
J. Lang, W. Cao, W. Huang and R. D. Russell (2003), 'A two-dimensional moving finite element method with local refinement based on *a posteriori* error estimates', *Appl. Numer. Math.* **46**, 75–94.
G. Lapenta and L. Chacón (2006), 'Cost-effectiveness of fully implicit moving mesh adaptation: A practical investigation in 1D', *J. Comput. Phys.* **219**, 86–103.
R. J. LeVeque (1990), *Numerical Methods for Conservation Laws*, Birkhäuser.
R. Li, T. Tang, and P.-W. Zhang (2002), 'A moving mesh finite element algorithm for singular problems in two and three space dimensions', *J. Comput. Phys.* **177**, 365–393.

https://doi.org/10.1017/S0962492906400015 Published online by Cambridge University Press

S. T. Li and L. R. Petzold (1997), 'Moving mesh methods with upwinding schemes for time dependent PDEs', *J. Comput Phys.* **131**, 368–377.

S. T. Li, L. R. Petzold and Y. Ren (1998), 'Stability of moving mesh systems of partial differential equations', *SIAM J. Sci. Comput.* **20**, 719–738.

G. Liao and D. Anderson (1992), 'A new approach to grid generation', *Appl. Anal.* **44**, 285–297.

G. Liao and J. Xue (2006), 'Moving meshes by the deformation method', *J. Comput. Appl. Math.* **195**, 83–92.

V. D. Liseikin (1999), *Grid Generation Methods*, Springer, Berlin.

A. Liu and B. Joe (1994), 'Relationship between tetrahedron quality measures', *BIT* **34**, 268–287.

J. Mackenzie (1999), 'Uniform convergence analysis of an upwind finite-difference approximation of a convection–diffusion boundary value problem on an adaptive grid', *IMA J. Numer. Anal.* **19**, 233–249.

J. A. Mackenzie and W. R. Mekwi (2007*a*), On the use of moving mesh methods to solve PDEs, in *Adaptive Computations: Theory and Algorithms* (T. Tang and J. Xu, eds), Science Press, Beijing, pp. 242–278.

J. A. Mackenzie and W. R. Mekwi (2007*b*), 'An analysis of stability and convergence of a finite-difference discretization of a model parabolic PDE in 1D using a moving mesh', *IMA J. Numer. Anal.* **27**, 507–528.

J. A. Mackenzie and M. L. Robertson (2002), 'A moving mesh method for the solution of the one-dimensional phase-field equations', *J. Comput. Phys.* **181**, 526–544.

R. I. McLachlan (1994), 'Symplectic integration of Hamiltonian wave equations', *Numer. Math.* **66**, 465–492.

A. Marquina (1994), 'Local piecewise hyperbolic resolution of numerical fluxes for nonlinear scalar conservation laws', *SIAM J. Sci. Comput.* **15**, 894–904.

C. T. Miller, S. N. Gleyzer and P. T. Imhoff (1998), Numerical modeling of NAPL dissolution fingering in porous media, in *Physical Nonequilibrium in Soils: Modeling and Application* (H. M. Selim and L. Ma, eds), Ann Arbor Press.

K. Miller (1981), 'Moving finite elements II', *SIAM J. Numer. Anal.* **18**, 1033–1057.

K. Miller and R. N. Miller (1981), 'Moving finite elements I', *SIAM J. Numer. Anal.* **18**, 1019–1032.

P. K. Moore and J. E. Flaherty (1992), 'Adaptive local overlapping grid methods for parabolic system in two space dimensions', *J. Comput. Phys.* **98**, 54–63.

J. Moser (1965), 'On the volume elements of a manifold', *Trans. Amer. Math. Soc.* **120**, 286–294.

L. S. Mulholland, W. Huang and D. M. Sloan (1998), 'Pseudospectral solution of near-singular problems using numerical coordinate transformations based on adaptivity', *SIAM J. Sci. Comput.* **19**, 1261–1298.

N. Nakamura (1994), 'Nonlinear equilibriation of two-dimensional Eady waves', Simulations with viscous geostrophic momentum equations', *J. Atmos. Sci.* **51**, 1023–1035.

V. I. Oliker and L. D. Prussner (1988), 'On the numerical solution of the equation $(\partial^2 z/\partial x^2)(\partial^2 z/\partial y^2) - ((\partial^2 z/\partial x \partial y))^2 = f$ and its discretizations I', *Numer. Math.* **54**, 271–293.

https://doi.org/10.1017/S0962492906400015 Published online by Cambridge University Press

P. J. Olver (1986), *Applications of Lie Groups to Differential Equations*, Springer, New York.

L. R. Petzold (1982), A description of DASSL: A differential/algebraic system solver. Technical report SAND82-8637, Sandia National Labs, Livermore, CA.

L. R. Petzold (1987), 'Observations on an adaptive moving grid method for one-dimensional systems for partial differential equations', *Appl. Numer. Math.* **3**, 347–360.

J. Pryce (1989), 'On the convergence of iterated remeshing', *IMA J. Numer. Anal.* **9**, 315–335.

Y. Qiu and D. M. Sloan (1998), 'Numerical solution of Fisher's equation using a moving mesh method', *J. Comput. Phys.* **146**, 726–746.

Y. Qiu and D. M. Sloan (1999), 'Analysis of difference approximations to a singularly perturbed two-point boundary value problem on an adaptively generated grid', *J. Comput. Appl. Math.* **101**, 1–25.

Y. Qiu, D. M. Sloan and T. Tang (2000), 'Numerical solution of a singularly perturbed two-point boundary value problem using equidistribution: Analysis of convergence', *J. Comput. Appl. Math.* **116**, 121–143.

S. T. Rachev and L. Rüschendorf (1998), *Mass Transportation Problems I: Theory*, Probability and its Applications, Springer, New York.

W. Ren and X. Wang (2000), 'An iterative grid redistribution method for singular problems in multiple dimensions', *J. Comput. Phys.* **159**, 246–273.

Y. G. Reshetnyak (1989), *Space Mappings with Bounded Distortion*, Vol. 73 of *Translations of Mathematical Monographs*, AMS, Providence, RI.

R. D. Russell, J. F. Williams, and X. Xu (2007), 'MOVCOL4: A moving mesh code for fourth-order time-dependent partial differential equations', *SIAM J. Sci. Comput.* **29**, 197–220

A. A. Samarskii, V. A. Galaktionov, S. P. Kurdyumov and A. P. Mikhailov (1995), *Blow-up in Quasilinear Parabolic Equations*, Vol. 19 of *De Gruyter Expositions in Mathematics*, Walter de Gruyter.

G. Sapiro (2003), Introduction to partial differential equations and variational formulations in image processing, in *Foundations of Computational Mathematics* (F. Cucker, ed.), Vol. 1, pp. 383–461.

P. Saucez, A. Vande Vouwer and P. A. Zegeling (2005), 'Adaptive method of lines solutions for the extended fifth order Korteveg–De Vries equation', *J. Comput. Math.* **183**, 343–357.

B. Semper and G. Liao (1995), 'A moving grid finite-element method using grid deformation', *Numer. Methods in PDEs* **11**, 603–615.

M. J. Sewell (1978), 'On Legendre transformations and umbilic catastrophes', *Math. Proc. Camb. Phil. Soc.* **83**, 273–288.

M. J. Sewell (2002), Some applications of transformation theory in mechanics, in *Large Scale Atmosphere–Ocean Dynamics*, Vol. II (J. Norbury and I. Roulstone, eds), Cambridge University Press, pp. 143–223.

R. Shewchuk (2002), Constrained Delaunay tetrahedralizations and provably good boundary recovery, in *IMR 2002*, Sandia National Laboratories, pp. 193–204.

G. E. Shilov and B. L. Gurevich (1978), *Integral, Measure and Derivative: A Unified Approach*, Dover.

https://doi.org/10.1017/S0962492906400015 Published online by Cambridge University Press

J. H. Smith (1996), Analysis of moving mesh methods for dissipative partial differential equations. PhD Thesis, Department of Computer Science, Stanford University.

J. Stockie, J. A. Mackenzie, and R. D. Russell (2000), 'A moving mesh method for one-dimensional hyperbolic conservation laws', *SIAM J. Sci. Comput.* **22**, 1791–1813.

C. Sulem and P. L. Sulem (1999), *The Nonlinear Schrödinger Equation: Self-Focusing and Wave Collapse*, Springer.

M. H. M. Sulman (2008) Optimal mass transport for adaptivity and image registration. PhD Thesis, Simon Fraser University.

Z. Tan (2007), 'Adaptive moving mesh methods for two-dimensional resistive magneto-hydrodynamic PDE models', *Computers and Fluids* **36**, 758–771.

Z. Tan, K. M. Lim and B. C. Khoo (2007), 'An adaptive mesh redistribution method for the incompressible mixture flows using phase-field model', *J. Comput. Phys.* **225**, 1137–1158.

H. Z. Tang and T. Tang (2003), 'Adaptive mesh methods for one- and two-dimensional hyperbolic conservation laws', *SIAM J. Numer. Anal.* **41**, 487–515.

T. Tang (2005), Moving mesh methods for computational fluid dynamics, in *Recent Advances in Adaptive Computations*, Vol. 383 of *Contemporary Mathematics*, AMS, pp. 141–173.

T. Tang and J. Xu, eds (2007), *Adaptive Computations: Theory and Algorithms*, Science Press, Beijing.

T. W. Tee and L. N. Trefethen (2006), 'A rational spectral collocation method with adaptively transformed Chebyshev grid points', *SIAM J. Sci. Comput.* **28**, 1798–1811.

J. F. Thompson (1985), 'A survey of dynamically-adaptive grids in the numerical solution of partial differential equations', *Appl. Numer. Math.* **1**, 3–27.

J. F. Thompson and N. P. Weatherill (1992), 'Structured and unstructured grid generation', *Critical Reviews Biomed. Eng.* **20**, 73–120.

J. F. Thompson, Z. U. A. Warsi, and C. W. Mastin (1982), 'Boundary-fitted coordinate systems for numerical solution of partial differential equations: A review', *J. Comput. Phys.* **47**, 1–108.

J. F. Thompson, Z. U. A. Warsi, and C. W. Mastin (1985), *Numerical Grid Generation*, North-Holland.

Y. Touringy and F. Hülseman (1998), 'A new moving mesh algorithm for the finite element solution of variational problems', *SIAM J. Numer. Anal.* **35**, 1416–1438.

A. E. P. Veldman and K. Rinzema (1992), 'Playing with nonuniform grids', *J. Engrg Math.* **26**, 119–130.

J. G. Verwer, J. G. Blom, R. M. Furzeland and P. A. Zegeling (1989), A moving-grid method for one-dimensional PDEs based on the method of lines, in *Adaptive Methods for Partial Differential Equations* (J. E. Flaherty, P. J. Paslow, M. S. Shepard and J. D. Vasilakis, eds), SIAM, Philadelphia, pp. 160–175.

C. Villani (2003), *Topics in Optimal Transportation*, Vol. 58 of *Graduate Studies in Mathematics*, AMS.

E. Walsh, C. J. Budd and J. F. Williams (2009), The PMA method for grid generation applied to the Eady problem in meteorology. University of Bath report.

https://doi.org/10.1017/S0962492906400015 Published online by Cambridge University Press

L.-L. Wang and J. Shen (2005), 'Error analysis for mapped Jacobi spectral methods', *J. Sci. Comput.* **24**, 183–218.
A. J. Wathen and M. J. Baines (1985), 'On the structure of the moving finite-element equations', *IMA J. Numer. Anal.* **5**, 161–182.
A. M. Winslow (1967), 'Numerical solution of the quasilinear Poisson equation in a nonuniform triangle mesh', *J. Comput. Phys.* **2**, 149–172.
A. M. Winslow (1981), Adaptive mesh rezoning by the equipotential method. Technical report UCID-19062, Lawrence Livermore Lab.
X. Xu, W.-H. Huang, R. D. Russell and J. F. Williams (2009), Convergence of de Boor's algorithm for generation of equidistributing meshes. Submitted.
N. N. Yanenko, E. A. Kroshko, V. V. Liseikin, V. M. Fomin, V. P. Shapeev and Y. A. Shitov (1976), *Methods for the Construction of Moving Grids for Problems of Fluid Dynamics with Big Deformations*, Vol. 59 of *Lecture Notes in Physics*, Springer.
P. A. Zegeling (1993), Moving-grid methods for time-dependent partial differential equations. CWI Tract 94.
P. A. Zegeling (2005), 'On resistive MHD models with adaptive moving meshes', *J. Sci. Comput.* **24**, 263–284.
P. A. Zegeling (2007), Theory and application of adaptive moving grid methods, in *Adaptive Computations: Theory and Algorithms*, Science Press, Beijing, pp. 279–332.
P. A. Zegeling and H. P. Kok (2004), 'Adaptive moving mesh computations for reaction–diffusion systems', *J. Comput. Appl. Math.* **168**, 519–528.
Z.-R Zhang and T. Tang (2002), 'An adaptive mesh redistribution algorithm for convection-dominated problems', *Comm. Pure Appl. Anal.* **1**, 341–357
B. Zitova and J. Flusser (2003), 'Image registration methods: A survey', *Image and Vision Comput.* **21**, 977–1000.
M. Zlamal (1968), 'On the finite element method', *Numer. Math.* **12**, 394–409.

https://doi.org/10.1017/S0962492906400015 Published online by Cambridge University Press